1997

Stable inversion based output tracking control of robotic systems

Hongchao Zhao
Iowa State University

INFORMATION TO USERS

This manuscript has been reproduced from the microfilm master. UMI films the text directly from the original or copy submitted. Thus, some thesis and dissertation copies are in typewriter face, while others may be from any type of computer printer.

The quality of this reproduction is dependent upon the quality of the copy submitted. Broken or indistinct print, colored or poor quality illustrations and photographs, print bleedthrough, substandard margins, and improper alignment can adversely affect reproduction.

In the unlikely event that the author did not send UMI a complete manuscript and there are missing pages, these will be noted. Also, if unauthorized copyright material had to be removed, a note will indicate the deletion.

Oversize materials (e.g., maps, drawings, charts) are reproduced by sectioning the original, beginning at the upper left-hand corner and continuing from left to right in equal sections with small overlaps. Each original is also photographed in one exposure and is included in reduced form at the back of the book.

Photographs included in the original manuscript have been reproduced xerographically in this copy. Higher quality 6" x 9" black and white photographic prints are available for any photographs or illustrations appearing in this copy for an additional charge. Contact UMI directly to order.

UMI

A Bell & Howell Information Company
300 North Zeeb Road, Ann Arbor MI 48106-1346 USA
313/761-4700 800/521-0600

Stable inversion based output tracking control of robotic systems

by

Hongchao Zhao

A dissertation submitted to the graduate faculty

in partial fulfillment of the requirements for the degree of

DOCTOR OF PHILOSOPHY

Major: Electrical Engineering (Control Systems)

Major Professor: Degang Chen

Iowa State University

Ames, Iowa

1997

Graduate College
Iowa State University

This is to certify that the Doctoral dissertation of

Hongchao Zhao

has met the dissertation requirements of Iowa State University

Signature was redacted for privacy.

Committee Member

Signature was redacted for privacy.

Committee Member

Signature was redacted for privacy.

Committee Member

Signature was redacted for privacy.

Committee Member

Signature was redacted for privacy.

Major Professor

Signature was redacted for privacy.

For the Major Program

Signature was redacted for privacy.

For the Graduate College

TABLE OF CONTENTS

ACKNOWLEDGMENTS

Very many thanks to my advisor, Dr. Degang Chen, for having been a constant source of inspiration and encouragement during this research. I am grateful to him for introducing me to this area of research in the first place, and his intellectual guidance throughout. I would also like to thank him for funding my study and research throughout my stay at Iowa State University.

A special appreciation is extended to Dr. Mustafa H. Khammash, Dr. Ping Lu, Dr. Bion L. Pierson, and Dr. Vijay Vittal for serving on my thesis committee. I would like to thank them for their time, support, and valuable and helpful comments and suggestions in shaping up this thesis.

Valuable discussions and suggestions given by fellow students in the control lab are sincerely appreciated.

My deepest thanks are due to my lovely wife, Mrs. Juan Shen, for her patience, understanding, and support.

ABSTRACT

This thesis addresses stable inversion based output tracking control and its applications to robotic systems. It considers the non-causal invertibility (stable inversion) problem of control systems in its various aspects including properties of stable inverses and algorithms for constructing stable inverses. Then, the stable inversion approach is applied to solve a control problem of long-standing interest: output tracking control for non-minimum phase nonlinear systems.

A minimum energy property of stable inverses is firstly established. The property claims that given any desired output trajectory, out of infinitely many possible inverse solutions, the one provided by the stable inversion process is the only one that has finite energy. Based on this property, a numerical procedure is developed to provide an efficient approach to construct stable inverses.

Secondly, a new output tracking control design is developed. The design incorporates stable inverses and assumes a controller structure of feed-forward plus feedback. It achieves high precision tracking together with closed-loop stability. Furthermore, when system uncertainties are considered and assumed to satisfy the so-called "matching conditions", a modified controller structure is presented and the corresponding robust tracking performance is discussed.

Finally, the stable inversion based tracking control design is applied to three flexible robotic systems. The first study is output tracking control of a flexible-joint robot. The application demonstrates how the new design deals with the undesirable non-minimum phase property and achieves desired output tracking. The second application is tip

trajectory tracking for a two-flexible-link manipulator. This thesis, for the first time, addresses the problem of stable tip trajectory tracking without any transient or steady-state errors for such non-minimum phase systems. In the third application, a new optimal motion control strategy for a flexible space robot is presented. The space robot system is assumed to consist of a two-link flexible manipulator attached to rigid spacecraft. Optimality is in the sense that a performance index measured by maneuvering time, control effort, and structural vibrations is minimized while the interference from the manipulator to spacecraft is kept satisfactorily small.

Studies on three applications demonstrate that the stable inversion based control design is very effective on output tracking for various robotic systems. This approach is expected to perform equivalently well for many other realistic non-minimum phase nonlinear systems.

CHAPTER 1 INTRODUCTION

As enormous computing power of microprocessors and computers is becoming available to control theorists and engineers, higher and higher quality performance is being demanded from control systems. This has led to better modeling of complex dynamic systems and control systems design incorporating features of the better models. Detailed modeling often results in highly nonlinear descriptions of physical systems. This imposes considerable limitations on the ability to use traditional linear control systems even though linear control theory has achieved a high degree of maturity. Only within a limited operating range may some physical systems be approximated by linear models based on which linear controllers are designed. Therefore, there has been a great deal of emphasis on nonlinear control systems. Because they are designed based on the complete nonlinear description of system dynamics, nonlinear control systems are expected to provide better performance.

1.1 Problem Statement

System inversion, as an approach to nonlinear control, provides a systematic control systems design technique. Control systems design via the system inversion approach explores a fundamental property, the (right) invertibility property, of control systems. This property means the ability of a control system to reproduce an arbitrary prescribed trajectory at the output by manipulating the control input (and the initial states).

It is known for a long time that inverse systems have been used to solve numerous control problems such as disturbance decoupling, model matching, and minimal realizations. Furthermore, the inversion problem is especially of direct interest in servo, output tracking, and feed-forward control. However, being causal solutions in classical inversion, inverse controls are necessarily unstable for those systems with unstable zero dynamics, the non-minimum phase systems. Many important engineering systems such as airplane flight control, rocket autopilot, and motion control of flexible robots are known to be nonlinear and of non-minimum phase. Therefore, stable inversion, a non-causal approach to system inversion, which investigates possibly bounded inverse controls for both minimum and non-minimum phase systems, is becoming of significant importance for such engineering systems.

For this reason, we in this thesis consider the non-causal invertibility problem (stable inversion) of control systems in its various aspects including properties of stable inverses and algorithms to construct the stable inverse solutions. Then, the stable inversion approach is applied to solve a control problem of long-standing interest: output tracking control for non-minimum phase nonlinear systems.

Generally speaking, the output tracking control problem is to design a control system such that the system output follows or "tracks" a prescribed reference trajectory (as a function of time) as closely as possible. In the meantime, all internal and external signals of the closed-loop control system connecting both physical system and controller remain stable. The overall performance of an output tracking control system is based on the ability of the system output to robustly respond to the reference signal despite possible changes in the system parameters or unmodeled dynamics, as well as the presence of external disturbances.

It has long been recognized that the non-minimum phase property of systems is a major obstacle in output tracking control. A system is of non-minimum phase if there exists a (nonlinear) feedback that can hold the system output identically zero while

the internal dynamics become unstable [29]. In the linear case those are the systems with unstable zeros. By incorporating stable inversion, this thesis aims at solving the problem of output tracking control for a class of non-minimum phase nonlinear systems with smooth dynamics and affine in control input. For the first time, a systematic output tracking design approach for such non-minimum phase systems is successfully applied to output tracking and motion control of various flexible robotic systems.

1.2 Outline of the Thesis

The outline of the thesis is as follows.

Chapter 2 is intended to serve as an introduction to stable inversion as well as its relevant background information. We start by briefly reviewing recent publications on invertibility problem of control systems and the theory of nonlinear differential geometric control. Various design approaches currently used in output tracking control are discussed. With a brief description of notations from differential geometry which are used throughout the thesis, we introduce the stable inversion theory by presenting its framework and some of its most important results.

Chapter 3 presents one of the main contributions of the thesis. It establishes a minimum energy property for stable inverses, the inverse solutions by stable inversion. The property claims that given any desired output trajectory, out of infinitely many possible inverse solutions, the one provided by the stable inversion process is the only one that has finite $\mathcal{L}_2(-\infty, +\infty)$-norm. Based on this property, a numerical procedure is developed to provide an efficient method to construct stable inverses by constructing and solving an optimal control problem. The problem searches for the minimum energy control among all exact-output-reproduction inputs. It is solved via an iteration on linearization, discretization, and pseudo-inversion processes.

Chapter 4 deals with output tracking control incorporating stable inverses. We develop a systematic design approach for the stable inversion based tracking controller which is expected to drive system output to accurately track prescribed trajectories in output and to maintain boundedness of all internal and external signals. Performance of asymptotic tracking and ϵ-tracking as defined in the thesis is established for the proposed tracking control system. A robustness result is also presented for system dynamics with uncertainties satisfying the so-called "matching conditions".

Chapter 5 applies the tracking control design developed in Chapter 4 to output tracking control of a single-link flexible-joint robot system. After development of forward system dynamics using the Lagrange's method, we define a stable inversion problem for such robot system. It is followed by construction of the stable inverse solution to the problem. Then, an output tracking controller incorporating the stable inverse with only partial state measurement is designed. A simulation study demonstrates the effectiveness of the design approach in dealing with the very undesirable non-minimum phase property of this robot system and in achieving desired output tracking performance.

Chapter 6 is an application on tip trajectory tracking using stable inversion for a two-link flexible manipulator. After a review of recent works published on modeling and control of robot manipulators, equations of motion are first developed using the assumed modes technique for a two-link flexible manipulator with tip position as output. From that, an inverse model is derived and a two-point boundary value condition is set up. This condition guarantees that the inverse solution for a given desired tip trajectory will be stable regardless of the fact that a flexible manipulator is a non-minimum phase system. The stable inverse solution is then used as a feed-forward signal together with a joint-angle stabilizing feedback to an output tracking controller. Excellent output tracking is achieved without any transient or steady-state errors. In a simulation study, simulation results compare very favorably against the performance of the well-known computed torque method.

Chapter 7 presents a new optimal motion control strategy using stable inversion for a flexible space robot system. The system consists of a two-link flexible manipulator attached to rigid spacecraft floating in space. Optimality is in the sense that a performance index measured by maneuvering time, control effort, and structural vibrations is minimized while the interference from the arm to spacecraft is kept satisfactorily small. After introducing forward system dynamics, the optimal motion control is formulated as a nonlinear optimal control problem. The problem is then reorganized into two stages. The inner-stage is an unconstrained exact output tracking problem that is automatically solved by applying stable inversion. The two-stage problem is then reduced to the outer-stage optimal trajectory planning problem. A suboptimal solution is pursued that leads to a planned tip trajectory. A stable inversion based output tracking controller is designed that drives the robot to track the planned trajectory. The controller assumes only joint-angle measurement and joint-torque control, but not any forces from spacecraft.

Conclusions are finally given in Chapter 8. It summarizes the contributions of the research presented in this thesis. Possible future work on improvement and extensions of current studies is also discussed.

CHAPTER 2 STABLE INVERSION

Stable inversion is by definition a part of the invertibility problem of control systems. It addresses the non-causal inversion of nonlinear (and linear) systems from the perspective of nonlinear differential geometric control theory. The introduction of stable inversion into the control world is motivated by the challenging problem of output tracking control for non-minimum phase nonlinear systems. Advances on all these three areas, system invertibility, differential geometric control, and output tracking, consequently pave the way to the development of stable inversion.

2.1 Literature Review

2.1.1 Invertibility of control systems

For every control system there is an input/output map associated with some prescribed initial conditions. The question of the (right) invertibility is essentially that of the surjectivity of this map. This fundamental problem has been extensively studied for over three decades. It was first attacked by Brockett and Mesarovic [6] in the mid-1960s. Later on, an easy-to-follow step-by-step procedure called Structure Algorithm [53] was developed by Silverman to construct (causal) inverses for a class of multivariable linear systems. Systematic studies of the invertibility problem for nonlinear systems began with Hirschorn's papers [25, 26, 27] in the late-1970s in which linear results were extended to nonlinear real-analytic systems. Singh in his papers [54, 55, 56] had obtained similar results on the development of nonlinear generalization of the Structure Algorithm

as well as its applications. There have also been other attempts in applying various techniques such as the differential algebraic approach [18, 19, 16] by Fliess and the geometric method [44, 45] by Nijmeijer. For discrete-time control systems, the inversion problem was addressed in an early paper [51] by Sain and Massey and later on by El Asmi and Fliess in their paper [17] and by Grizzle's paper [24]. A rather thorough treatment in this discrete-time case of the inversion problem and its applications to systems synthesis can be found in a recently published book [34] by Kotta.

2.1.2 Nonlinear differential geometric control

While much of the material on the theory of nonlinear geometric control can be traced to recent publications, it is well collected and presented in two books, *Nonlinear Control Systems* [29] by Isidori and *Nonlinear Dynamical Control Systems* [47] by Nijmeijer and van der Schaft. Nonlinear systems with affine input have in particular attracted much attention. A paper [28] published in 1983 by Hunt, Su, and Meyer was one of the early widely recognized works dealing with exact state linearization by using feedback and coordinate transformation. Issues of input-output linearization and input-output decoupling were discussed in many papers including [31] by Isidori et al., [58] by Singh and Rugh, and [57] by Singh. The concept of zero dynamics plays a key role in the differential geometric control. The relation of the zero dynamics to transmission zeros in linear systems was introduced in papers [32, 35] by Isidori et al. A related notion of zeros at infinity was discussed in a paper [46] by Nijmeijer and Schumacher. Recent advances of differential geometric control theory have provided a solid theoretic basis for the development of the stable inversion theory.

2.1.3 Output tracking control

The problem of asymptotic output tracking control for linear time-invariant systems was solved early in 1970s and summarized as the Internal Model Principle [21] by Fran-

cis and Wonham. Interested readers may refer to papers [13] by Davison and [20] by Francis for additional references. Based on the differential geometric control theory, the matrix equations defining asymptotic tracking controllers for linear systems were translated into nonlinear partial differential equations lately by Isidori and Byrnes [30] to deal with tracking control for nonlinear systems. This approach, known as nonlinear regulation, uses a controller structure of feed-forward plus feedback and provides zero steady-state error output tracking for a class of reference trajectories generated from given autonomous exosystems. The feed-forward signal is obtained by solving a set of partial differential equations of the same order as that of the forward dynamics. The feedback is an exponentially stabilizing control law. A application of this regulation approach to a flexible robot manipulator for tip trajectory tracking can be found in a paper [15] by De Luca and Siciliano. Besides the numerical tractability of nonlinear partial differential equations, a major concern is the possibly large transient error that is not controlled in this regulation approach.

The transient behavior can be precisely controlled by using a classical inversion based output tracking control approach [26, 54]. This approach assumes the same controller structure of feed-forward plus feedback as that used by the regulation approach. The same stabilizing feedback is used. The feed-forward signal is, however, generated by solving an inverse system as an initial value problem for a given output function. For minimum phase systems, this approach has been successfully used in designing output tracking control systems. Inversion based control of robot manipulators can be found in papers [14] by De Luca and Siciliano and [37] by Madhavan and Singh and many others. For flight control applications, see publications by Wise [64], Morton [42], and Azam and Singh [1] for examples. In addition to the basic system invertibility problem, the fundamental difficulty of this inversion based tracking control is the phenomenon of unbounded inverse control signals generated for non-minimum phase systems.

2.2 Stable Inversion

2.2.1 Characterization and preliminaries

Stable inversion, expected to play a key role in achieving high precision output tracking control for non-minimum phase nonlinear systems, was introduced to the control world lately by Chen and Paden [11, 12]. It considers multivariable nonlinear control systems of the following state-space form

$$\dot{x} = f(x) + \sum_{i=1}^{m} g_i(x)u_i, \tag{2.1}$$

$$y_i = h_i(x), \qquad 1 \leq i \leq m. \tag{2.2}$$

In a more compact form, it can be written as

$$\dot{x} = f(x) + g(x)u, \tag{2.3}$$

$$y = h(x), \tag{2.4}$$

where system state x is defined on an open neighborhood of the origin of $\mathbb{R}^n$ and $u \in \mathbb{R}^m$ and $y \in \mathbb{R}^m$. It is assumed that $f(x)$ and $g_i(x)$ for $i = 1, 2, \ldots, m$ are smooth vector fields and $h_i(x)$ for $i = 1, 2, \ldots, m$ are smooth functions defined on the neighborhood with $f(0) = 0$ and $h(0) = 0$.

The class (2.3)-(2.4) describes a large number of physical systems of interest in many engineering applications, including of course linear systems. For such systems, the stable inversion problem can be stated as follows.

Definition 1 (Stable Inversion Problem) *Given any smooth reference output trajectory y_d with compact support (Assumption 2), find a bounded control input u_d and a bounded state trajectory x_d such that $u_d \to 0$ and $x_d \to 0$ as $t \to \pm\infty$ and their image by the input/output map of the control system (2.3)-(2.4) is exactly y_d.*

The pair (x_d, u_d) is the stable inverse solution for a given reference output y_d. It is called stable inverse because of the boundedness and convergence provided by the definition. We also call x_d the desired state trajectory and u_d the nominal control input.

For convenience, notations from differential geometry are used throughout this thesis. With $\mathbb{N} \stackrel{\text{def}}{=} \{1, 2, \ldots\}$ and $y: \mathbb{R}^n \to \mathbb{R}^m$, we define

$$r \stackrel{\text{def}}{=} [r_1, r_1, \ldots, r_m]^T \in \mathbb{N}^m, \tag{2.5}$$

$$y^{(r)} \stackrel{\text{def}}{=} [y_1^{(r_1)}, y_2^{(r_2)}, \ldots, y_m^{(r_m)}]^T. \tag{2.6}$$

For $h: \mathbb{R}^n \to \mathbb{R}^m$, $f: \mathbb{R}^n \to \mathbb{R}^n$, and $g = [g_1, \ldots, g_m]$ with $g_i: \mathbb{R}^n \to \mathbb{R}^n$, we define

$$L_f^r h \stackrel{\text{def}}{=} [L_f^{r_1} h_1, L_f^{r_2} h_2, \ldots, L_f^{r_m} h_m]^T, \tag{2.7}$$

$$L_g h \stackrel{\text{def}}{=} [L_{g_1} h, L_{g_2} h, \ldots, L_{g_k} h]. \tag{2.8}$$

where the notation $L_f^{r_i} h_i$ and so on are defined as follows.

For a real-valued function h_i and a vector field f both defined on an open neighborhood of the origin of $\mathbb{R}^n$, the function called the derivative of h_i along f is defined as

$$L_f h_i(x) \stackrel{\text{def}}{=} \frac{\partial h_i}{\partial x} f(x) = \sum_{k=1}^{n} \frac{\partial h_i}{\partial x_k} f_k(x), \tag{2.9}$$

at each x of the neighborhood. By taking the derivative of h_i first along a vector field f and then along another vector field g_j, we define a new function

$$L_{g_j} L_f h_i(x) \stackrel{\text{def}}{=} \frac{\partial (L_f h_i)}{\partial x} g_j(x). \tag{2.10}$$

Thus, $L_f^{r_i} h_i(x)$ satisfies

$$L_f^{r_i} h_i = \frac{\partial (L_f^{r_i - 1} h_i(x))}{\partial x} f(x), \tag{2.11}$$

with $L_f^0 h_i(x) = h_i(x)$.

For the time being, only systems of the form (2.3)-(2.4) with a well-defined relative degree are considered. Using the notations introduced, this assumption can be stated as follows.

Assumption 1 *The nonlinear system in the form of (2.3)-(2.4) has a well-defined vector relative degree $r \in \mathbb{N}^m$ at the origin, i.e. in an open neighborhood of the origin,*

(i) for all $1 \leq j \leq m$, for all $1 \leq i \leq m$, for all $0 \leq k < r_i - 1$, and for all x,

$$L_{g_j} L_f^k h_i(x) = 0; \tag{2.12}$$

(ii) the following $m \times m$ matrix is nonsingular at the origin $x = 0$:

$$\beta(x) \stackrel{\text{def}}{=} L_g L_f^{r-1} h(x) = \begin{bmatrix} L_{g_1} L_f^{r_1-1} h_1(x) & \dots & L_{g_m} L_f^{r_1-1} h_1(x) \\ L_{g_1} L_f^{r_2-1} h_2(x) & \dots & L_{g_m} L_f^{r_2-1} h_2(x) \\ \dots & \dots & \dots \\ L_{g_1} L_f^{r_m-1} h_m(x) & \dots & L_{g_m} L_f^{r_m-1} h_m(x) \end{bmatrix}. \tag{2.13}$$

It is noticed that the number r_i is exactly the number of times one has to differentiate the ith output $y_i(x)$ in order to have at least one component of the input vector u explicitly appearing. It is also noticed that because the control u does not appear in output equation (2.4), we have $r_i \geq 1$ for all $i = 1, 2, \dots, m$.

In the definition of the stable inversion problem, we require the reference output trajectory y_d to have compact support. This requirement can be stated as follows.

Assumption 2 *The reference output trajectory y_d is a sufficiently smooth function of time satisfying $y_d(t) \equiv 0$ for all $t \leq t_0$ and $t \geq t_f$ where $t_f > t_0$ are both finite.*

The results of stable inversion reviewed in this section can be extended with little effort to cover reference trajectories whose first derivatives have compact support. This extension covers a large class of realistic trajectories. For those trajectories, all contributions of the thesis from Chapter 3 to Chapter 7 remain valid except for Theorem 4. The only additional requirement in addition to the assumptions stated throughout the thesis is that $r_i \geq 2$ corresponding to the output component i with such extension.

2.2.2 Construction of stable inverses

Under Assumption 1, system dynamics (2.3) can be partially linearized [29]. To do this, we define

$$\begin{aligned}\xi &\stackrel{\text{def}}{=} [\xi_1^1, \xi_2^1, \ldots, \xi_{r_1}^1, \xi_1^2, \ldots, \xi_{r_2}^2, \ldots, \xi_{r_m}^m]^T \\ &\stackrel{\text{def}}{=} [y_1, \dot{y}_1, \ldots, y_1^{(r_1-1)}, y_2, \ldots, y_2^{(r_2-1)}, \ldots, y_m^{(r_m-1)}]^T. \end{aligned} \tag{2.14}$$

In the trivial case when $r_1+\cdots+r_m=n$, the dynamics can be completely linearized by a state feedback and the inversion problem becomes a kinematic or algebraic inversion. Hence, it is assumed that $r_1+\cdots+r_m<n$. Choose η such that

$$[\xi^T, \eta^T]^T = [\phi_\xi^T(x), \phi_\eta^T(x)]^T = \Phi(x) \tag{2.15}$$

forms a local coordinate transformation with $\Phi(0) = 0$. To qualify as a change of coordinates, $\Phi(x)$ should be chosen such that it has a Jacobian matrix that is nonsingular at the origin. In the new coordinate, dynamics equation (2.3) becomes

$$\begin{aligned}\dot{\xi}_1^i &= \xi_2^i \\ &\vdots \\ \dot{\xi}_{r_i-1}^i &= \xi_{r_i}^i \\ \dot{\xi}_{r_i}^i &= \alpha_i(\xi,\eta) + \beta_i(\xi,\eta)u \\ \dot{\eta} &= \alpha_\eta(\xi,\eta) + \beta_\eta(\xi,\eta)u, \end{aligned} \tag{2.16}$$

for $i = 1, 2, \ldots, m$. In a more compact form, it is equivalent to

$$y^{(r)} = \alpha(\xi,\eta) + \beta(\xi,\eta)u, \tag{2.17}$$

$$\dot{\eta} = \alpha_\eta(\xi,\eta) + \beta_\eta(\xi,\eta)u, \tag{2.18}$$

where

$$\alpha(\xi,\eta) \stackrel{\text{def}}{=} L_f^r h(\Phi^{-1}(\xi,\eta)), \tag{2.19}$$

$$\beta(\xi,\eta) \stackrel{\text{def}}{=} L_g L_f^{r-1} h(\Phi^{-1}(\xi,\eta)), \tag{2.20}$$

$$\alpha_\eta(\xi,\eta) \stackrel{\text{def}}{=} L_f \phi_\eta(\Phi^{-1}(\xi,\eta)), \tag{2.21}$$

$$\beta_\eta(\xi,\eta) \stackrel{\text{def}}{=} L_g \phi_\eta(\Phi^{-1}(\xi,\eta)), \tag{2.22}$$

and α_i and β_i are the ith row of $\alpha(\,)$ and $\beta(\,)$ respectively.

Let y_d be any prescribed output trajectory. Set $y(t) \equiv y_d(t)$. Then, we immediately have

$$\xi = \xi_d \stackrel{\text{def}}{=} [\, y_{d1}, \dot{y}_{d1}, \ldots, y_{d1}^{(r_1-1)}, y_{d2}, \ldots, y_{d2}^{(r_2-1)}, \ldots, y_{dm}^{(r_m-1)} \,]^T. \tag{2.23}$$

and $y^{(r)} = y_d^{(r)}$. Solving for u from equation (2.17), we obtain

$$u = \beta^{-1}(\xi_d,\eta)[\, y_d^{(r)} - \alpha(\xi_d,\eta) \,]. \tag{2.24}$$

The invertibility of $\beta(\,)$ is guaranteed by Assumption 1. Upon substituting (2.24), equation (2.18) becomes the so-called reference dynamics:

$$\dot{\eta} = p(\bar{\xi}_d,\eta), \tag{2.25}$$

where

$$\bar{\xi}_d \stackrel{\text{def}}{=} \begin{bmatrix} \xi_d \\ y_d^{(r)} \end{bmatrix}; \tag{2.26}$$

$$p(\bar{\xi}_d,\eta) \stackrel{\text{def}}{=} \alpha_\eta(\xi_d,\eta) + \beta_\eta(\xi_d,\eta)\beta^{-1}(\xi_d,\eta)[\, y_d^{(r)} - \alpha(\xi_d,\eta) \,]. \tag{2.27}$$

Reference dynamics (2.25) together with equation (2.24) constitutes inverse system dynamics for given y_d. When $y_d \equiv 0$ (and consequently $\bar{\xi}_d \equiv 0$), the reference dynamics becomes autonomous zero dynamics:

$$\dot{\eta} = p(0,\eta). \tag{2.28}$$

It is interesting to notice that the linear approximation of the zero dynamics (2.28) at $\eta = 0$ coincides with the zero dynamics of the linear approximation of the entire system (2.3)-(2.4). In other words, the linear approximation at $\eta = 0$ of the zero

dynamics has eigenvalues which coincide with the zeros of the transfer function of the linear approximation at $x = 0$ of the entire system.

The zero dynamics (2.28) corresponds to the dynamics describing the "internal" behavior of the system when input and initial conditions have been chosen in such a way as to constrain the output to remain identically zero. Nonlinear systems with unstable zero dynamics are said to have non-minimum phase.

It is noticed that the reference dynamics does become the zero dynamics for t outside the compact interval $[t_0, t_f]$ (by Assumption 2).

Assumption 3 *The linear approximation at $\eta = 0$ of the zero dynamics (2.28) has no eigenvalues on the imaginary axis.*

In other words, the assumption requires that the zero dynamics has a hyperbolic equilibrium point at the origin.

Theorem 1 (See Chen and Paden [12] for a proof.) *Under Assumptions 1-3, the stable inversion problem has a solution if and only if the following two-point boundary value problem has a solution*

$$\dot{\eta} = p(\bar{\xi}_d, \eta), \tag{2.29}$$

subject to

$$\begin{cases} \eta(t_0) \in \mathbf{W}^u \\ \eta(t_f) \in \mathbf{W}^s, \end{cases} \tag{2.30}$$

where $\mathbf{W}^u$ and $\mathbf{W}^s$ are respectively the invariant unstable manifold and the stable manifold of the zero dynamics (2.28).

The solution of this two-point boundary value problem η_d will provide a way to compute the stable inverse pair (x_d, u_d) through the inverse coordinate transformation of (2.15) and equation (2.24) which is the output equation of inverse dynamics:

$$x_d = \Phi^{-1}(\xi_d, \eta_d), \tag{2.31}$$

$$u_d = \beta^{-1}(x_d)[\, y_d^{(r)} - \alpha(x_d)\,]. \tag{2.32}$$

The properties of existence and uniqueness of stable inverses are given by the following theorem.

Theorem 2 (See Chen and Paden [12] for a proof.) *Under Assumptions 1-3, the two-point boundary value problem (2.29)-(2.30) locally has a unique solution.*

In a paper [9] by Chen, an approach was developed to solve the two-point boundary value problem (2.29)-(2.30) by iteratively linearizing the nonlinear problem into a linear time-varying problem at each iteration step. The linear problem in each iteration is then solved by applying a method similar to the so-called Sweep Method [7] from linear quadratic optimal control. The main idea in this approach is to try to separate stable and unstable dynamics and then to integrate the stable part forward in time while to integrate the unstable part backward in time. The procedure will be utilized in a tip trajectory tracking design studied in Chapter 7. See Appendix A for more details on this algorithm.

It is noticed that stable inversion designs a possibly non-causal inverse system for a given desired output trajectory. The non-causality comes from the fact that stable inverses are defined and of possible non-zero values over the entire time horizon whereas the output functions are required to have compact support over $[t_0, t_f]$. This non-causality of the inversion process is perfectly fine from an engineering point of view because an inverse system is not a physical system but a general nonlinear map (from a given output to an input). For minimum phase systems stable inversion coincides with the Hirschorn's classical (causal) inversion.

CHAPTER 3 PROPERTIES OF STABLE INVERSES

Stable inverses have some properties by definition: boundedness, convergence, and non-causality. The properties of existence, uniqueness, and continuous dependence on reference output trajectories can be established from Theorem 2 and its proof. In addition to these important features, energy quantity associated with the stable inverse solutions is studied in this chapter.

3.1 Minimal Energy Properties

The goal of this section is to establish that out of an infinite number of input and state trajectories that are capable of producing exactly a given output trajectory, the desired state trajectory and the nominal control input given by the stable inversion process is the only pair yielding a finite $\mathcal{L}_2(-\infty, +\infty)$-norm. This is a very important property of stable inversion. It immediately suggests its value in many applications where output tracking, input energy consumption, and internal vibrations are of concern.

Before we start, we recall two standard theorems from theory of ordinary differential equations, Theorem 10 and Theorem 11. Both are quoted in Appendix B. Theorem 10 concerns a local property of solutions on stable or unstable manifolds of a hyperbolic equilibrium point. The solutions are expected to approach the equilibrium point exponentially. Theorem 11 addresses a local property of solutions that are on neither stable nor unstable manifolds of a hyperbolic equilibrium point. In this case, the solutions must leave a prescribed spherical neighborhood with center at the equilibrium point at

some finite time.

In the proof of Theorem 3, these two theorems will be applied to the reference dynamics (2.29) for $t \leq t_0$ and $t \geq t_f$ during which the dynamics becomes the autonomous zero dynamics (2.28). With these preparations, we start by showing in Theorem 3 that the boundary condition (2.30) ensures finite energy of the solution to the two-point boundary value problem, but those not satisfying the boundary condition (2.30) all have infinite energy.

3.1.1 Modes of reference dynamics

Theorem 3 *Suppose Assumptions 1-3 are all satisfied. Then, among all the solutions of the reference dynamics (2.29), the η_d that satisfies the boundary condition (2.30) is the only one yielding a finite $\mathcal{L}_2(-\infty, +\infty)$-norm.*

Proof: By Theorem 2, Assumptions 1-3 guarantee the existence of a unique $\eta_d(t)$ for all $t \in (-\infty, +\infty)$. Consider

$$\int_{-\infty}^{+\infty} \| \eta_d(t) \|_2^2 \, dt = \int_{-\infty}^{t_0} \| \eta_d(t) \|_2^2 \, dt + \int_{t_0}^{t_f} \| \eta_d(t) \|_2^2 \, dt + \int_{t_f}^{+\infty} \| \eta_d(t) \|_2^2 \, dt. \tag{3.1}$$

Since η_d is continuous, it is bounded over a compact interval. Denote

$$\kappa_1 = \sup\{ \| \eta_d(t) \|_2 \mid t_0 \leq t \leq t_f \}. \tag{3.2}$$

From the boundary condition (2.30) we have $\eta_d(t_f) \in \mathbf{W}^s$ for all $t \geq t_f$ since $\mathbf{W}^s$ is time invariant. By Theorem 10, there exist finite constants $\alpha_1 > 0$ and $\beta_1 > 0$ such that

$$\begin{aligned} \| \eta_d(t) \|_2 &\leq \alpha_1 \| \eta_d(t_f) \|_2 \exp\{-\beta_1 [t - t_f]\} \\ &\leq \alpha_1 \kappa_1 \exp\{-\beta_1 [t - t_f]\}, \quad \forall t \geq t_f. \end{aligned} \tag{3.3}$$

Similarly the boundary condition (2.30) also implies that $\eta_d(t_0) \in \mathbf{W}^u$ for all $t \leq t_0$ and that there exist finite constants $\alpha_2 > 0$ and $\beta_2 > 0$ such that

$$\begin{aligned} \| \eta_d(t) \|_2 &\leq \alpha_2 \| \eta_d(t_0) \|_2 \exp\{\beta_2 [t - t_0]\} \\ &\leq \alpha_2 \kappa_1 \exp\{\beta_2 (t - t_0)\}, \quad \forall t \leq t_0. \end{aligned} \tag{3.4}$$

Hence,

$$\int_{-\infty}^{t_0} \| \eta_d(t) \|_2^2 \, dt \leq \int_{-\infty}^{t_0} \alpha_2^2 \kappa_1^2 \exp\{2\beta_2[t - t_0]\} \, dt = \frac{\alpha_2^2 \kappa_1^2}{2\beta_2}. \tag{3.5}$$

$$\int_{t_0}^{t_f} \| \eta_d(t) \|_2^2 \, dt \leq \kappa_1^2 [t_f - t_0], \tag{3.6}$$

$$\int_{t_f}^{+\infty} \| \eta_d(t) \|_2^2 \, dt \leq \int_{t_f}^{+\infty} \alpha_1^2 \kappa_1^2 \exp\{-2\beta_1[t - t_f]\} \, dt = \frac{\alpha_1^2 \kappa_1^2}{2\beta_1}. \tag{3.7}$$

Substituting (3.5)-(3.7) into (3.1) we get

$$\| \eta_d \|_{\mathcal{L}_2(-\infty,+\infty)}^2 = \int_{-\infty}^{+\infty} \| \eta_d(t) \|_2^2 \, dt \leq \kappa_\eta < +\infty, \tag{3.8}$$

where the constant

$$\kappa_\eta \stackrel{\text{def}}{=} \frac{\alpha_2^2 \kappa_1^2}{2\beta_2} + \kappa_1^2 [t_f - t_0] + \frac{\alpha_1^2 \kappa_1^2}{2\beta_1}. \tag{3.9}$$

On the other hand, consider any other solution $\eta(t)$ of equation (2.29) that does not satisfy the boundary condition (2.30), that is,

$$\eta(t_0) \notin \mathbf{W}^u \quad \textit{and/or} \quad \eta(t_f) \notin \mathbf{W}^s.$$

Suppose $\eta(t_f) \notin \mathbf{W}^s$, then $\eta(t) \notin \mathbf{W}^s$ for all $t \geq t_f$ due to the invariance of $\mathbf{W}^s$. We want to show that the $\mathcal{L}_2(-\infty, +\infty)$-norm of this solution is infinite by showing

$$\int_{t_f}^{+\infty} \| \eta(t) \|_2^2 \, dt = +\infty. \tag{3.10}$$

Select a constant $\delta_1 = 2\delta > 0$ as in Theorem 11. Without loss of generality, we assume that $\|\eta(t)\|_2 = 2\delta$ is not an equilibrium since otherwise we immediately have (3.10). Let $\{t_k,\ k = 1, 2, 3, ...,\ t_{k+1} > t_k \geq t_f\}$ be the set of all time points at which η enters the ball $B(\delta_1)$. If this set is empty and $\eta(t_f) \in B(2\delta)$, η will leave the ball in finite time according to Theorem 11 and stay outside for the rest of the time, or if $\eta(t_f) \notin B(2\delta)$ it will remain outside the ball for all $t \geq t_f$. In either case, equation (3.10) is obviously true. If the set is nonempty, we construct a new set $\{t'_k,\ k = 1, 2, 3, ...,\ t'_{k+1} > t'_k \geq t_f\}$ as follows. Let $t'_1 = t_1$ and $I_1 = [t'_1,\ t'_1 + \Delta t]$. Then find the first $t_j \notin I_1$ in the t_k set and

let $t_2' = t_j$ and $I_2 = [t_2', t_2' + \Delta t]$. Continue this process until the t_k set is exhausted. The constant Δt in this process is defined by

$$\Delta t = \frac{\delta}{max\| p(y_d^{(r)}, \xi_d, \eta \in B(2\delta))(t) \|_2}. \tag{3.11}$$

With this Δt, it follows easily that $\| \eta(t) \|_2 \geq \delta$ for all $t \in I_k$ since $\| \eta(t_k') \|_2 = 2\delta$.

Two situations need to be considered. First, the set t_k' contains finite number of points. By Theorem 11, $\eta(t)$ will leave the ball in finite time after each I_k. Therefore the total amount of time during which $\eta(t)$ is inside the ball is finite and during the rest of the time it is outside the ball, or, $\| \eta(t) \|_2 > 2\delta$. Consequently, equation (3.10) is true.

In the second situation, the set $\{t_k'\}$ contains infinite number of points. In this case, noticing that all these I_k's are disjoint, we have

$$\int_{t_f}^{+\infty} \| \eta(t) \|_2^2 \, dt \geq \int_{\cup_{k=1}^{\infty} I_k} \| \eta(t) \|_2^2 \, dt \geq \sum_{k=1}^{\infty} \int_{I_k} \delta^2 \, dt = \sum_{k=1}^{\infty} \delta^2 \Delta t. \tag{3.12}$$

which is unbounded and implies equation (3.10).

A similar argument can be made when $\eta(t_0) \notin \mathbf{W}^u$. Hence, violating any part of the boundary condition (2.30) always leads to $\| \eta \|_{\mathcal{L}_2(-\infty,+\infty)} = \infty$.

□

3.1.2 State and input trajectories

Based on Theorem 3, we establish a minimum energy property of the desired state trajectory x_d. The following technical assumption will be assumed in the proof of the property.

Assumption 4 *For any smooth reference output trajectory y_d, the reference dynamics (2.29) does not have a finite escape time.*

Theorem 4 *Suppose Assumptions 1-4 are all satisfied. Then, among the infinitely many state trajectories x which map exactly into a desired output trajectory y_d, the x_d computed by $x_d = \Phi^{-1}(\xi_d, \eta_d)$, where η_d is the solution of (2.29) subjected to (2.30), is the only one yielding a finite $\mathcal{L}_2(-\infty, +\infty)$-norm.*

Proof: The inverse coordinate transformation $x_d = \Phi^{-1}(\xi_d, \eta_d)$ with $\Phi^{-1}(0,0) = 0$ is a local diffeomorphism which implies that $\Phi^{-1}(\,)$ is locally Lipschitz continuous. Since both ξ_d and η_d are bounded, there exists a suitable compact set over which there are Lipschitz constants κ_1 and κ_2 such that

$$\begin{aligned} \| x_d \|_{\mathcal{L}_2(-\infty,+\infty)} &\leq \kappa_1 \| \xi_d \|_{\mathcal{L}_2(-\infty,+\infty)} + \kappa_2 \| \eta_d \|_{\mathcal{L}_2(-\infty,+\infty)} \\ &= \kappa_1 \| \xi_d \|_{\mathcal{L}_2[t_0,t_f]} + \kappa_2 \| \eta_d \|_{\mathcal{L}_2(-\infty,+\infty)}. \end{aligned} \tag{3.13}$$

Both terms on the right hand side are finite by Assumption 2 and Theorem 3. Therefore, so is the $\mathcal{L}_2(-\infty, +\infty)$-norm of x_d.

Notice that any other state trajectories that map exactly into the reference trajectory $y_d(t)$ can be found by the change of coordinate $x = \Phi^{-1}(\xi_d, \eta)$ where η is a solution of the reference dynamics (2.29) that does not satisfy (2.30). Since $\Phi(\,)$ is also a local diffeomorphism, it is locally Lipschitz continuous in x. However, in this case neither x nor η can be guaranteed to be small. To deal with this complication, let us divide $\mathbb{R}$ into $I_l + I_g$ such that

$$x(t) \in B(\delta_0) \quad \forall t \in I_l,$$

$$x(t) \notin B(\delta_0) \quad \forall t \in I_g,$$

for some small positive number δ_0. If I_g is infinite, then $\| x \|_{\mathcal{L}_2(-\infty,+\infty)} = \infty$ since $\| x(t) \|_2 > \delta_0$ for $t \in I_g$. Now assume I_g has finite measure. Let κ_3 be a Lipschitz constant of $\Phi(\,)$ over $B(\delta_0)$. Then for all $t \in I_l$ we have

$$\| \eta(t) \|_2 \leq \left\| \begin{bmatrix} \xi_d(t) \\ \eta(t) \end{bmatrix} \right\|_2 = \| \Phi(x)(t) \|_2 \leq \kappa_3 \| x(t) \|_2. \tag{3.14}$$

Hence,

$$\| x \|_{\mathcal{L}_2(-\infty,+\infty)} = \left[\int_{-\infty}^{+\infty} \| x(t) \|_2^2 \, dt\right]^{\frac{1}{2}} \geq \left[\int_{I_t} \| x(t) \|_2^2 \, dt\right]^{\frac{1}{2}} \geq \left[\frac{1}{\kappa_3^2}\int_{I_t} \| \eta(t) \|_2^2 \, dt\right]^{\frac{1}{2}}$$

$$= \frac{1}{\kappa_3}\left[\int_{-\infty}^{+\infty} \| \eta(t) \|_2^2 \, dt - \int_{I_g} \| \eta(t) \|_2^2 \, dt\right]^{\frac{1}{2}} = \frac{1}{\kappa_3}[\infty - \kappa_x]^{\frac{1}{2}} = \infty. \qquad (3.15)$$

Notice that in the last equation we used the results of Theorem 3 and Assumption 4 that there is no finite escape time to the reference dynamics. Therefore, the integral over a finite domain I_g is a finite number κ_x. Consequently, we have $\| x \|_{\mathcal{L}_2(-\infty,+\infty)} = \infty$ in both situations of I_g having finite measure and infinite measure.

□

To establish the minimum energy property of the nominal control input u_d, we pose another technical assumption as follows.

Assumption 5 *On the zero dynamics manifold $\xi = 0$,*

(i) $\beta(x) \stackrel{\text{def}}{=} L_g L_f^{r-1} h(x)$ is globally uniformly bounded;

(ii) given any $\delta > 0$, $\Delta t > 0$, there exists an $\epsilon(\Delta t, \delta) > 0$ such that for all t, $\| \eta(\tau) \|_2 > \delta$ for all $\tau \in [t, t + \Delta t]$ implies that $\| \alpha(0, \eta) \|^2_{\mathcal{L}_2[t,t+\Delta t]} \geq \epsilon$.

It is noticed from equation (2.17) that matrix $\beta(\,)$ is the high frequency gain from input to output which is bounded for any practical systems. Therefore, the first condition in the assumption does not pose any practical constraints. The second condition is related to the system's observability. In the linear case, if the zero dynamics is observable from $\alpha(\,)$, then the condition is satisfied.

Theorem 5 *Suppose Assumptions 1-5 are all satisfied. Then, among all the control inputs u which would reproduce exactly the reference trajectory y_d, the u_d computed by $u_d = \beta^{-1}(\xi_d, \eta_d)[y_d^{(r)} - \alpha(\xi_d, \eta_d)]$, where η_d is the solution of (2.29) subjected to (2.30), is the only one yielding a finite $\mathcal{L}_2(-\infty, +\infty)$-norm.*

Proof: Recall that by definition the stable inverses are all bounded. Denote

$$\kappa_1 = \sup\{ \| u_d(t) \|_2 \mid t_0 \leq t \leq t_f \}. \tag{3.16}$$

Thus,

$$\int_{t_0}^{t_f} \| u_d(t) \|_2^2 \, dt \leq \kappa_1^2 [t_f - t_0]. \tag{3.17}$$

As the reference trajectory y_d is of compact support, we have for $t \notin [t_0, t_f]$,

$$u_d = -\beta^{-1}(0, \eta_d)\alpha(0, \eta_d). \tag{3.18}$$

By smoothness we have that $\beta^{-1}(0, \eta_d)\alpha(0, \eta_d)$ is locally Lipschitz continuous with respect to η_d. From the boundedness of η_d there exists an appropriate compact set over which there are Lipschitz constants κ_2 and κ_3 such that

$$\| u_d \|_{\mathcal{L}_2(-\infty, t_0]} = \| \beta^{-1}(0, \eta_d)\alpha(0, \eta_d) \|_{\mathcal{L}_2(-\infty, t_0]} \leq \kappa_2 \| \eta_d \|_{\mathcal{L}_2(-\infty, t_0]}, \tag{3.19}$$

$$\| u_d \|_{\mathcal{L}_2[t_f, +\infty)} = \| \beta^{-1}(0, \eta_d)\alpha(0, \eta_d) \|_{\mathcal{L}_2[t_f, +\infty)} \leq \kappa_3 \| \eta_d \|_{\mathcal{L}_2[t_f, +\infty)}. \tag{3.20}$$

Notice that in the above we have used the fact $\alpha(0, 0) = 0$ which is a consequence of $f(0) = 0$. Combining equations (3.17)-(3.20) we can conclude that the $\mathcal{L}_2(-\infty, +\infty)$-norm of u_d is of a finite value.

Now consider any other control input u that also reproduce exactly the reference trajectory. It is noticed that u can also be written as $u = \beta^{-1}(\xi_d, \eta)[y_d^{(r)} - \alpha(\xi_d, \eta)]$, where η is a solution of (2.29) that does not satisfy the boundary condition (2.30). For t outside the compact interval $[t_0, t_f]$, we have $\xi_d \equiv 0$ and the input becomes $u = -\beta^{-1}(0, \eta)\alpha(0, \eta)$. By Assumption 5 on global uniform boundedness of the matrix $\beta(0, \eta)$, there exists a finite constant κ_4, such that

$$\| u(t) \|_2 \geq \frac{1}{\| \beta(0, \eta)(t) \|_2} \| \alpha(0, \eta)(t) \|_2 \geq \frac{1}{\kappa_4} \| \alpha(0, \eta)(t) \|_2. \tag{3.21}$$

Assumption 5 assumes that there exists a positive constant $\epsilon > 0$ such that

$$\| \alpha(0, \eta) \|_{\mathcal{L}_2[t, t+\Delta t]}^2 \geq \epsilon, \qquad \text{whenever} \qquad \| \eta(t) \|_2 \geq \delta.$$

Let δ and Δt be chosen as in the proof of Theorem 3. The rest of the proof shows $\| \alpha(0,\eta) \|_{\mathcal{L}_2(-\infty,+\infty)} = \infty$ and it follows identically the same lines as in the corresponding part of the proof of Theorem 3.

Therefore, we conclude from (3.21) that $\| u \|_{\mathcal{L}_2(-\infty,+\infty)} = +\infty$.

□

It is noticed that even though the stable inverse is shown to be the only inverse solution pair yielding a finite $\mathcal{L}_2(-\infty,+\infty)$-norm, however, it is impossible in practice to work with the infinite horizon $(-\infty,+\infty)$. Instead, a finite interval $[\bar{t}_0, \bar{t}_f]$ will be used where $\bar{t}_0 \leq t_0$ and $\bar{t}_f \geq t_f$.

Let u_{inv} be any control input defined on $[\bar{t}_0, \bar{t}_f]$ and it produces $y(t) \equiv y_d(t)$ on $[\bar{t}_0, \bar{t}_f]$. As an immediate consequence of Theorem 5, we have the following result.

Corollary 1 *Given any finite $\delta_m > 0$, there exists a finite $t_m > 0$ such that for all $\bar{t}_0 \leq t_0 - t_m$ and $\bar{t}_f \geq t_f + t_m$,*

$$\| u_{inv} \|_{\mathcal{L}_2[\bar{t}_0,\bar{t}_f]} - \| u_d \|_{\mathcal{L}_2[\bar{t}_0,\bar{t}_f]} > \delta_m. \tag{3.22}$$

It is noticed that in order for this corollary to be true, the interval $[\bar{t}_0, \bar{t}_f]$ has to be large enough. In this sense, the nominal control input u_d is the minimum energy control among all exact-output-reproduction inputs.

3.2 An Algorithm to Stable Inverses

The solution of the two-point boundary value problem (2.29)-(2.30) η_d provides a way to compute the stable inverse pair through the inverse coordinate transformation (2.31) and inverse output equation (2.32). However, integration of the reference dynamics (2.29) is still a nontrivial problem. The difficulty arises from the instability of the dynamics in both positive and negative time directions.

In this section, a numerical algorithm based on the minimum energy property of the nominal control input (Theorems 5) is developed to provide an approach to compute stable inverses. Without loss of generality we assume that the open-loop unforced dynamics of the systems (2.3)-(2.4) has been exponentially stabilized. See discussions in Section 4.1 for reasons of this generalization. For simplicity, we also take a stronger assumption as follows.

Assumption 6 *The local linearization at the origin of the forward system (2.3)-(2.4) is completely reachable.*

3.2.1 Nominal control vs. optimal control

Instead of solving the corresponding two-point boundary value problem (2.29)-(2.30), this numerical procedure tries to approximate the nominal control input u_d by a solution of an optimal control problem minimizing control input energy over a finite time horizon $[\tilde{t}_0, \bar{t}_f]$, where $\tilde{t}_0 < \bar{t}_0$, $\bar{t}_0 \leq t_0$, and $\bar{t}_f \geq t_f$. This optimal control problem is constructed as follows:

Definition 2 (Optimal Control Problem I (OCP I))

$$\min_{u \in \mathcal{L}_\infty^m[\tilde{t}_0, \bar{t}_f]} \mathcal{J}(u) = \| u \|^2_{\mathcal{L}_2[\tilde{t}_0, \bar{t}_f]} \tag{3.23}$$

subject to

$$\begin{cases} \dot{x} = f(x) + g(x)u, \quad x(\tilde{t}_0) = 0, \\ y = h(x), \\ y(t) = y_d(t), \quad \forall t \in [\bar{t}_0, \bar{t}_f], \end{cases} \tag{3.24}$$

where y_d is a prescribed output trajectory satisfying Assumption 2.

We claim that the $\mathcal{L}_\infty[\tilde{t}_0, \bar{t}_f]$-norm of the error between an optimal solution u^* to (OCP I) and the nominal control input u_d can be made arbitrarily small provided that $\bar{t}_0$ is chosen sufficiently small whereas $\bar{t}_f$ sufficiently large.

Lemma 1 *Suppose Assumptions 1-6 are all satisfied. Then, there exists a finite* $t_u > 0$ *such that for all* $\bar{t}_0 \leq t_0 - t_u$ *and* $\bar{t}_f \geq t_f + t_u$,

$$u^*(t) = u_d(t), \quad \forall t \in [\bar{t}_0, \bar{t}_f]. \tag{3.25}$$

Proof: By Assumption 6 on reachability of linearization, we conclude that the nonlinear system (2.3)-(2.4) is locally reachable near the origin $x = 0$ [29]. That is, as long as $\| x_d(\bar{t}_0) \|_2$ is sufficiently small, we have $x_d(\bar{t}_0)$ is reachable from $x(\bar{t}_0) = 0$. The smallness of $\| x_d(\bar{t}_0) \|_2$ can be ensured by both the property of exponential decay of $x_d(t)$ as $t \to \pm\infty$ (a consequence of exponential convergence of $\eta_d(t)$) and the selection of $\bar{t}_0$ to be sufficiently small, say $\bar{t}_0 \leq t_0 - \bar{t}_u$ for a finite $\bar{t}_u > 0$.

Define

$$\mathbb{S}_u = \{ u \in \mathcal{L}_\infty^m[\bar{t}_0, \bar{t}_f] \mid u(t) = u_d(t), \ \forall t \in [\bar{t}_0, \bar{t}_f] \}. \tag{3.26}$$

The reachability of $x_d(\bar{t}_0)$ implies that there exists at least one $u_x \in \mathbb{S}_u$ satisfying the constraints (3.24) in (OCP I).

The fact $u_x \in \mathcal{L}_\infty^m[\bar{t}_0, \bar{t}_f]$ implies that there exists a finite $\delta_m > 0$ such that

$$\| u_x \|^2_{\mathcal{L}_2[\bar{t}_0, \bar{t}_0]} \leq \delta_m. \tag{3.27}$$

$$\mathcal{J}(u_x) = \| u_s \|^2_{\mathcal{L}_2[\bar{t}_0, \bar{t}_f]} \leq \delta_m + \| u_d \|^2_{\mathcal{L}_2[\bar{t}_0, \bar{t}_f]}. \tag{3.28}$$

From Corollary 1 there exists a finite $t_m > 0$ such that (3.22) holds. Now choose $t_u = \max\{\bar{t}_u, t_m\}$. Then, for any $\bar{t}_0 \leq t_0 - t_u$ and $\bar{t}_f \geq t_f + t_u$, suppose $u^*(t) \neq u_d(t)$ for some $t \in [\bar{t}_0, \bar{t}_f]$. We in the rest of the proof aim to show that this assumption is not true.

Because of constraint (3.24), u^* is one of u_{inv} defined in Corollary 1. Thus, substituting u^* into (3.22) we have

$$\| u^* \|^2_{\mathcal{L}_2[\bar{t}_0, \bar{t}_f]} - \| u_d \|^2_{\mathcal{L}_2[\bar{t}_0, \bar{t}_f]} > \delta_m. \tag{3.29}$$

Then,

$$\mathcal{J}(u^*) = \| u^* \|^2_{\mathcal{L}_2[\bar{t}_0,\bar{t}_f]} \geq \| u^* \|^2_{\mathcal{L}_2[\bar{t}_0,\bar{t}_f]} > \delta_m + \| u_d \|^2_{\mathcal{L}_2[\bar{t}_0,\bar{t}_f]}. \tag{3.30}$$

From (3.28) and (3.30) we conclude that $\mathcal{J}(u^*) > \mathcal{J}(u_x)$. However, this can not be true since u^* is an optimal solution. Thus, we must have

$$u^*(t) = u_d(t), \quad \forall t \in [\bar{t}_0, \bar{t}_f]. \tag{3.31}$$

□

From this lemma, u^* and u_d are shown to be identical over the interval $[\bar{t}_0, \bar{t}_f]$. Therefore, to establish the claim on closeness of u^* and u_d over $[\tilde{t}_0, \bar{t}_f]$, we only need to show the closeness of u^* and u_d over interval $[\tilde{t}_0, \bar{t}_0]$.

By Lemma 1, the (OCP I) is reduced to the following optimal control problem which minimizes the performance index $\mathcal{J}$ over the smaller interval $[\tilde{t}_0, \bar{t}_0]$.

Definition 3 (Optimal Control Problem II (OCP II))

$$\min_{u_t \in \mathcal{L}^m_\infty[\tilde{t}_0,\bar{t}_0]} \mathcal{J}_t(u_t) = \| u_t \|^2_{\mathcal{L}_2[\tilde{t}_0,\bar{t}_0]} \tag{3.32}$$

subject to

$$\begin{cases} \dot{x} = f(x) + g(x)u_t, \quad x(\tilde{t}_0) = 0, \\ x(\bar{t}_0) = x_d(\bar{t}_0). \end{cases} \tag{3.33}$$

The nominal control input u_d and optimal solutions to the two optimal control problems (OCP I) and (OCP II) are related as follows:

$$u^*(t) = \begin{cases} u_t^*(t), & \tilde{t}_0 \leq t < \bar{t}_0 \\ u_d(t), & \bar{t}_0 \leq t \leq \bar{t}_f. \end{cases} \tag{3.34}$$

Lemma 2 *Suppose Assumptions 1-6 are all satisfied. Then, given any $\delta_u > 0$, there exists a finite $t_\delta > 0$ such that $\bar{t}_0 \leq t_0 - t_\delta$ implies*

$$\| u^* - u_d \|_{\mathcal{L}_\infty[\tilde{t}_0,\bar{t}_0]} < \delta_u. \tag{3.35}$$

Proof: When $\bar{t}_0$ is sufficiently small, both $\| x_d(\bar{t}_0) \|_2$ and $\| x_d(\bar{t}_0) \|_2$ are small due to their exponential convergence to zero as $t \to -\infty$. Thus, dynamic constraint (3.33) in the (OCP II) may be approximated by its first approximation at the origin. The constraint (3.33) then reads as

$$\begin{cases} \dot{x} = A_t x + B_t u_t, \quad x(\tilde{t}_0) = 0, \\ x(\bar{t}_0) = x_d(\bar{t}_0), \end{cases} \tag{3.36}$$

where

$$A_t = \left. \frac{\partial f(x)}{\partial x} \right|_{x=0}, \quad \text{and} \quad B_t = g(0). \tag{3.37}$$

The analytical solution to this approximate linear optimal control problem with fixed final state $x(\bar{t}_0) = x_d(\bar{t}_0)$ is given by

$$\begin{aligned} u_t^*(t) &= -B_t^T e^{A_t^T[\bar{t}_0 - t]} G^{-1}(\tilde{t}_0, \bar{t}_0) \left[x(\bar{t}_0) - e^{A_t[\bar{t}_0 - \tilde{t}_0]} x(\tilde{t}_0) \right] \\ &= -B_t^T e^{A_t^T[\bar{t}_0 - t]} G^{-1}(\tilde{t}_0, \bar{t}_0) x_d(\bar{t}_0), \qquad \forall t \in [\tilde{t}_0, \bar{t}_0]. \end{aligned} \tag{3.38}$$

where

$$G(\tilde{t}_0, \bar{t}_0) \stackrel{\text{def}}{=} \int_{\tilde{t}_0}^{\bar{t}_0} e^{A_t[\bar{t}_0 - t]} B_t B_t^T e^{A_t^T[\bar{t}_0 - t]} \, dt.$$

Assumption 6 on system reachability guarantees the invertibility of $G(\tilde{t}_0, \bar{t}_0)$. By smoothness of vector fields and functions of system dynamics, from (3.38) we conclude that there exists a finite constant $\kappa_1 > 0$ such that

$$\| u^*(t) \|_\infty = \| u_t^*(t) \|_\infty \leq \kappa_1 \| x_d(t) \|_\infty, \qquad \forall t \in [\tilde{t}_0, \bar{t}_0]. \tag{3.39}$$

On the other hand, by smoothness of $\beta^{-1}(0, \eta_d)\alpha(0, \eta_d)$, the right hand side of equation (3.18), there exists a finite $\kappa_2 > 0$ such that

$$\| u_d(t) \|_\infty \leq \kappa_2 \| \eta_d(t) \|_\infty, \qquad \forall t \in [\tilde{t}_0, \bar{t}_0]. \tag{3.40}$$

Since both $x_d(t)$ and $\eta_d(t)$ exponentially approach zero as t goes to negative infinity, both $\| u^*(t) \|_\infty$ and $\| u_d(t) \|_\infty$ are also exponentially decaying by (3.39) and (3.40). The conclusion follows immediately.

□

3.2.2 An iterative approach to optimal control

In order to construct an optimal solution u^* to (OCP I) to approximate u_d, we take an iterative approach. At each iteration step, the forward system dynamics (2.3)-(2.4) is linearized along the solutions, both state and input trajectories, obtained from the immediately previous step and then discretized. Let n_0 and n_1 be the total samples over intervals $[\bar{t}_0, \bar{t}_f]$ and $[\bar{t}_0, \bar{t}_f]$ respectively. By a standard discretization approach, the (OCP I) becomes:

Definition 4 (Optimal Control in Discretization (OCD))

$$\min_u \ \mathcal{J}_d(u) = \sum_{i=1}^{n_0} \| u_i \|_2^2 \tag{3.41}$$

subject to

$$\begin{cases} x_{k+1} = A_k x_k + B_k u_k + E_k, & \forall k = 1, \ldots, n_0, \\ x_1 = 0, & \\ y_k = C_k x_k + D_k, & \forall k = n_0 - n_1 + 1, \ldots, n_0, \\ y_k = y_{dk}, & \forall k = n_0 - n_1 + 1, \ldots, n_0. \end{cases} \tag{3.42}$$

It happened that this optimization problem has a unique solution and can be solved via the Moore-Penrose generalized inversion approach [48] after some manipulations.

Rewrite the constraint (3.42) in (OCD) as follows by both evaluating output y_k at each sampling time as a linear combination of u_j's and E_j's with $j < k$ and setting $y_k = y_{dk}$ for all y_k in the interval $[\bar{t}_0, \bar{t}_f]$:

$$\begin{aligned} y_{dk} \ = \ & C_k[B_{k-1}u_{k-1} + A_{k-1}B_{k-2}u_{k-2} + \cdots + A_{k-1}A_{k-2}\ldots A_2 B_1 u_1] + \\ & + C_k[E_{k-1} + A_{k-1}E_{k-2} + \cdots + A_{k-1}A_{k-2}\ldots A_2 E_1] + D_k, \\ & \forall k = n_0 - n_1 + 1, \ldots, n_0. \end{aligned} \tag{3.43}$$

Let Y_d be the column vector formed by stacking the y_{dk}'s together, that is, y_{dk} is the kth block row of Y_d. Similarly, let U be the column vector obtained by stacking the u_k's

together. Then, the set of n_1 equations of the form (3.43) can be written in a compact linear algebraic matrix equation

$$Y_d = M_\alpha U + M_\beta. \tag{3.44}$$

It is noticed that there are more unknowns in U ($\dim(U) = n_0 m$) than the number of equations ($\dim(Y_d) = n_1 m$) in (3.44). The well-defined relative degree guarantees that the matrix M_α has a full row rank as long as $n_0 - n_1 \geq \max\{r_1, \ldots, r_m\}$. Therefore, there are infinitely many U which will solve the equation (3.44) and the minimum energy solution is given by

$$U^* = M_\alpha^\dagger [Y_d - M_\beta], \tag{3.45}$$

where $M_\alpha^\dagger$ is the Moore-Penrose generalized inverse matrix [48]. Then, forward time simulation on the linearization of the forward system dynamics (2.3) using the computed input U^*, equivalently $u^*(t)$, as a function of time, will generate the approximated state x^* of the current step. Simulation stops when the states computed in the adjacent two steps are sufficiently close to each other.

When the sampling period is taken to be sufficiently small, the linear time-varying system, the linearization of the original forward system dynamics, can then be viewed as a time-invariant system within any one short sampling period. Thus, the computation of the transition matrices needed in obtaining the sampled-data systems in constraint (3.42)would be much simpler. This would greatly reduce the computing effort in the discretization at each iteration. It is also noticed that all matrices in (OCD) can be pre-computed for all k once the linearized forward system dynamics is known.

The numerical procedure developed in this subsection is briefly summarized as follows:

- Step 1: Set $x^0(t) = 0$ and $u^0(t) = 0$ for all t.

- Step 2: Linearize the stabilized forward system dynamics along $x^0(t)$ and $u^0(t)$ and sample it to obtain (OCD).

- Step 3: Derive the linear algebraic equation (3.44) and compute optimal solution u^* by (3.45).

- Step 4: Integrate the linearized dynamics using u^* to obtain the corresponding state trajectory x^*.

- Step 5: If $\|x^0 - x^*\|_{\mathcal{L}_\infty[\bar{t}_0,\bar{t}_f]}$ is greater than a given threshold, then set $x^0(t) = x^*(t)$ and $u^0(t) = u^*(t)$, go to step 2, else continue to step 6.

- Step 6: Set the nominal control input u_d by the solution of step 3.

CHAPTER 4 TRACKING CONTROL SYSTEMS DESIGN

The stable inverse pair (x_d, u_d) by definition solves the exact output tracking problem. However, it is firstly noticed that for non-minimum phase systems, u_d has to be applied at $t = -\infty$ which is practically impossible. Thus, left tail truncated inverse solutions have to be used. Secondly, the nonlinear system may be unstable. Any perturbation could result in divergence from desired values for those unstable systems. Therefore, we are in this chapter exploring tracking control systems design incorporating stable inverses.

4.1 Two Design Approaches

Up to now stabilization of a general nonlinear system is still an open problem. Only for systems with certain properties or structures are there linearization based and Lyapunov based stabilization designs. Anyhow, this is an independent topic of our system inversion study. Given a nonlinear system of the form (2.3)-(2.4), we assume that a stabilizing control law $u = \gamma(x)$ is known and it renders the origin of the closed-loop dynamics an exponentially stable equilibrium point.

By using $u = \gamma(x) + \nu$, the closed-loop dynamics of the stabilized system is then of the form

$$\dot{x} = f(x) + g(x)\gamma(x) + g(x)\nu, \tag{4.1}$$

$$y = h(x). \tag{4.2}$$

It can be easily verified that the original system (2.3)-(2.4) and the stabilized system (4.1)-(4.2) have the identical relative degree vector. Both systems share the same coordinate transformation and have the same zero dynamics and reference dynamics. These identity results lead to the observation: (x_d, u_d) is the unique stable inverse pair for system (2.3)-(2.4) if and only if (x_d, ν_d) is the one for system (4.1)-(4.2) where

$$\nu_d = u_d - \gamma(x_d). \tag{4.3}$$

From this observation, there are two equivalent approaches to our tracking control systems design as illustrated in Figure 4.1.

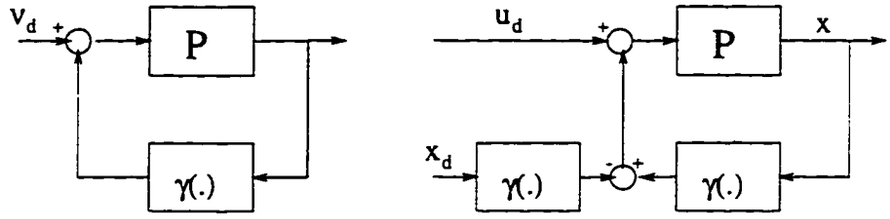

Figure 4.1 Two Equivalent Tracking Control Systems

The first design is that the nonlinear system is stabilized and then stably inverted to obtain the stable inverse solution (x_d, ν_d) for the stabilized system. The nominal control input $\nu_d(t)$ is used to drive the stabilized system. This is Approach I. The second is that the stable inverse pair (x_d, u_d) is computed based on the original system. Then the controller assumes a structure of feed-forward plus feedback of the form

$$u = u_d + \gamma(x) - \gamma(x_d). \tag{4.4}$$

This renders Approach II.

Clearly, tracking control systems via both approaches result in the same closed-loop dynamics due to the relationship (4.3). Control systems with such closed-loop dynamics achieve desired tracking performance with closed-loop stability. The performance analysis is given as follows.

4.2 Tracking Performance Analysis

4.2.1 Tracking error dynamics

We consider the case when the truncated nominal control input u_d is applied starting at $\bar{t}_0 = t_0 - T$. The closed-loop dynamics is then given by

$$\dot{x} = f(x) + g(x)[u_d + \gamma(x) - \gamma(x_d)], \quad x(t_0 - T) = 0, \tag{4.5}$$

$$y = h(x). \tag{4.6}$$

On the other hand, by definition of stable inversion we have

$$\dot{x}_d = f(x_d) + g(x_d)u_d, \quad x(-\infty) = 0, \tag{4.7}$$

$$y_d = h(x_d). \tag{4.8}$$

In this subsection, we show the following two results. The error ($x_e \stackrel{\text{def}}{=} x - x_d$) dynamics is exponentially stable at the origin provided that both $\| x_d \|_{\mathcal{L}_\infty(-\infty,+\infty)}$ and $\| u_d \|_{\mathcal{L}_\infty(-\infty,+\infty)}$ are sufficiently small. The smallness requirement on the stable inverse pair is equivalent to require the smallness of the reference output trajectory measured by $\| \bar{\xi}_d \|_{\mathcal{L}_\infty(-\infty,+\infty)}$.

Lemma 3 *Suppose Assumptions 1-6 are all satisfied. Then, there exists a constant $m_e > 0$ such that both $\| x_d \|_{\mathcal{L}_\infty(-\infty,+\infty)} < m_e$ and $\| u_d \|_{\mathcal{L}_\infty(-\infty,+\infty)} < m_e$ imply that the zero error is an exponentially stable equilibrium point of the error x_e-dynamics.*

Proof: Subtracting dynamics (4.7) from (4.5) we obtain the error dynamics

$$\dot{x}_e = f(x) - f(x_d) + g(x)[u_d + \gamma(x) - \gamma(x_d)] - g(x_d)u_d. \tag{4.9}$$

Define

$$F(x) \stackrel{\text{def}}{=} f(x) + g(x)\gamma(x). \tag{4.10}$$

The error dynamics (4.9) can be regrouped as follows:

$$\dot{x}_e = F(x_e + x_d) - F(x_d) + [\,g(x_e + x_d) - g(x_d)\,][\,u_d - \gamma(x_d)\,]. \tag{4.11}$$

By Taylors theorem,

$$\begin{aligned} \dot{x}_e &= \left.\frac{\partial F(x_e + x_d)}{\partial x_e}\right|_{x_e=0} x_e + \mathcal{O}(\|x_e\|^2) + [\,g(x_e + x_d) - g(x_d)\,][\,u_d - \gamma(x_d)\,] \\ &= A_e x_e + \Delta_e(x_d)x_e + \mathcal{O}(\|x_e\|^2) + \mathcal{O}(\|x_e\|)[\,u_d - \gamma(x_d)\,], \end{aligned} \tag{4.12}$$

where

$$A_e \stackrel{\text{def}}{=} \left.\frac{\partial F(x)}{\partial x}\right|_{x=0}, \tag{4.13}$$

and

$$\Delta(x_d) \stackrel{\text{def}}{=} \left.\frac{\partial F(x)}{\partial x}\right|_{x=x_d} - \left.\frac{\partial F(x)}{\partial x}\right|_{x=0} \tag{4.14}$$

with $\Delta(0) = 0$.

By the assumption that the origin of $\dot{x} = F(x)$ is an exponentially stable equilibrium point, from Theorem 12 (Appendix B), $\dot{x} = A_e x$ is also exponentially stable at $x = 0$.

Now for any given $\epsilon > 0$ there exists an $m_e > 0$ such that $\| x_d \|_{\mathcal{L}_\infty(-\infty,+\infty)} < m_e$, $\| u_d \|_{\mathcal{L}_\infty(-\infty,+\infty)} < m_e$. and $\| x_e \|_{\mathcal{L}_\infty(-\infty,+\infty)} < m_e$ imply

$$\left\| \left[\, \Delta_e(x_d)x_e + \mathcal{O}(\|x_e\|^2) + \mathcal{O}(\|x_e\|)[u_d - \gamma(x_d)] \,\right](t) \right\|_2 \leq \epsilon \| x_e(t) \|_2. \tag{4.15}$$

Applying the converse Lyapunov theorem (Theorem 13 in Appendix B) and choosing ϵ accordingly, the exponential stability of the error dynamics (4.11) at $x_e = 0$ follows from a standard Lyapunov argument.

□

It is noticed that the tracking is only local. The smallness of the stable inverse solution is required. However, we claim that the smallness requirement on the stable inverse pair can be satisfied provided that the reference output is sufficiently small.

Recall that given any reference output y_d, the nominal control input u_d can be regarded as the output of the stable inverse system. The stable inverse dynamics has been derived in Chapter 2. For easy reference, we regroup them as follows.

$$\dot{\eta}_d = \alpha_\eta(\xi_d, \eta_d) + \beta_\eta(\xi_d, \eta_d)\beta^{-1}(\xi_d, \eta_d)[\, y_d^{(r)} - \alpha(\xi_d, \eta_d)\,]. \tag{4.16}$$

$$\begin{cases} \eta_d(t_0) \in \mathbf{W}^u, \\ \eta_d(t_f) \in \mathbf{W}^s, \end{cases} \tag{4.17}$$

$$u_d = \beta^{-1}(\xi_d, \eta_d)[\, y_d^{(r)} - \alpha(\xi_d, \eta_d)\,]. \tag{4.18}$$

They are respectively equations (2.29), (2.30), and (2.32) in Section 2.2.

To establish the claim, we need the concept of transversality, a geometric notion which deals with the intersection of surfaces or manifolds. Denote

$$n_\eta = n - [\, r_1 + r_2 + \cdots + r_m\,]. \tag{4.19}$$

Then, $\mathbf{W}^u$ and $\mathbf{W}^s$ are differentiable manifolds in $\mathbb{R}^{n_\eta}$. Let η be a point in $\mathbb{R}^{n_\eta}$. $\mathbf{W}^u$ and $\mathbf{W}^s$ are said to be transversal at η if $\eta \notin \mathbf{W}^u \cap \mathbf{W}^s$; or if $\eta \in \mathbf{W}^u \cap \mathbf{W}^s$, then $T_\eta \mathbf{W}^u + T_\eta \mathbf{W}^s = \mathbb{R}^{n_\eta}$, where $T_\eta \mathbf{W}^u$ and $T_\eta \mathbf{W}^s$ denote the tangent spaces of $\mathbf{W}^u$ and $\mathbf{W}^s$, respectively, at the point η. The two manifolds are said to be transversal if they are transversal at every point $\eta \in \mathbb{R}^{n_\eta}$.

Lemma 4 *Suppose Assumptions 1-6 are all satisfied and* $\mathbf{W}^u$ *and* $\mathbf{W}^s$ *are transversal. Then, given any* $\epsilon > 0$, *there exists a* $\delta > 0$ *such that if* $\| \bar{\xi}_d \|_{\mathcal{L}_\infty(-\infty,+\infty)} < \delta$, *then*

$$\| u_d \|_{\mathcal{L}_\infty(-\infty,+\infty)} < \epsilon, \quad \textit{and} \quad \| x_d \|_{\mathcal{L}_\infty(-\infty,+\infty)} < \epsilon. \tag{4.20}$$

Proof: Consider the dynamics equation (4.16) with $\bar{\xi}_d \equiv 0$ (equivalently, the zero dynamics (2.28)):

$$\dot{\eta}_d = \alpha_\eta(0, \eta_d) - \beta\eta(0, \eta_d)\beta^{-1}(0, \eta_d)\alpha(0, \eta_d), \tag{4.21}$$

Since the stable and unstable manifolds are transversal, Assumption 3 on hyperbolicity of the zero dynamics implies that the only point at which these two manifolds intersect is the origin. Thus, the trivial solution $\eta_d = 0$ is the only solution to (4.21).

By continuous dependence of solutions on parameters, for any $\epsilon_1 > 0$, there exists a $\delta_1 > 0$ such that for all $t \geq t_0$ if $\| \bar{\xi}_d(t) \|_\infty < \delta_1$, then $\| \eta_d(t) \|_\infty < \epsilon_1$.

Since $x_d = \Phi^{-1}(\xi_d, \eta_d)$ is a local diffeomorphism and $\Phi^{-1}(0,0) = 0$, there exists a constant $\kappa_1 > 0$ such that

$$\| x_d(t) \|_\infty \leq \kappa_1 \left\| \begin{bmatrix} \xi_d(t) \\ \eta_d(t) \end{bmatrix} \right\|_\infty \leq \max\{ \kappa_1 \| \bar{\xi}_d(t) \|_\infty, \kappa_1 \| \eta_d(t) \|_\infty \}. \tag{4.22}$$

Similarly, continuity of $u_d(\bar{\xi}_d, \eta_d)$ on both $\bar{\xi}_d$ and η_d and $u_d(0,0) = 0$ (by $f(0) = 0$) imply that there exists another constant $\kappa_2 > 0$ such that

$$\| u_d(t) \|_\infty \leq \max\{ \kappa_2 \| \bar{\xi}_d(t) \|_\infty, \kappa_2 \| \eta_d(t) \|_\infty \}. \tag{4.23}$$

Now, given any $\epsilon > 0$, take

$$\epsilon_1 < \frac{\epsilon}{\max\{\kappa_1, \kappa_2\}}. \tag{4.24}$$

Then, take $\delta < \min\{\delta_1, \epsilon_1\}$, from (4.22) and (4.23) we have

$$\| u_d(t) \|_\infty < \epsilon, \text{ and, } \| x_d(t) \|_\infty < \epsilon, \ \forall t \geq t_0. \tag{4.25}$$

Arguments over interval $(-\infty, t_0]$ can be made by noticing the exponential decay to zero of both $u_d(t)$ and $x_d(t)$ as $t \to -\infty$. Taking the supremum over $(-\infty, +\infty)$ completes the proof.

□

4.2.2 Tracking by truncated control

Under Lemma 3 and the exponential convergence property of x_d, we claim that the control system (4.5)-(4.6) achieves asymptotic tracking and the so-called ϵ-tracking. The definition of ϵ-tracking is given as follows:

Definition 5 (ϵ-Tracking I) *Consider closed-loop system dynamics (4.5)-(4.6). Given any $\epsilon > 0$, there exists a $T > 0$ such that $\| y - y_d \|_{\mathcal{L}_\infty(-\infty,+\infty)} < \epsilon$.*

Theorem 6 *Suppose Assumptions 1-6 are all satisfied. Then, the closed-loop dynamics (4.5)-(4.6) achieves 1) asymptotic tracking, 2) ϵ-tracking I. Furthermore, the tracking error $\epsilon \to 0$ as $T \to \infty$.*

Proof: The asymptotic tracking follows directly from the exponential stability of error dynamics and the smoothness of $h(\,)$.

To show the ϵ-tracking, we apply the property that x_d exponentially decays as time goes to plus or minus infinity. By this property and Lemma 3, there exist constants α_1, α_2, β_1 and β_2 such that $\forall t \geq t_0 - T$,

$$\begin{aligned} \| x_e(t) \| &\leq \alpha_1 e^{-\beta_1[t-t_0+T]} \| x_e(t_0 - T) \| \\ &= \alpha_1 e^{-\beta_1[t-t_0+T]} \| x_d(t_0 - T) \| \\ &\leq \alpha_1 \| x_d(t_0 - T) \| \\ &\leq \alpha_1 \alpha_2 e^{\beta_2[t_0-T-t_0]} \| x_d(t_0) \| \\ &= \alpha_1 \alpha_2 \| x_d(t_0) \| e^{-\beta_2 T}. \end{aligned} \tag{4.26}$$

On the other hand, $\forall t \leq t_0 - T$,

$$\begin{aligned} \|x_e(t)\| &= \| x_d(t) \| \leq \alpha_2 e^{\beta_2[t-t_0]} \| x_d(t_0) \| \\ &\leq \alpha_2 e^{\beta_2[t_0-T-t_0]} \| x_d(t_0) \| = \alpha_2 \| x_d(t_0) \| e^{-\beta_2 T}. \end{aligned} \tag{4.27}$$

Thus, choosing T sufficiently large, inequalities (4.26)-(4.27) and the smoothness of $h(\,)$ guarantee that the ϵ-tracking can be achieved.

Finally, the property of the output tracking error $\epsilon \to 0$ as $T \to \infty$ can also be concluded from these two inequalities (4.26)-(4.27) and the smoothness of $h(\,)$.

□

4.2.3 Tracking under computing error

Tracking performance considering computing error is discussed in this subsection. Because solving for stable inverses involves numerical procedures, computing error always exists. Therefore, instead of the nominal control input u_d, an approximate solution $\hat{u}_d$ will actually be used to output tracking. Now, $\hat{u}_d$ is truncated and applied at $\bar{t}_0 = t_0 - T$. We claim that as long as the error between u_d and $\hat{u}_d$ is small, a nice tracking performance can still be achieved. Here we define another measurement of performance, the ϵ-tracking II.

Definition 6 (ϵ-Tracking II) *Consider closed-loop dynamics (4.5)-(4.6) with input u_d replaced by its approximattion $\hat{u}_d$. Given any $\epsilon > 0$, there exist $T > 0$ and $\delta > 0$ such that $\| \hat{u}_d - u_d \|_{\mathcal{L}_\infty(-\infty,+\infty)} < \delta$ implies $\| y - y_d \|_{\mathcal{L}_\infty(-\infty,+\infty)} < \epsilon$.*

Theorem 7 *Suppose Assumptions 1-6 are all satisfied. Then, the closed-loop dynamics (4.5)-(4.6) with input $\hat{u}_d$ achieves ϵ-Tracking II. Furthermore, the tracking error ϵ can be made arbitrarily small by decreasing $\| \hat{u}_d - u_d \|_{\mathcal{L}_\infty(-\infty,+\infty)}$.*

Proof: The proof is straight forward and it mainly follows from the conclusions of Lemma 3 and Theorem 15.

The error dynamics now becomes

$$\dot{x}_e = f(x) - f(x_d) + g(x)[\, u_d + \gamma(x) - \gamma(x_d)\,] - g(x_d)u_d + g(x)[\, \hat{u}_d - u_d\,], \qquad (4.28)$$

where $x \stackrel{\text{def}}{=} x_e + x_d$.

Consider term $g(x)[\hat{u}_d - u_d]$ as a perturbation to the nominal system (4.9). Since the nominal dynamics (4.9) is exponentially stable by Lemma 3, if $\| \hat{u}_d - u_d \|_{\mathcal{L}_\infty(-\infty,+\infty)}$ is not too large, then $x_e(t)$ is ultimately bounded by Theorem 15 (Appendix B).

It is noticed that the ultimate bound is proportional to the upper bound on the perturbation. Smoothness of $h(\,)$ implies that the output tracking error ϵ is also ultimately

bounded. Thus, the bound on ϵ can be made arbitrarily small be decreasing the bound on perturbation, equivalently, on $\| \hat{u}_d - u_d \|_{\mathcal{L}_\infty(-\infty,+\infty)}$.

□

4.3 Robustness Analysis

Consider systems with uncertainties. Assume that the so-called "matching conditions" are satisfied. Then all uncertain elements can be "lumped" and the closed-loop system dynamics can be described by

$$\dot{x} = f(x) + g(x)\gamma(x) + g(x)\nu + g(x)\Delta(x,t), \quad x(t_0 - T) = 0, \tag{4.29}$$

$$y = h(x). \tag{4.30}$$

In Section 4.2, by feedback control law (4.4) closed-loop system (4.1)-(4.2) without any uncertainties has been shown to achieve desired tracking performance. For systems with uncertainty $\Delta(x,t)$, we propose a modified control input as follows:

$$\nu = \nu_d + \nu_0. \tag{4.31}$$

Equivalently,

$$u = u_d + \gamma(x) - \gamma(x_d) + \nu_0. \tag{4.32}$$

With the modified control input, the error dynamics becomes

$$\dot{x}_e = F_e(x_e,t) + g(x_e + x_d)\nu_0 + g(x_e + x_d)\Delta(x_e + x_d, t), \tag{4.33}$$

where

$$x_e \stackrel{\text{def}}{=} x - x_d, \tag{4.34}$$

$$F_e(x_e,t) \stackrel{\text{def}}{=} f(x_e + x_d) + g(x_e + x_d)\gamma(x_e + x_d) - f(x_d) - g(x_d)\gamma(x_d) + [\, g(x_e + x_d) - g(x_d)\,]\nu_d. \tag{4.35}$$

From Lemma 3 we have that $\dot{x}_e = F(x_e, t)$ is exponentially stable for small (x_d, ν_d). Thus by the converse Lyapunov theorem (Theorem 13 in Appendix B), there exists a C^1 function $V(x_e, t)$ such that

$$c_1 \| x_e(t) \|_2^2 \leq V(x_e, t) \leq c_2 \| x_e(t) \|_2^2, \tag{4.36}$$

$$\frac{\partial V}{\partial t} + \frac{\partial V}{\partial x_e} F_e(x_e, t) \leq -c_3 \| x_e(t) \|_2^2. \tag{4.37}$$

By assuming the knowledge of both the bounding function on uncertainty $\Delta(x, t)$ and the Lyapunov function $V(x_e, t)$, we have robust output tracking control results as follows.

4.3.1 Robust asymptotic tracking

The following theorem claims that with the knowledge of the bounding function on $\Delta(x, t)$ and the Lyapunov function $V(x_e, t)$, output tracking with no steady-state error can be achieved.

Theorem 8 *Suppose Assumptions 1-6 are all satisfied and* $\| \Delta(x_e + x_d)(t) \|_2 \leq \rho(x_e, t)$. *Then, there exist* $\epsilon_0 > 0$ *and* $\beta_0 > 0$ *such that the closed-loop dynamics (4.29)-(4.30) achieved asymptotic tracking using*

$$\nu_0 = -\rho(x_e, t) \frac{\mu(x_e, t)}{\| \mu(x_e, t) \|_2 + \epsilon_0 e^{-\beta_0 t}}, \tag{4.38}$$

where

$$\mu(x_e, t) \stackrel{\text{def}}{=} g^T(x_e + x_d) \left[\frac{\partial V}{\partial x_e} \right]^T \rho(x_e, t). \tag{4.39}$$

Proof: Using $V(x_e, t)$ as the Lyapunov candidate, we have

$$\begin{aligned} \dot{V} &= \frac{\partial V}{\partial t} + \frac{\partial V}{\partial x_e} F_e(x_e, t) + \frac{\partial V}{\partial x_e} [\, g(x_e + x_d)\nu_0 + g(x_e + x_d)\Delta(x_e + x_d) \,] \\ &\leq -c_3 \| x_e(t) \|_2^2 - \frac{\partial V}{\partial x_e} g(x_e + x_d)\rho(x_e, t) \frac{\mu(x_e, t)}{\| \mu(x_e, t) \|_2 + \epsilon_0 e^{-\beta_0 t}} + \| \mu(x_e, t) \|_2 \\ &= -c_3 \| x_e(t) \|_2^2 + \frac{\| \mu(x_e, t) \|_2 \epsilon_0 e^{-\beta_0 t}}{\| \mu(x_e, t) \|_2 + \epsilon_0 e^{-\beta_0 t}}. \end{aligned} \tag{4.40}$$

Because

$$0 \leq \frac{ab}{a+b} \leq a, \qquad \forall a, b \geq 0,$$

we have

$$\dot{V} \leq -c_3 \| x_e(t) \|_2^2 + \epsilon_0 e^{-\beta_0 t}. \tag{4.41}$$

That is,

$$\begin{aligned} 0 &\leq c_1 \| x_e(t) \|_2^2 && (4.42) \\ &\leq V(x_e, t) \\ &= V(x_e(t_0 - T), t_0 - T) + \int_{t_0-T}^{t} \dot{V}(x_e, \tau)\, d\tau \\ &\leq c_2 \| x_e(t_0 - T) \|_2^2 - \int_{t_0-T}^{t} c_3 \| x_e(t) \|_2^2 \, d\tau + \frac{\epsilon_0}{\beta_0}[e^{-\beta_0[t_0-T]} - e^{-\beta_0 t}]. && (4.43) \end{aligned}$$

From this we obtain the following two inequalities:

$$c_1 \| x_e(t) \|_2^2 \leq c_2 \| x_d(t_0 - T) \|_2^2 + \frac{\epsilon_0}{\beta_0} e^{-\beta_0[t_0-T]}, \tag{4.44}$$

and

$$\lim_{t\to\infty} \int_{t_0-T}^{t} c_3 \| x_e(t) \|_2^2 \, d\tau \leq c_2 \| x_d(t_0 - T) \|_2^2 + \frac{\epsilon_0}{\beta_0} e^{-\beta_0[t_0-T]}. \tag{4.45}$$

Thus $x_e \in \mathcal{L}_2 \cap \mathcal{L}_\infty$. Since $\dot{x}_e$ is also bounded, by the Barbalat's lemma (Lemma 5 in Appendix B) we have

$$\lim_{t\to\infty} x_e(t) = 0. \tag{4.46}$$

□

4.3.2 Robust ϵ-tracking

Assuming the same knowledge on $\Delta(x, t)$ and $V(x_e, t)$, the following theorem claims that the output tracking error can still be made arbitrarily small for system dynamics with uncertainty provided that the control input is applied sufficiently early.

Theorem 9 *Suppose Assumptions 1-6 are all satisfied and* $\| \Delta(x_e + x_d)(t) \|_2 \leq \rho(x_e, t)$. *Then, given any* $\epsilon > 0$, *there exist* $T > 0$ *and* $\epsilon_0 > 0$ *such that* $\| y - y_d \|_{\mathcal{L}_\infty(-\infty,+\infty)} < \epsilon$ *can be achieved by*

$$\nu_0 = -\rho(x_e, t) \frac{\mu(x_e, t)}{\| \mu(x_e, t) \|_2 + \epsilon_0}. \tag{4.47}$$

Proof: Following the argument in the proof of the previous Theorem 8 we similarly obtain

$$\dot{V} \leq -c_3 \| x_e(t) \|_2^2 + \epsilon_0. \tag{4.48}$$

Let $0 < \theta < 1$.

$$\dot{V} \leq -c_3(1-\theta) \| x_e(t) \|_2^2 - c_3 \theta \| x_e(t) \|_2^2 + \epsilon_0. \tag{4.49}$$

Then,

$$\dot{V} \leq -c_3(1-\theta) \| x_e(t) \|_2^2, \qquad \forall \| x_e(t) \|_2 \geq \sqrt{\frac{\epsilon_0}{c_3 \theta}}. \tag{4.50}$$

By Theorem 14 (Appendix B), there exists a $t_v \geq t_0 - T$ such that $\forall t_0 - T \leq t \leq t_v$,

$$\| x_e(t) \|_2 \leq \sqrt{\frac{c_2}{c_1}} \| x_e(t_0 - T) \|_2 \exp\left\{ -\frac{[1-\theta]c_3}{2c_2} [t - [t_0 - T]] \right\}, \tag{4.51}$$

and $\forall t \geq t_v$,

$$\| x_e(t) \|_2 \leq \sqrt{\frac{\epsilon_0 c_2}{c_1 c_3 \theta}}. \tag{4.52}$$

The conclusion comes immediately following from the inequalities (4.51)-(4.52) and the smoothness of $h(\,)$.

□

CHAPTER 5 OUTPUT TRACKING CONTROL OF A FLEXIBLE-JOINT ROBOT

The most elementary task in robot control is to drive the end-effector of a robot arm to follow a given desired trajectory. Precise positioning and appropriate speed control of the end-effector along a given path are key requirements in many industrial applications such as arc welding, spray painting, pressure casting, tool machine serving, assembling, and thermal treatment processing. All of these applications demand good designs on output tracking controllers for various robotic systems.

5.1 Introduction

Design of output tracking controllers for non-minimum phase nonlinear systems is highly challenging. Among existing methods the nonlinear regulation approach leads to possibly large transient errors whereas the classical inversion approach results in unbounded internal dynamics for non-minimum phase systems. In this chapter, a new stable inversion based design approach developed in Chapter 4 is applied to output tracking control for a flexible-joint robot system. It aims at demonstrating the effectiveness of the design for non-minimum phase nonlinear systems.

The robot system studied in this chapter is a single robot link attached to a wobbly platform with a flexible joint. It is a design example from a recent book by Freeman and Kokotovic [23]. The system is also discussed in Freeman's PhD dissertation [22]. By neglecting the rotational motion of the platform, model reduction had been carried out

by the singular perturbation technique which renders a reduced-order minimum phase system. Based on this minimum phase system, an input/output linearization design leads to an asymptotic tracking controller with full-state feedback. The full-state feedback requirement can be dropped by using an observer based controller. Backstepping technique had also been used to design a partial state feedback output tracking controller. All design approaches discussed are based on an approximate model which is a minimum phase system.

The design using stable inversion is directly based on the complete model even though it is of non-minimum phase. Forward system dynamics of this robot system is developed in Section 5.2 using the Lagrange's method. In Section 5.3, following the general framework of stable inversion reviewed in Section 2.2, a stable inversion problem for this specific robot system is defined and it is followed by construction of the stable inverse solution to the problem. Section 5.4 applies the Approach II developed in Section 4.1 to design an output trajectory tracking controller that incorporates stable inverses. Simulation study demonstrates the effectiveness of this approach in achieving excellent output tracking for non-minimum phase systems.

5.2 Forward System Dynamics

5.2.1 System configuration

Consider the robot system shown in Figure 5.1. It contains a single link (L) attached with a flexible joint to the rotor (R) of a motor mounted on a platform (P). The platform is attached to a fixed base (B). It is assumed that there is no motion in the vertical direction. Thus, only the motion in the horizontal plane will be considered and modeled. There are five degrees of freedom in the system: linear displacement (x_p, y_p) and angular displacement θ_p of the platform, angular displacement θ_r of the rotor, and angular

displacement θ_l of the link. The three angles θ_p, θ_r, and θ_l are measured with respect to the X-axis as shown in Figure 5.1.

We assume that the point (x_p, y_p) is the center of mass of both the platform and the rotor. We also assume that the platform is subject to linear and angular restoring forces proportional to its deviation from an initial position, and the link is subject to an angular restoring force proportional to its deviation $(\theta_l - \theta_r)$ from alignment with the rotor. All motions are also assumed to subject to viscous friction forces proportional to their velocities respectively.

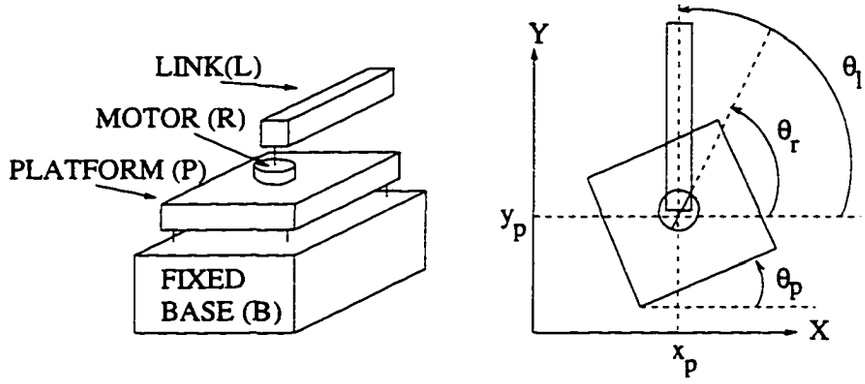

Figure 5.1 Flexible-Joint Robot with Wobbly Platform

The angle of the link relative to the platform, $\theta_l - \theta_p$, is defined as the system's output whereas u, the torque generated by the motor, is the control input. The system with parameters listed in Table 5.1 is utilized as the physical model in this study.

5.2.2 The Lagrange's method

To apply the Lagrange's method [5], the kinetic energy of the whole system containing three bodies (platform, rotor and link) is firstly found as follows:

$$KE = \frac{1}{2}M[\dot{x}_p^2 + \dot{y}_p^2] + mr_0\dot{\theta}_l[-\dot{x}_p \sin\theta_l + \dot{y}_p \cos\theta_l] + \frac{1}{2}I_l\dot{\theta}_l^2 + \frac{1}{2}I_r\dot{\theta}_r^2 + \frac{1}{2}I_p\dot{\theta}_p^2. \quad (5.1)$$

Secondly, the total potential energy stored in all springs is given by

$$PE = \frac{1}{2}k_1[x_p^2 + y_p^2] + \frac{1}{2}k_2\theta_p^2 + \frac{1}{2}k_3[\theta_l - \theta_r]^2. \quad (5.2)$$

Table 5.1 Parameters for the Robot System in SI Units

$M(5.0\,kg)$	total mass of L, R, and P
$m(0.5\,kg)$	mass of L
$r_0(0.3\,m)$	distance from L-center to (x_p, y_p)
$I_l(0.6\,kg\,m^2)$	moment of inertia of L w/ (x_p, y_p)
$I_r(0.05\,kg\,m^2)$	moment of inertia of R w/ (x_p, y_p)
$I_p(5.0\,kg\,m^2)$	moment of inertia of P w/ (x_p, y_p)
$k_1(2600\,N/m)$	linear spring const btwn P and B
$k_2(2960\,N/rad)$	angular spring const btwn P and B
$k_3(8.0\,N/rad)$	spring const btwn L and R
$b_1(14.0\,N\,s/m)$	linear friction coef btwn P and B
$b_2(15.0\,N\,s/rad)$	angular friction coef btwn P and B
$b_3(0.04\,N\,s/rad)$	friction coef btwn L and R
$b_4(0.007\,N\,s/rad)$	friction coef btwn P and R

Let

$$\psi \stackrel{\text{def}}{=} [\,x_p, y_p, \theta_l, \theta_r, \theta_p\,]^T \tag{5.3}$$

be the system's generalized coordinates. The Lagrange's equation is given by

$$\frac{d}{dt}\frac{\partial L}{\partial \dot{\psi}} - \frac{\partial L}{\partial \psi} = F_\tau, \tag{5.4}$$

where $L = KE - PE$ is the Lagrangian and F_τ is the generalized force including motor driving force and viscous friction forces. Substituting (5.1), (5.2), and (5.3) into the Lagrange's equation (5.4), the left hand side of the equation yields:

$$\frac{d}{dt}\frac{\partial L}{\partial \dot{x}_p} - \frac{\partial L}{\partial x_p} = M\ddot{x}_p - mr_0[\,\ddot{\theta}_l \sin\theta_l + \dot{\theta}_l^2 \cos\theta_l\,] + k_1 x_p, \tag{5.5}$$

$$\frac{d}{dt}\frac{\partial L}{\partial \dot{y}_p} - \frac{\partial L}{\partial y_p} = M\ddot{y}_p + mr_0[\,\ddot{\theta}_l \cos\theta_l - \dot{\theta}_l^2 \sin\theta_l\,] + k_1 y_p, \tag{5.6}$$

$$\frac{d}{dt}\frac{\partial L}{\partial \dot{\theta}_l} - \frac{\partial L}{\partial \theta_l} = I_l\ddot{\theta}_l - mr_0[\,\ddot{x}_p \sin\theta_l - \ddot{y}_p \cos\theta_l\,] \tag{5.7}$$

$$+k_3[\,\theta_l - \theta_r\,] - mr_0\dot{\theta}_l[\,\dot{x}_p \cos\theta_l + \dot{y}_p \sin\theta_l\,], \tag{5.8}$$

$$\frac{d}{dt}\frac{\partial L}{\partial \dot{\theta}_r} - \frac{\partial L}{\partial \theta_r} = I_r\ddot{\theta}_r - k_3[\,\theta_l - \theta_r\,], \tag{5.9}$$

$$\frac{d}{dt}\frac{\partial L}{\partial \dot{\theta}_p} - \frac{\partial L}{\partial \theta_p} = I_p\ddot{\theta}_p + k_2\theta_p. \tag{5.10}$$

The Lagrange's equation thus yields the following system dynamics:

$$\begin{cases} M\ddot{x}_p - mr_0[\ddot{\theta}_l \sin\theta_l + \dot{\theta}_l^2 \cos\theta_l] + b_1\dot{x}_p + k_1 x_p = 0, \\ M\ddot{y}_p + mr_0[\ddot{\theta}_l \cos\theta_l - \dot{\theta}_l^2 \sin\theta_l] + b_1\dot{y}_p + k_1 y_p = 0, \\ I_l\ddot{\theta}_l - mr_0[\ddot{x}_p \sin\theta_l - \ddot{y}_p \cos\theta_l] + b_3[\dot{\theta}_l - \dot{\theta}_r] \\ \qquad +k_3[\theta_l - \theta_r] - mr_0\dot{\theta}_l[\dot{x}_p \cos\theta_l + \dot{y}_p \sin\theta_l] = 0, \\ I_r\ddot{\theta}_r - b_3[\dot{\theta}_l - \dot{\theta}_r] - k_3[\theta_l - \theta_r] + b_4[\dot{\theta}_r - \dot{\theta}_p] = u, \\ I_p\ddot{\theta}_p + b_2\dot{\theta}_p + k_2\theta_p - b_4[\dot{\theta}_r - \dot{\theta}_p] = -u. \end{cases} \tag{5.11}$$

Dynamic equations in (5.11) can be written in a more compact form (5.12). Together with the definition of system's output, the forward dynamics of the robot system is then given by

$$M_1(\psi)\ddot{\psi} + H(\dot{\psi}, \psi) + M_2\dot{\psi} + M_3\psi = B_u u, \tag{5.12}$$

$$y = h(\psi), \tag{5.13}$$

where

$$h(\psi) \stackrel{\text{def}}{=} \theta_l - \theta_p. \tag{5.14}$$

The inertia matrix $M_1(\psi)$ is given by

$$M_1(\psi) = \begin{bmatrix} M & 0 & -mr_0 \sin\theta_l & 0 & 0 \\ 0 & M & mr_0 \cos\theta_l & 0 & 0 \\ -mr_0 \sin\theta_l & mr_0 \cos\theta_l & I_l & 0 & 0 \\ 0 & 0 & 0 & I_r & 0 \\ 0 & 0 & 0 & 0 & I_p \end{bmatrix}. \tag{5.15}$$

The centrifugal/Coriolis term $H(\dot{\psi}, \psi)$, the damping matrix M_2, the stiffness matrix M_3, and the torque distribution matrix B_u can all be directly obtained from dynamics equations in (5.11).

5.3 The Stable Inversion Problem

The forward dynamics (5.12)-(5.13) of the robot system can be written in the following state-space form:

$$\begin{cases} \dot{\psi} = \dot{\psi}, \\ \ddot{\psi} = -M_1^{-1}(\psi)[\,H(\dot{\psi},\psi) + M_2\dot{\psi} + M_3\psi\,] + M_1^{-1}(\psi)B_u u, \end{cases} \tag{5.16}$$

$$y = h(\psi). \tag{5.17}$$

Being an inertia matrix, M_1 is symmetric positive definite and thus M_1^{-1} is well-defined. It is noticed from this form that this single-input single-output nonlinear system is affine in its control input. Furthermore, the right hand sides of both dynamics and output equations are smooth on $(\psi, \dot{\psi})$. Thus, it fits into the general framework of the stable inversion problem described in Section 2.2. Following the procedure in that framework, we define the stable inversion problem for the robot system (5.16)-(5.17) as follows: *Given any smooth reference output trajectory y_d whose first-order derivative $\dot{y}_d$ having compact support on $[t_0, t_f]$, find a bounded control input u_d and a bounded state trajectory $(\psi_d, \dot{\psi}_d)$ such that $u_d \to 0$ and $(\psi_d, \dot{\psi}_d) \to 0$ as $t \to \pm\infty$ and their image by the input/output map of the control system (5.16)-(5.17) is exactly y_d.*

5.3.1 Inverse system dynamics

In order to solve the problem to find the stable inverse pair u_d and $(\psi_d, \dot{\psi}_d)$, we again follow the procedure described in the stable inversion framework. Firstly, we compute the time-derivatives of the output until the input u appears explicitly:

$$\dot{y} = \dot{\psi}_3 - \dot{\psi}_5, \tag{5.18}$$

$$\ddot{y} = \alpha(\psi, \dot{\psi}) + \frac{1}{I_p}u, \tag{5.19}$$

where the expression of $\alpha(\psi, \dot{\psi})$ can be obtained after some algebra from the forward dynamics (5.16)-(5.17). It is clear from equation (5.19) that the system has a well-defined relative degree $r = 2$.

Secondly, a coordinate transformation is made. In addition to the output and its first derivative, we also choose all the flexible modes of the system

$$\bar{\eta} \stackrel{\text{def}}{=} [\, x_p, y_p, \theta_l - \theta_r, \theta_p \,]^T, \tag{5.20}$$

together with the first derivative $\dot{\bar{\eta}}$ as the new set of coordinates. The linear independence of the selected coordinates can be easily verified. It turns out that the transformation is linear and can be written as follows:

$$\begin{bmatrix} y & \dot{y} & \bar{\eta}^T & \dot{\bar{\eta}}^T \end{bmatrix}^T = M_\phi \begin{bmatrix} \psi \\ \dot{\psi} \end{bmatrix}, \quad \bar{\eta} \in \mathbb{R}^4. \tag{5.21}$$

The transformation matrix M_ϕ is given by

$$M_\phi \stackrel{\text{def}}{=} \begin{bmatrix} M_{\phi 1} & O \\ O & M_{\phi 1} \\ M_{\phi 2} & O \\ O & M_{\phi 2} \end{bmatrix}, \tag{5.22}$$

where

$$M_{\phi 1} \stackrel{\text{def}}{=} \begin{bmatrix} 0 & 0 & 1 & 0 & -1 \end{bmatrix}, \tag{5.23}$$

and

$$M_{\phi 2} \stackrel{\text{def}}{=} \begin{bmatrix} 1 & 0 & 0 & 0 & 0 \\ 0 & 1 & 0 & 0 & 0 \\ 0 & 0 & 1 & -1 & 0 \\ 0 & 0 & 0 & 0 & 1 \end{bmatrix}. \tag{5.24}$$

Set $y \equiv y_d$. Solving for u from equation (5.19), we obtain the output equation of the inverse dynamics

$$u = I_p \left[\ddot{y}_d - \alpha(\psi, \dot{\psi}) \right], \tag{5.25}$$

The system dynamics under the new coordinates is given by

$$\begin{cases} \dot{y} = \dot{y}_d, \\ \ddot{y} = \ddot{y}_d, \\ \dot{\bar{\eta}} = \dot{\bar{\eta}}, \\ \ddot{\bar{\eta}} = \bar{p}(y_d, \dot{y}_d, \ddot{y}_d, \bar{\eta}, \dot{\bar{\eta}}). \end{cases} \tag{5.26}$$

A convenient way to find the expression for $\bar{p}(\,)$ is to derive it directly from dynamic equations (5.11). Adding the last two equations in (5.11) together and substituting θ_l by $\theta_p + y_d$ yield

$$\begin{cases} M\ddot{x}_p - mr_0[\,\ddot{\theta}_p + \ddot{y}_d\,]\sin(\theta_p + y_d) \\ \qquad +mr_0[\,\dot{\theta}_p + \dot{y}_d\,]^2\cos(\theta_p + y_d) + b_1\dot{x}_p + k_1x_p = 0, \\ M\ddot{y}_p + mr_0[\,\ddot{\theta}_p + \ddot{y}_d\,]\cos(\theta_p + y_d) \\ \qquad -mr_0[\,\dot{\theta}_p + \dot{y}_d\,]^2\sin(\theta_p + y_d) + b_1\dot{y}_p + k_1y_p = 0, \\ I_l[\,\ddot{\theta}_p + \ddot{y}_d\,] + mr_0[\,-\ddot{x}_p\sin(\theta_p + y_d) + \ddot{y}_p\cos(\theta_p + y_d)\,] \\ \qquad -mr_0[\,\dot{\theta}_p + \dot{y}_d\,][\,\dot{x}_p\cos(\theta_p + y_d) + \dot{y}_p\sin(\theta_p + y_d)\,] \\ \qquad +b_3\dot{\theta}_{lr} + k_3\theta_{lr} = 0, \\ [\,I_r + I_p\,]\,\ddot{\theta}_p - I_r\ddot{\theta}_{lr} + I_r\ddot{y}_d - b_3\dot{\theta}_{lr} + b_2\dot{\theta}_p \\ \qquad -k_3\theta_{lr} + k_2\theta_p = 0, \end{cases} \tag{5.27}$$

where

$$\theta_{lr} \stackrel{\text{def}}{=} \theta_l - \theta_r. \tag{5.28}$$

Equation (5.27) is the equivalence of the last two equations in (5.26) and it is the reference dynamics in its state-space form. In addition, by setting $y_d(t) \equiv 0$ in the reference dynamics, it becomes the well-known zero dynamics [29]:

$$\begin{cases} \dot{\bar{\eta}} = \dot{\bar{\eta}}, \\ \ddot{\bar{\eta}} = \bar{p}(0, 0, 0, \bar{\eta}, \dot{\bar{\eta}}). \end{cases} \tag{5.29}$$

5.3.2 Stable inverse solutions

Using parameters in Table 5.1, eigenvalues of the linear approximation at the origin of the zero dynamics (5.29) are calculated as shown in Table 5.2. Hyperbolicity of the equilibrium point at the origin can be easily seen since there is no eigenvalues with zero real part. It is also noticed that this system is of non-minimum phase due to the existence of two unstable eigenvalues to the linear part of the zero dynamics. By the theory of differential equations [63], locally near the origin there exist a stable manifold $\mathbf{W}^s$ of dimension six and an unstable manifold $\mathbf{W}^u$ of dimension two.

Table 5.2 Eigenvalues of Linearized Zero Dynamics

$-1.40 \pm j22.76$	$-1.41 \pm j22.82$	$6.12 \pm j29.84$	$-9.91 \pm j27.47$

Consider the following two-point boundary value problem:

$$\ddot{\bar{\eta}} = \bar{p}(y_d, \dot{y}_d, \ddot{y}_d, \bar{\eta}, \dot{\bar{\eta}}), \tag{5.30}$$

subject to

$$\begin{cases} (\bar{\eta}(t_0), \dot{\bar{\eta}}(t_0)) \in \mathbf{W}^u, \\ (\bar{\eta}(t_f), \dot{\bar{\eta}}(t_f)) \in \mathbf{W}^s. \end{cases} \tag{5.31}$$

The boundary condition (5.31) requires that at $t = t_0$ the desired internal dynamics should stay inside the unstable manifold whereas at $t = t_f$ stays inside the stable manifold.

Recall two theorems stated in Section 2.2. Theorem 2 claims that the two-point boundary value problem (5.30)-(5.31) locally has a unique solution $(\bar{\eta}_d, \dot{\bar{\eta}}_d)$ and Theorem 1 claims that the stable inverse pair can be constructed from $(\bar{\eta}_d, \dot{\bar{\eta}}_d)$ through inverse transformation (5.21) and inverse dynamics output equation (5.25):

$$\begin{bmatrix} \psi_d \\ \dot{\psi}_d \end{bmatrix} = M_\phi^{-1} \begin{bmatrix} y_d & \dot{y}_d & \bar{\eta}_d^T & \dot{\bar{\eta}}_d^T \end{bmatrix}^T, \tag{5.32}$$

and

$$u_d = I_p \left[\ddot{y}_d - \alpha(\psi_d, \dot{\psi}_d) \right]. \tag{5.33}$$

5.4 Output Tracking Control

In this section we first compute the stable inverse pair by solving the two-point boundary value problem (5.30)-(5.31) and utilizing equations (5.32)-(5.33). Then, a tracking controller is designed by using the stable inverse solution to drive the link to track a prescribed reference trajectory.

5.4.1 An approximate stable inverse

Let the desired output trajectory be defined as follows with $t_0 = 1$ second and $t_f = 2$ second:

$$y_d = \begin{cases} 0, & t \leq t_0, \\ 2[t - t_0] - \pi^{-1} \sin(2\pi[t - t_0]), & t_0 < t \leq t_f, \\ 2, & t > t_f. \end{cases} \tag{5.34}$$

To find the stable inverse pair u_d and $(\psi_d, \dot{\psi}_d)$, two numerical algorithms could be used. One is aimed at solving the two-point boundary value problem by decoupling stable/unstable manifolds. See Appendix A for details. Another is by solving an optimal control problem minimizing control input energy that is developed in Section 3.2. Instead of carrying out those algorithms, we choose in this example to solve the two-point boundary value problem (5.30)-(5.31) simply by "decoupling" the stable/unstable manifolds via a linear coordinate transformation. Thus, only an approximate stable inverse solution is computed. Details are as follows.

Rewrite the differential equation (5.30) in the two-point boundary value problem in the following state-space form:

$$\begin{bmatrix} \dot{\bar{\eta}} \\ \ddot{\bar{\eta}} \end{bmatrix} = A_\eta \begin{bmatrix} \bar{\eta} \\ \dot{\bar{\eta}} \end{bmatrix} + R(y_d, \dot{y}_d, \ddot{y}_d, \bar{\eta}, \dot{\bar{\eta}}), \tag{5.35}$$

where

$$R(0,0,0,\bar{\eta},\dot{\bar{\eta}}) = \mathcal{O}(|\,(\bar{\eta},\dot{\bar{\eta}})\,|^2), \tag{5.36}$$

and A_η is the first approximation of the zero dynamics (set $y_d \equiv 0$ in (5.30)) at the origin. From elementary linear algebra, there exists a linear transformation

$$\begin{bmatrix} \bar{\eta} \\ \dot{\bar{\eta}} \end{bmatrix} = M_T \begin{bmatrix} z_1 \\ z_2 \end{bmatrix} \tag{5.37}$$

which transforms equation (5.35) into

$$\begin{cases} \dot{z}_1 = A_{z1} z_1 + R_{z1}(y_d, \dot{y}_d, \ddot{y}_d, z_1, z_2), \\ \dot{z}_2 = A_{z2} z_2 + R_{z2}(y_d, \dot{y}_d, \ddot{y}_d, z_1, z_2), \end{cases} \tag{5.38}$$

where both A_{z1} and $-A_{z2}$ are Hurwitz. Recall that the boundary condition (5.31) requires that at t_0 the $(\bar{\eta},\dot{\bar{\eta}})$ stays in the unstable manifold whereas at t_f stays in the stable manifold. We approximate the boundary condition simply by

$$\begin{cases} z_1(t_0) = 0, \\ z_2(t_f) = 0, \end{cases} \tag{5.39}$$

because, roughly speaking, z_1 and z_2 pick up the stable and unstable parts of the zero dynamics respectively. The approximate stable inverse pair is then obtained through the following iterative steps:

- step 1: Set $z_1^0(t) = 0$ for all t.
- step 2: Integrate the unstable part of equation (5.38) from $t = t_f$ to $t = 0$ backward in time with final value $z_2(t_f) = 0$ to obtain z_2.
- step 3: Integrate the stable part of equation (5.38) from $t = t_0$ to $t = 3$ second forward in time with initial value $z_1(t_0) = 0$ to obtain z_1.
- step 4: If $\|z_1 - z_1^0\|$ is greater than a given threshold, set $z_1^0 = z_1$ and go to step 2, otherwise continue to step 5.

- step 5: Use transformation (5.37) to find an approximate solution $(\bar{\eta}_d, \dot{\bar{\eta}}_d)$.

- step 6: Construct $(\psi_d, \dot{\psi}_d)$ via equation (5.32) and u_d through (5.33).

5.4.2 Tracking control designs

Using only $\theta_r - \theta_p$ and $\dot{\theta}_r - \dot{\theta}_p$, the measurements of rotor position and rotor velocity relative to the platform, controller incorporating stable inversion by the Approach II is simply designed as follows: use u_d as a feed-forward signal that is superimposed by a PD stabilizing feedback:

$$\gamma(\psi) = -a_p[\,\theta_r - \theta_p\,] - a_d[\,\dot{\theta}_r - \dot{\theta}_p\,]. \tag{5.40}$$

The input/output map from u to $\theta_r - \theta_p$ can be verified to be of minimum phase. The closed-loop stability is thus guaranteed [10]. The overall control law is given by

$$u = u_d - a_p[\,(\theta_r - \theta_p) - (\theta_r - \theta_p)_d\,] - a_d[\,(\dot{\theta}_r - \dot{\theta}_p) - (\dot{\theta}_r - \dot{\theta}_p)_d\,], \tag{5.41}$$

where a_p and a_d are two design parameters. It is noticed that the measurements of $(\theta_r - \theta_p)_d$ and $(\dot{\theta}_r - \dot{\theta}_p)_d$ can be easily implemented by installing an encoder on the motor.

Forward simulation starts from $t = 0.5$ second with a rest initial condition. Simulation results using $a_p = 30300$ and $a_d = 1616$ are shown in Figure 5.2. It is seen from the upper part of the figure that the excellent tracking performance by this controller: there is neither transient error nor steady-state error in tracking. The lower part of the figure shows the bounded computed stable inverse u_d. It is seen that even though the output trajectory starts moving at $t = t_0 = 1$ second and stops at $t = t_f = 2$ second, the control needs to be applied to pre-shape the system some time before t_0 and it is also in effect after t_f for a period of time. This is due to the non-minimum phase property

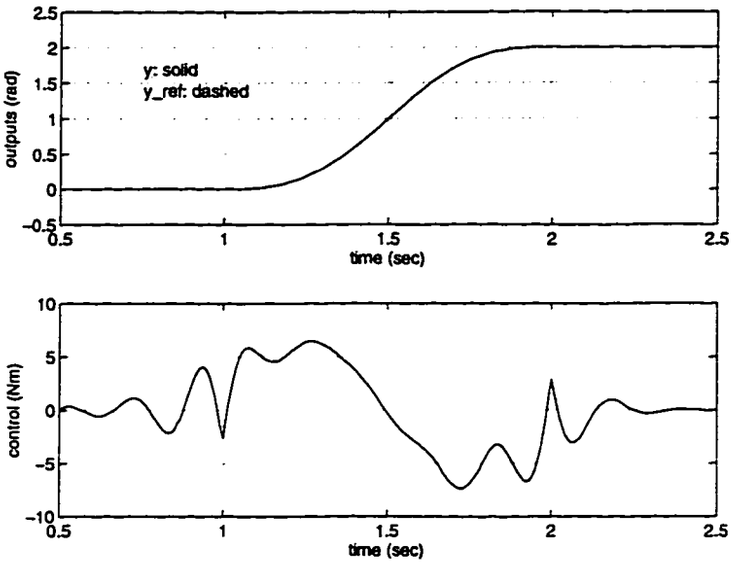

Figure 5.2 Tracking Performance and Nominal Control

of the system.

It is interesting to notice that in this robot system the angular motion, $(\theta_p, \dot{\theta}_p)$, of the platform is rather small. By neglecting this motion the system may be approximated by a minimum phase model with its order reduced by two. See [22] for a detailed description of the model reduction and a corresponding input/output linearization control design. Simulation results by this input/output linearization approach are shown in Figure 5.3. It is noticed that this input/output linearization tracking design based on the reduced-order minimum phase model also achieves output tracking with a satisfactorily small tracking error. However, it is also noticed that this method, unlike the stable inversion approach, requires a full-state measurement for feedback.

5.5 Conclusions

Stable inversion, an approach to the design of output tracking control for nonlinear non-minimum phase systems, is successfully applied to output tracking of a single-link flexible-joint robot system. The key assumptions, a well-defined relative degree and hy-

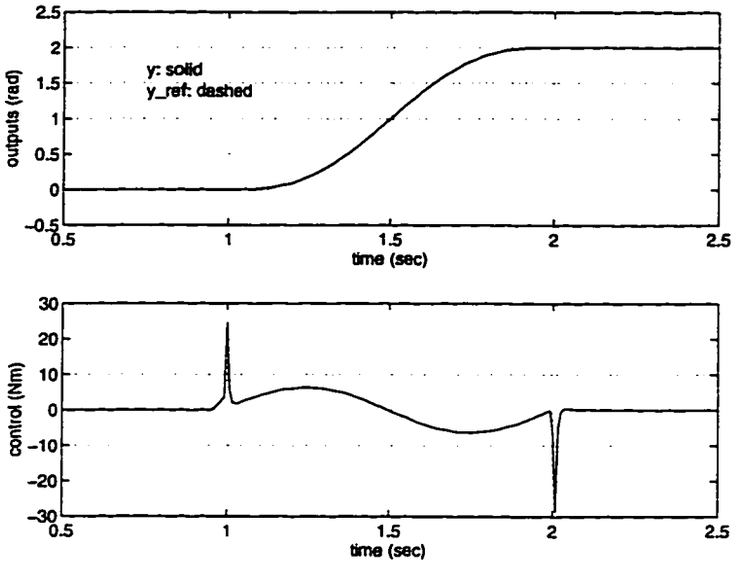

Figure 5.3 Tracking by Input/Output Linearization

perbolicity of the fixed point of the zero dynamics, in applying stable inversion based controller design are both satisfied by this system. Simulation results demonstrate that this stable inversion based approach is very effective for obtaining accurate output tracking with only partial state measurements for this non-minimum phase system.

It is interesting to notice that both the stable inversion based design and the input/output linearization based design achieve remarkably accurate output tracking. This is due to the small rotational motion of the platform. It is this motion that contributes to the non-minimum phase property. Thus, the robot system has a "weak" non-minimum phase property. The weakness means that the unstable zeros are located farther away form the imaginary axis than other system zeros. This can be seen from Table 5.2 where two zeros with position real part are introduced by platform's rotational motion. In such case, neglecting motion that renders non-minimum phase property could possibly result in a satisfactory control design.

CHAPTER 6 TIP TRAJECTORY TRACKING OF A TWO-LINK FLEXIBLE MANIPULATOR

Stable inversion provides a promising design method for output tracking control. In this chapter, the stable inversion based design is applied to tip trajectory tracking for a two-link flexible manipulator. While last chapter considers flexible-joint robot, the robot studied in this chapter undergoes link deformation due to its flexibility. The controller takes the structure of the Approach II proposed in Chapter 4.

6.1 Introduction

Stable inversion based output tracking of a multi-link flexible manipulator is a model based control which requires a detailed, carefully predetermined dynamic model of an actual system. Equations of motion of a flexible manipulator are mixed partial and ordinary differential equations which contain terms in the integral form [59]. With few exceptions, closed form solutions of partial differential equations are not practical. Therefore, motion prediction usually relies on approximations made by a set of admissible space functions. These shape functions may be obtained analytically by using the mode shapes of a fixed-free cantilever beam [8]. When obtained numerically, the shape functions can be found by the finite element technique. For example, a method that utilizes the eigenvectors obtained from the finite element analysis as approximation functions was developed by Sunada and Dubowsky [60]. The assumed modes method, which will be used in this study, is another way to obtain the shape functions numeri-

cally. The approach by the assumed modes technique has been used extensively in the research of the flexible manipulators [37].

The study on control of flexible robot manipulators was pioneered by Cannon and Schmitz [8] in 1980s where a linear-quadratic optimal control approach was successfully applied to the end-effector tracking control of a one-link flexible robot arm in which the non-minimum phase effect was first demonstrated. After that, many researchers have considered different approaches to the control of one-link flexible arms which are linear systems for small deflection. Among those, Siciliano and Book [52] used a singular perturbation approach to deal with the flexible modes. Bayo [2] applied Fourier transform to obtain stable but non-causal control input. As for the nonlinear control of multi-link flexible manipulators, Lucibello and Siciliano [15] applied the nonlinear regulation theory and asymptotic tracking of periodic output trajectories was achieved. Simulation results demonstrated asymptotic tracking of a finite trajectory with transient errors existing at both the beginning and the end of maneuver.

This transient behavior can be precisely controlled by applying the classical inversion method that uses stabilizing feedback together with feed-forward signals generated by an inverse system. Conditions for the invertibility of linear systems were developed by Brockett [6], Silverman [53], and Sain [51] while for nonlinear systems were established by Hirschorn [26] and Singh [54]. All these inversion algorithms produce causal inverses for a given desired output and a fixed initial condition, but unbounded control and state trajectories will be produced for non-minimum phase systems. This fundamental difficulty has been noticed for a long time.

The new tracking control design incorporating stable inverses avoids difficulties in both nonlinear regulation and classical inversion while preserves the advantages of both. Section 6.2 develops a mathematical model for a two-link flexible manipulator using the assumed modes technique with tip position as output. From that, in Section 6.3 an inverse model is derived and the two-point boundary value condition corresponding

to stable inversion is set up. In Section 6.4, conditions for applying stable inversion are verified, and the effectiveness of stable inversion to output tracking for such non-minimum phase systems is demonstrated by comparing favorably against a carefully fine-tuned computed torque method.

6.2 Equations of Motion of Flexible Manipulators

For rigid-body mechanical systems, the dynamic modeling is well understood and easily handled by the Lagrange's principle [49]. So is the case for single-link flexible robot arms [36]. However, the dynamics of multi-link articulated flexible structures is significantly more complicated. Some researchers have used finite element method to numerically construct the dynamic equations [3]. Others have used the assumed modes approach [5, 14]. The modeling approach for multi-link flexible manipulators provided in this section is compact and self-contained. It follows the Lagrange's principle using the assumed modes technique. We believe that our treatment is especially easy to follow for those without any mechanical engineering background.

6.2.1 The assumed modes approach

A robot is often considered as an assembly of several rigid links. However, the assumption may lead to unsatisfactory performance if the links of the robot undergo elastic deformation. In such cases, a basic link is generally modeled as composed of a flexible beam with a rigid hub at the base end and a point mass at the opposite end. For multi-link robot arms, the links are connected with joints at their ends. The joints of the arm are considered to be revolute and input torque is applied at these joints. Each flexible beam is assumed to satisfy the Euler-Bernoulli beam assumption. The deformation in the axial direction and the thickness of the beam itself are both

neglected. We also assume that the links are maneuvered in the horizontal plane and the out-of-plane deflection is negligible.

Notations for physical properties of each link are as follows. Suppose that each link i has total length l_i, mass per unit length ρ_i, product of area moment inertia of the cross section about the neutral axis and Young's modulus e_i. The end tip mass of link i is denoted as m_{e_i} and the mass moment of inertia of this portion of the link is assumed to be negligible. For the other end, i_{b_i} stands for the inertia of the rigid hub.

To introduce the Lagrange's method using the assumed modes technique, let us first consider a basic flexible link that is shown in Figure 6.1.

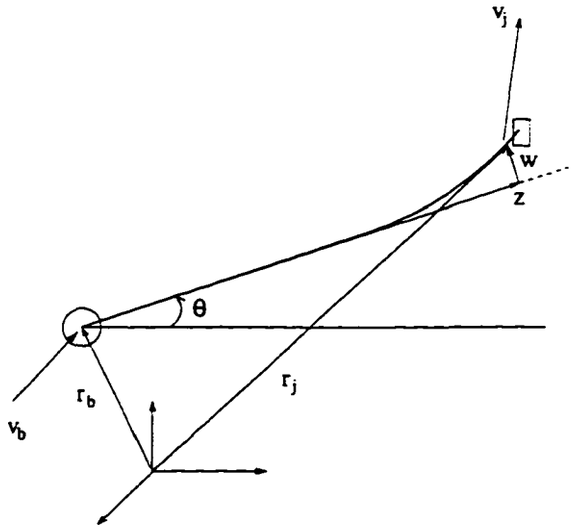

Figure 6.1 Model of A Basic Flexible Link

Let $\vec{e}_z$ be the unit vector in the tangent direction of the link and $\vec{e}_w$ be the unit vector perpendicular to $\vec{e}_z$. Then, the position of any point along the beam can be written as follows with $\vec{r}_b$ and $\vec{v}_b$ being the position and velocity of the hub relative to the ground reference frame,

$$\vec{r}_j = \vec{r}_b + \vec{z} + \vec{w} = \vec{r}_b + z\vec{e}_z + w(z,t)\vec{e}_w, \tag{6.1}$$

where z measures the distance between the point and the hub in $\vec{e}_z$ direction and $w(z,t)$ is the deflection along $\vec{e}_w$ of the elastic beam measured from its undeformed configuration.

Differentiating (6.1) with respect to time, the velocity of any point along the beam is of the following form

$$\vec{v}_j = \vec{v}_b + \dot{\vec{\theta}} \times \vec{z} + \dot{\vec{w}}, \tag{6.2}$$

where $\dot{\vec{\theta}}$ is the angular velocity of the rigid hub measured with respect to the inertial frame and the symbol "$\times$" represents vector cross product.

Using this expression (6.2), we can write the kinetic energy of a flexible link of length l as follows:

$$KE = \frac{1}{2} i_b \dot{\theta}^2 + \frac{1}{2} \int_0^l \rho^* \vec{v}_j \cdot \vec{v}_j \, dz, \tag{6.3}$$

where "$\cdot$" stands for inner product, $\rho^* \stackrel{\text{def}}{=} \rho(z) + m_e \delta(z - l)$, and $\delta(\,)$ is the Dirac delta function. Assume the potential energy contains only the elastic energy part while the gravitational potential energy is neglected. The potential energy of the flexible link can then be computed by

$$PE = \frac{1}{2} \int_0^l e[w''(z,t)]^2 \, dz, \tag{6.4}$$

where $(\cdot)''$ denotes the second derivative of $(\cdot)$ with respect to its spatial variable. The Lagrangian of the flexible link is the difference between the kinetic energy KE and the potential energy PE:

$$L = KE - PE. \tag{6.5}$$

When a multi-link flexible arm is considered, the Lagrangian of the whole system is obtained by summing up the Lagrangian of all the individual links of the flexible arm. Now, by the Lagrange's method, the equations of motion can be expressed as

$$\frac{d}{dt} \frac{\partial L}{\partial \dot{\psi}} - \frac{\partial L}{\partial \psi} = F_\tau, \tag{6.6}$$

where ψ is a set of generalized coordinates for the system, and F_τ is the generalized force acting on the generalized coordinates.

Equation (6.6) is a set of partial differential/integral equations. To simplify, assumed modes [38] can be invoked to approximate the links deformation. In the approximation,

a set of admissible functions are chosen so that they are linearly independent and satisfy all the geometric boundary conditions of the system. They must also be as many times differentiable as the number of the boundary conditions. Accuracy of the approximation can be improved as the number of admissible functions chosen to approximate the deformation increases.

Let $\sigma_{ij}(z_i)$ be the jth admissible function of the ith link and $q_{ij}(t)$ the corresponding generalized coordinates. Then the distributed deflection of the ith link, $w_i(z_i,t)$, is approximated by

$$w_i(z_i,t) = \sum_{j=1}^{n_j} \sigma_{ij}(z_i) q_{ij}(t) \stackrel{\text{def}}{=} \sigma_i^T q_i. \tag{6.7}$$

In this study, two flexible modes are assigned to each link: $n_j = 2$. The admissible functions are chosen to be the ones for the clamped-free beam [37]. One simple choice of the admissible functions that meet the above mentioned requirements are those of the form:

$$\sigma_{ij}(z_i) = \left[\frac{z_i}{l_i}\right]^{j+1}, \qquad \forall j = 1,\ldots,n_j. \tag{6.8}$$

The geometric boundary conditions are all satisfied since the polynomials in (6.8) always have $\sigma_{ij}(0) = \sigma'_{ij}(0) = 0$.

6.2.2 Manipulators with two flexible links

The two-link flexible manipulator shown in Figure 6.2 is modeled as follows. The rotation angle θ_1 of link one is the angle between the tangent direction of the link and the horizontal axis of the ground reference frame. The angle θ_2 is the joint rotation of the rigid base on the second link measuring the tangent direction of this link from the tangent line at the end-tip of the first link.

Let $\vec{r}_1$ and $\vec{r}_2$ be the position vectors of a point on link one and link two respectively. Then,

$$\vec{r}_1 = z_1\vec{e}_{z_1} + w_1\vec{e}_{w_1}, \tag{6.9}$$

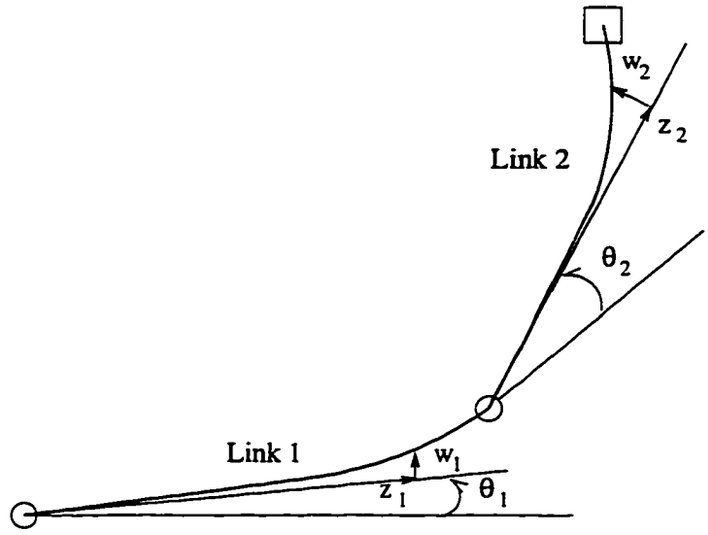

Figure 6.2 Two-Link Flexible Manipulator

$$\vec{r}_2 = l_1\vec{e}_{z_1} + w_1(l_1)\vec{e}_{w_1} + z_2\vec{e}_{z_2} + w_2\vec{e}_{w_2}, \tag{6.10}$$

where l_1 is the length of the first link. The velocity vectors can be obtained by

$$\vec{v}_1 = [\, z_1\dot{\theta}_1 + \dot{w}_1 \,]\vec{e}_{w_1}, \tag{6.11}$$

$$\vec{v}_2 = [\, l_1\dot{\theta}_1 + \dot{w}_1(l_1) \,]\vec{e}_{w_1} + [\, z_2[\, \dot{\theta}_1 + \dot{\theta}_2 + \dot{w}_1'(l_1) \,] + \dot{w}_2 \,]\vec{e}_{w_2}. \tag{6.12}$$

Note that different symbols have been used to separate the derivatives with respect to time t and those with respect to spatial variable z_1. The squares of the magnitude of the velocities are then found as follows:

$$\vec{v}_1 \cdot \vec{v}_1 = [\, z_1\dot{\theta}_1 + \dot{w}_1 \,]^2, \tag{6.13}$$

$$\begin{aligned}\vec{v}_2 \cdot \vec{v}_2 = {} & [\, l_1\dot{\theta}_1 + \dot{w}_1(l_1) \,]^2 + [\, z_2[\, \dot{\theta}_1 + \dot{\theta}_2 + \dot{w}_1'(l_1) \,] + \dot{w}_2 \,]^2 \\ & + 2[\, z_2[\dot{\theta}_1 + \dot{\theta}_2 + \dot{w}_1'(l_1)] + \dot{w}_2 \,][l_1\dot{\theta}_1 + \dot{w}_1(l_1)]\cos(\theta_2 + w_1'(l_1)).\end{aligned} \tag{6.14}$$

Thus, the potential and the kinetic energy of link one and link two are given by

$$PE_1 = \frac{1}{2}\int_0^{l_1} e_1[w_1'']^2\, dz_1 = \frac{1}{2}q_1^T\left[\int_0^{l_1} e_1[\sigma_1''][\sigma_1'']^T\, dz_1\right] q_1, \tag{6.15}$$

$$PE_2 = \frac{1}{2}\int_0^{l_2} e_2[w_2'']^2\, dz_2 = \frac{1}{2}q_2^T\left[\int_0^{l_2} e_2[\sigma_2''][\sigma_2'']^T\, dz_2\right] q_2, \tag{6.16}$$

$$KE_1 = \frac{1}{2} i_{b_1} \dot{\theta}_1^2 + \frac{1}{2} \int_0^{l_1} \rho_1^* \vec{v}_1 \cdot \vec{v}_1 \, dz_1. \tag{6.17}$$

$$KE_2 = \frac{1}{2} i_{b_2} [\dot{\theta}_1 + \dot{\theta}_2 + \dot{w}_1'(l_1)]^2 + \frac{1}{2} \int_0^{l_1} \rho_2^* \vec{v}_2 \cdot \vec{v}_2 \, dz_2, \tag{6.18}$$

Clearly, both PE_1 and PE_2 are quadratic functions of q_1 and q_2 respectively. Noticing that $\dot{w}_i = \sigma_i^T \dot{q}_i$ and $\dot{w}_1' = [\sigma_i']^T \dot{q}_1$, we see that both $\acute{K}E_1$ and $\acute{K}E_2$ are quadratic functions of $\dot{\theta}_1$, $\dot{\theta}_2$, $\dot{q}_1$ and $\dot{q}_2$.

Denote the system's generalized coordinate

$$\psi \stackrel{\text{def}}{=} [\theta^T, q^T]^T \stackrel{\text{def}}{=} [\theta_1, \theta_2, q_{11}, q_{12}, q_{21}, q_{22}]^T. \tag{6.19}$$

The potential and the kinetic energy of the system can then be written as

$$PE = PE_1 + PE_2 = \frac{1}{2} \psi^T \acute{K} \psi. \tag{6.20}$$

$$\acute{K}E = \acute{K}E_1 + \acute{K}E_2 = \frac{1}{2} \dot{\psi}^T M(\psi) \dot{\psi}, \tag{6.21}$$

where $M(\psi)$ is the system inertia matrix. $\acute{K}$ is the stiffness matrix of the form

$$\acute{K} \stackrel{\text{def}}{=} \begin{bmatrix} O_{2\times 2} & O_{2\times 4} \\ O_{4\times 2} & M_3 \end{bmatrix}, \tag{6.22}$$

$$M_3 \stackrel{\text{def}}{=} \begin{bmatrix} \acute{K}^1_{2\times 2} & O_{2\times 2} \\ O_{2\times 2} & \acute{K}^2_{2\times 2} \end{bmatrix}, \tag{6.23}$$

where $\acute{K}^1$ and $\acute{K}^2$ are the kernels in equations (6.15) and (6.16) respectively. Substituting (6.20)-(6.21) into (6.6) we obtain

$$M(\psi)\ddot{\psi} + \dot{M}(\psi)\dot{\psi} - \frac{1}{2} \frac{\partial(\dot{\psi}^T M(\psi)\dot{\psi})}{\partial \psi} + \acute{K}\psi = B_u u - F_d, \tag{6.24}$$

where $u = [u_1, u_2]^T$ is the vector joint torque, $B_u = [I_{2\times 2}, O_{2\times 4}]^T$ the torque distribution matrix, and F_d is the Rayleigh dissipation force due to structural damping of the flexible links and is assumed to have the form

$$F_d = C\dot{\psi}, \tag{6.25}$$

where C is taken to be proportional to the stiffness matrix K by a damping ratio α_d:

$$C = \begin{bmatrix} O_{2\times 2} & O_{2\times 4} \\ O_{4\times 2} & M_2 \end{bmatrix}, \tag{6.26}$$

where

$$M_2 = \alpha_d M_3. \tag{6.27}$$

Defining the term which involves centrifugal and Coriolis forces

$$H(\psi, \dot{\psi}) \stackrel{\text{def}}{=} \dot{M}(\psi)\dot{\psi} - \frac{1}{2}\frac{\partial(\dot{\psi}^T M(\psi)\dot{\psi})}{\partial \psi}, \tag{6.28}$$

we obtain the system dynamics from equation (6.24)

$$M(\psi)\ddot{\psi} + H(\psi, \dot{\psi}) + C\dot{\psi} + K\psi = B_u u. \tag{6.29}$$

There are many ways to choose the system output. Depending on which points along the links are selected as output, the whole system can be either minimum phase or non-minimum phase. If the output is selected to be the joint angles. i.e. the sensors and actuators are collocated, the system is known to be minimum phase. A more meaningful choice of output is the tip position and this choice renders the system non-minimum phase. In this study, we choose

$$y = [y_1, y_2]^T = [\theta_1, \theta_2]^T + \left[\arctan\left(\frac{w_1(l_1, t)}{l_1}\right), \arctan\left(\frac{w_2(l_2, t)}{l_2}\right) \right]^T. \tag{6.30}$$

When elastic deformation of the first link is small, the output y is approximately the tip angular positions of the links. It can be seen that both output components chosen are practically measurable. For small elastic deformation,

$$\arctan\left(\frac{w_i(l_i, t)}{l_i}\right) \approx \frac{w_i(l_i, t)}{l_i}. \tag{6.31}$$

By substituting equation (6.7) into equation (6.30), we obtain the simplified output equation

$$y = D\psi, \tag{6.32}$$

where $D = [D_1 \;\; D_2]$ with $D_1 = I_{2\times 2}$, and

$$D_2 = \begin{bmatrix} l_1^{-1}\sigma_{11}(l_1) & l_1^{-1}\sigma_{12}(l_1) & 0 & 0 \\ 0 & 0 & l_2^{-1}\sigma_{21}(l_2) & l_2^{-1}\sigma_{22}(l_2) \end{bmatrix}. \tag{6.33}$$

System dynamics equation (6.29) together with its output equation (6.32) constitutes the forward system dynamics of the two-link flexible manipulator system.

6.3 Stable Inversion of Flexible Manipulators

To design stable inversion based output tracking control, inverse dynamics needs to be constructed. Based on the inverse dynamics a stable inverse is found for any given output trajectory. The boundedness and the convergence of the stable inverse are guaranteed by setting up a two-point boundary value problem which is then solved in this study by following the iterative procedure described in Appendix A.

6.3.1 Inverse dynamics

Inverse dynamics usually consists of reference dynamics (2.25) and an (inverse) output equation (2.24). For a flexible manipulator system, the inverse dynamics can be simply derived as follows.

Partition and rewrite the forward dynamics (6.29) and (6.32) as follows:

$$M_{11}(\psi)\ddot{\theta} + M_{12}(\psi)\ddot{q} + H_1(\psi, \dot{\psi}) = u, \tag{6.34}$$

$$M_{21}(\psi)\ddot{\theta} + M_{22}(\psi)\ddot{q} + H_2(\psi, \dot{\psi}) + M_2\dot{q} + M_3 q = 0, \tag{6.35}$$

$$y = \theta + D_2 q, \tag{6.36}$$

where D_2 is defined in (6.33) and M_2 and M_3 are defined in (6.27) and (6.23) respectively. From (6.36), we have

$$\theta = y - D_2 q. \tag{6.37}$$

Let $y_d(t)$ be the reference output trajectory. Set $y \equiv y_d$. Substituting (6.37) into equation (6.35), we obtain a dynamic equation governing the flexible coordinates q:

$$M_1(y_d, q)\ddot{q} + M_2\dot{q} + M_3 q + H_2(y_d, \dot{y}_d, q, \dot{q}) = M_4(y_d, q)\ddot{y}_d, \tag{6.38}$$

where

$$M_1(y_d, q) = M_{22}(y_d, q) - M_{21}(y_d, q)D_2, \tag{6.39}$$

$$M_4(y_d, q) = -M_{21}(y_d, q). \tag{6.40}$$

Equation (6.38) is the reference dynamics equation (2.25) in second order form.

The equivalence of the general inverse output equation (2.24) for the flexible manipulator can be easily obtained from equation (6.34) with a substitution of (6.37) and $y \equiv y_d$:

$$u = [\, M_{12}(y_d, q) - M_{11}(y_d, q)D_2 \,]\,\ddot{q} + [\, M_{11}(y_d, q)\ddot{y}_d + H_1(y_d, \dot{y}_d, q, \dot{q}) \,]\,. \tag{6.41}$$

Equations (6.38)-(6.41) characterize the inverse dynamics of the two-link flexible manipulator system.

6.3.2 Linear two-point boundary value problems

To ensure a stable solution from the inverse dynamics, a two-point boundary condition (2.30) needs to be imposed on the flexible mode q. However, instead of (2.30), we directly derive the linear two-point boundary value problem (A.1)-(A.2) for our flexible manipulators, based on which the iterative procedure described in Appendix A can be carried out to find stable inverses.

Firstly, we need to find the linearized equation for the reference dynamics (6.38). A notation for convenience is in order. Let $\mathcal{M}(x)$ be a $k \times l$ matrix function of $x \in \mathbb{R}^n$ and $\bar{x} \in \mathbb{R}^n$ be a column vector. The derivative of $\mathcal{M}$ at a point x_0 in the direction of $\bar{x}$ is defined as

$$D_x^{x_0}\mathcal{M}\bar{x} \stackrel{\text{def}}{=} \sum_{i=1}^{n} \frac{\partial \mathcal{M}}{\partial x_i}\bigg|_{x=x_0} \bar{x}_i. \tag{6.42}$$

Using this notation and neglecting higher order terms, the first term $M_1\ddot{q}$ in the reference dynamics equation (6.38) can be linearized as

$$\begin{aligned} M_1\ddot{q} &\approx \left[M_1^0 + D_q^0 M_1 [\, q - q_0 \,] \right] [\, \ddot{q}_0 + [\, \ddot{q} - \ddot{q}_0 \,]] \\ &\approx M_1^0\ddot{q} + [\, D_q^0 M_1 q \,]\ddot{q}_0 - [\, D_q^0 M_1 q_0 \,]\ddot{q}_0, \end{aligned} \tag{6.43}$$

where the superscript 0 stands for evaluation along q_0 and/or $\dot{q}_0$ (solutions of the previous iteration) no matter whichever is applicable. Since it can be easily verified that

$$[\, D_x M\tilde{x} \,]\,\tilde{x} = [\, D_x M\tilde{x} \,]\,\tilde{x}, \tag{6.44}$$

where $\tilde{x} \in \mathbb{R}^n$, we obtain

$$M_1\ddot{q} = M_1^0\ddot{q} + \left[D_q^0 M_1\ddot{q}_0 \right] q - \left[D_q^0 M_1\ddot{q}_0 \right] q_0. \tag{6.45}$$

Both M_2 and M_3 are constant matrices. For the term $H_2(y_d, \dot{y}_d, q, \dot{q})$, we have

$$\begin{aligned} H_2 &\approx H_2^0 + D_q^0 H_2 [\, q - q_0 \,] + D_{\dot{q}}^0 H_2 [\, \dot{q} - \dot{q}_0 \,] \\ &= H_2^0 - D_q^0 H_2 q_0 - D_{\dot{q}}^0 H_2 \dot{q}_0 + D_q^0 H_2 q + D_{\dot{q}}^0 H_2 \dot{q}. \end{aligned} \tag{6.46}$$

Similar to the derivation for the first term $M_1\ddot{q}$, we can get the linearized form of $M_4\ddot{y}_d$ as

$$M_4\ddot{y}_d \approx M_4^0\ddot{y}_d - \left[D_q^0 M_4\ddot{y}_d \right] q_0 + \left[D_q^0 M_4\ddot{y}_d \right] q. \tag{6.47}$$

Thus, combining the equations (6.45) through (6.47), the linearized inverse dynamics can be expressed as

$$L_1\ddot{q} + L_2\dot{q} + L_3 q = L_4, \tag{6.48}$$

where

$$L_1 = M_1^0; \tag{6.49}$$

$$L_2 = M_2 + D_{\dot{q}}^0 H_2; \tag{6.50}$$

$$L_3 = D_q^0 M_1\ddot{q}_0 + M_3 + D_q^0 H_2 - D_q^0 M_4\ddot{y}_d; \tag{6.51}$$

$$L_4 = M_4^0\ddot{y}_d - \left[D_q^0 M_4\ddot{y}_d \right] q_0 + \left[D_q^0 M_1\ddot{q}_0 \right] q_0 + D_q^0 H_2 q_0 + D_{\dot{q}}^0 H_2\dot{q}_0 - H_2^0. \tag{6.52}$$

Let $\eta = [q^T, \dot{q}^T]^T$, and

$$A(t) = \begin{bmatrix} 0 & I \\ -L_1^{-1}L_3 & -L_1^{-1}L_2 \end{bmatrix}, \quad \text{and} \quad B(t) = \begin{bmatrix} 0 \\ L_1^{-1}L_4 \end{bmatrix}. \tag{6.53}$$

Then, equation (6.48) is an equation (A.1) in second order form.

Secondly, the linear boundary conditions (A.6)-(A.9) are derived. Instead of updating the transformation matrices C_s and C_u at each iteration, in this study we compute one C_s and one C_u for all iterations by evaluating matrix $A(t)$ in (6.53) at $q_0 = 0$ and $y_d = [0°, 90°]^T$. It is found later in simulation by computing the eigenvalues of $A(t_0)$ and $A(t_f)$ that at both t_0 and t_f the zero dynamics has five stable eigenvalues and three unstable ones. Thus, following the procedure in Appendix A, the transformation matrices C_s and C_u would be of dimension five by eight and three by eight respectively.

6.4 Tip Trajectory Tracking Control

In this simulation study, we demonstrate the effectiveness of our tracking control design using stable inversion. First of all, a simulation setup is presented. Then, conditions are verified to ensure the applicability of stable inversion. This is followed by two tracking controllers design using stable inversion and the well-known computed torque method respectively. Some simulation results are presented.

6.4.1 Simulation setup

Table 6.1 lists key parameters of the two-link flexible arm model used in this study. The two links of the manipulator are also assumed to have the same structural damping $\alpha_d = 0.01$.

In addition to satisfy Assumption 2, the reference output trajectory is selected following considerations given by Bayo and Paden [4]. Firstly, the acceleration profile should not have exceedingly high frequency components. The reason is that if the acceleration

Table 6.1 Properties of Two-Flexible-Link Arm

No of link	l	ρ	e	m_e	i_b
Link One	1.0 m	0.3 kg/m^2	3.9375 N/m^2	0.15 kg	0.200 $kg\,m^2$
Link two	1.0 m	0.1 kg/m^2	0.4375 N/m^2	0.10 kg	0.067 $kg\,m^2$

changes too rapidly, then the calculated torque profile will contain high peak impulse which may excite the natural frequencies of the flexible manipulators. Secondly, the maximum acceleration limit should be chosen so as not to saturate the actuator. With these considerations, we have chosen the reference tip trajectory for link two (the second component of the output) as shown in Figure 6.3, in which the acceleration profile is composed of a pure sinusoidal function. A similar reference trajectory profile has been chosen for link one.

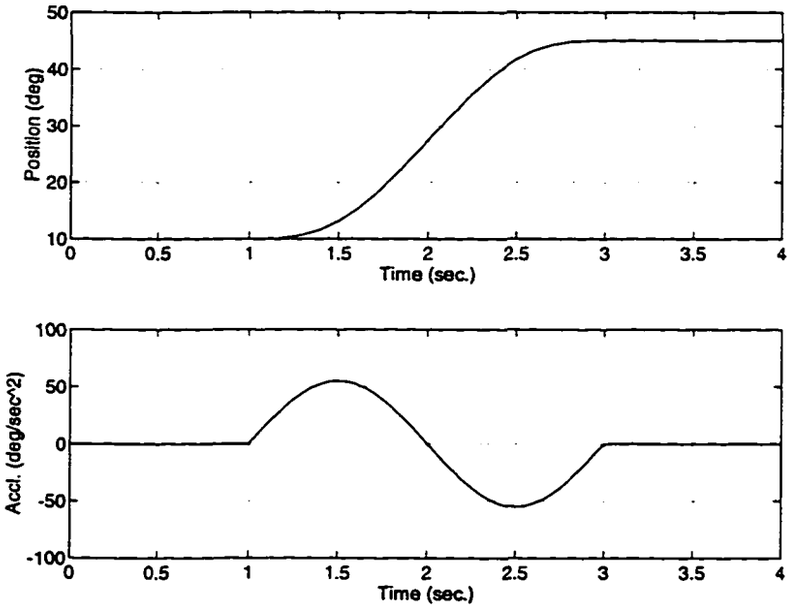

Figure 6.3 Desired Tip Trajectory Profiles for Link Two

6.4.2 Verification of system properties

In order to apply the stable inversion approach, two conditions need to be verified: the system should have a well-defined relative degree and its zero dynamics should have a hyperbolic equilibrium point at the origin.

Before we verify these, we first show the non-minimum phase property of the system. Otherwise, the output trajectory tracking can be accomplished using the classical inversion approach. To make notations simple, we assume that the two links are identical. Let l, m, and e denote their length, mass, and product of area moment inertia and Young's modulus respectively. Besides, let m_e and i_b denote the end-point mass and hub inertia of the second link respectively.

Zero dynamics is first derived from reference dynamics (6.38) with $y_d = [0°, 90°]^T$ and derivatives of y_d of all orders to zero (an equilibrium point). Then, a standard linearization on the obtained zero dynamics yields linearized zero dynamics as follows:

$$A_1\ddot{q} + A_2\dot{q} + A_3 q = 0, \tag{6.54}$$

where $A_2 = \alpha_d A_3$, and

$$A_1 = \begin{bmatrix} \frac{37}{60}m + 2m_e + 2\frac{i_b}{l^2} & \frac{5}{4}m + 4m_e + 4\frac{i_b}{l^2} & -\frac{1}{6}m - 2\frac{i_b}{l^2} & -\frac{4}{15}m - 2\frac{i_b}{l^2} \\ \frac{29}{30}m + 3m_e + 3\frac{i_b}{l^2} & \frac{68}{35}m + 6m_e + 6\frac{i_b}{l^2} & -\frac{1}{4}m - 3\frac{i_b}{l^2} & -\frac{2}{5}m - 3\frac{i_b}{l^2} \\ \frac{1}{4}m + m_e & \frac{1}{2}m + 2m_e & -\frac{1}{20}m & -\frac{1}{12}m \\ \frac{1}{5}m + m_e & \frac{2}{5}m + 2m_e & -\frac{1}{30}m & -\frac{2}{35}m \end{bmatrix}, \tag{6.55}$$

$$A_3 = \begin{bmatrix} 4e & 6e & 0 & 0 \\ 6e & 12e & 0 & 0 \\ 0 & 0 & 4e & 6e \\ 0 & 0 & 6e & 12e \end{bmatrix}, \tag{6.56}$$

and α_d is the damping ratio. Notice that we have exactly

$$\det A_3 = 144e^4 > 0, \tag{6.57}$$

and

$$\det A_1 = -\frac{1}{13230000}m^4 - \frac{13}{10584000}m^3 m_e - \frac{13}{5292000}m^3\frac{i_b}{l^2} - \frac{13}{44100}m^2 m_e\frac{i_b}{l^2} < 0. \quad (6.58)$$

Equations (6.57)-(6.58) imply that the product of all eigenvalues of the system is negative. Since the total number of the eigenvalues is an even number, we conclude that there exists at least one positive real eigenvalue for the linearization of the zero dynamics (6.54). The non-minimum-phase property is thus verified. It is noticed from the above argument that the non-minimum phase property is independent of α_d, the damping ratio. Thus, even in the case when structural damping is neglected ($\alpha_d = 0$), the flexible manipulator system is still non-minimum phase.

To verify the hyperbolicity of the zero dynamics, we further assume that $m_e = 0$ and $i_b = 0$ for notational simplicity. First, zero eigenvalues can be easily excluded from the fact $\det A_3 \neq 0$. Next, suppose the zero dynamics has pure imaginary eigenvalues $\pm i\lambda$ with $\lambda \neq 0$. Substituting them into the characteristic equation of the zero dynamics leads to

$$\det(-\lambda^2 A_1 \pm i\lambda A_2 + A_3) = 0. \quad (6.59)$$

$$\det(-\lambda^2 A_1 A_3^{-1} + [1 \pm i\alpha_d\lambda]I) = 0. \quad (6.60)$$

Equation (6.60) says that there exists an eigenvalue $\bar{\lambda}$ of matrix $A_1 A_3^{-1}$ such that

$$-\lambda^2\bar{\lambda} + [1 \pm i\alpha_d\lambda] = 0. \quad (6.61)$$

$$\bar{\lambda} = \frac{1}{\lambda^2}[1 \pm i\alpha_d\lambda]. \quad (6.62)$$

But the characteristic equation of matrix $em^{-1}A_1 A_3^{-1}$ is exactly given by

$$s^4 - \frac{61}{420}s^3 - \frac{331}{2116800}s^2 + \frac{127}{42336000}s - \frac{1}{1905120000} = 0. \quad (6.63)$$

It can be easily verified that this characteristic equation has all four real roots. Thus, condition (6.62) can not be true. Hence, the linearization of the zero dynamics (6.54) can

not have purely imaginary eigenvalues $\pm i\lambda$. However, it is noticed that no conclusion can be made about the hyperbolicity of the zero dynamics when structural damping in neglected ($\alpha_d = 0$).

The well-defined relative degree property can be seen by arranging the forward dynamics as follows. Substituting (6.37) into dynamics equation (6.35) yields

$$[\, M_{22}(\psi) - M_{21}(\psi)D_2\,]\ddot{q} + H_2(\psi, \dot{\psi}) + M_2\dot{q} + M_3 q + M_{21}(\psi)\ddot{y} = 0. \tag{6.64}$$

It can be easily seen that matrix $M_{22}(\psi) - M_{21}(\psi)D_2$ evaluated at $\theta_2 = 90^\circ$ is exactly the matrix A_1 in equation (6.54) because equation (6.64) with $y \equiv y_d$ is the reference dynamics (6.38). Equation (6.58) says that this matrix A_1 is nonsingular. Thus, substituting equations (6.37) and (6.64) into another part of the forward system dynamics (6.34) gives

$$M_{r1}(\psi)\ddot{y} + H_1(\psi, \dot{\psi}) - M_{r2}(\psi)[\, H_2(\psi, \dot{\psi}) + M_2\dot{q} + M_3 q\,] = u, \tag{6.65}$$

where

$$M_{r1}(\psi) = M_{11}(\psi) - M_{r2}(\psi)M_{21}(\psi), \tag{6.66}$$

$$M_{r2}(\psi) = [\, M_{12}(\psi) - M_{11}(\psi)D_2\,][\, M_{22}(\psi) - M_{21}(\psi)D_2\,]^{-1}. \tag{6.67}$$

It can be easily verified that M_r, the coefficient matrix of $\ddot{y}$, is invertible under the same simplifications as made in the verification of the hyperbolicity. Thus, the existence of a locally well-defined relative degree is verified, that is, both output components have relative degree two at the equilibrium point $\theta = [0^o, 90^o]^T$. It can further be verified that the above argument is still valid over the range of $5^0 \leq \theta_2 \leq 90^o$. The range is selected such that it covers the reference trajectory chosen in the simulation study.

6.4.3 Stable inversion vs. computed torque

In this subsection, we present simulation results and study the performance of our stable inversion based tracking controllers by comparing it with the well-known computed torque approach.

To apply stable inversion, the iterative procedure discussed in Appendix A is carried out to compute stable inverses. For the selected reference output trajectory, the nominal control input u_d and the desired joint-angle trajectory θ_d are calculated through the following steps:

- Step 1: Set $q_0(t) = 0$ for all t.
- Step 2: Linearize (6.38) along $q_0(t)$ and $\dot{q}_0(t)$ to get (6.48), (A.6)-(A.8) and (A.12)-(A.18).
- Step 3: Integrate equation (A.16) backward in time to get $S(t)$.
- Step 4: Integrate equation (A.17) backward in time to get $\sigma(t)$.
- Step 5: Integrate equation (A.18) forward in time to get $\zeta_1(t)$ and get $\zeta_2(t)$ by (A.14).
- Step 6: Compute $\begin{bmatrix} q(t) \\ \dot{q}(t) \end{bmatrix} = \begin{bmatrix} C_s \\ C_u \end{bmatrix}^{-1} \begin{bmatrix} \zeta_1 \\ \zeta_2 \end{bmatrix}$.
- Step 7: If $\|q - q_0\|$ is greater than a given threshold, set $q_0 = q$ and go to step 2, otherwise go to step 8.
- Step 8: Compute the nominal input u_d from (6.41) and desired rigid mode θ_d from (6.37).

The numerical procedure stops when it leads to a relative error of 5×10^{-4} in q between the third and the fourth iterations. It takes less than five minutes on a DEC workstation with the algorithm coded in Matlab. Figure 6.4 shows the nominal control input u_d, the joint torque needed to produce the desired tip trajectories in output. As expected, the torque needs to be applied to pre-shape the links some time before the tip starts moving due to the non-minimum phase property of the system.

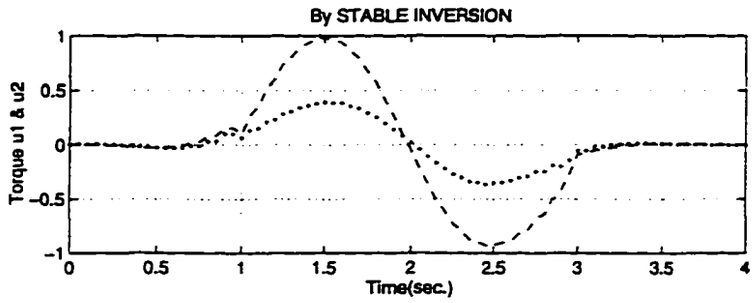

Figure 6.4 Nominal Control Input by Stable Inversion

Table 6.2 lists eigenvalues of the linearized forward system dynamics. They are computed from the linear approximation of forward dynamics (6.29) at $\theta = [0^o, 90^o]^T$ and $q = 0$. It is clear that the open-loop forward dynamics is unstable due to four poles at the origin. Those poles are corresponding to rigid modes θ and $\dot{\theta}$.

Table 6.2 Eigenvalues of Open-Loop Forward Dynamics

0	0	0	0
-16.2886+i4.7029	-16.2886-i4.7029	-0.2219+i0.6581	-0.2219-i0.6581
-42.6746+i81.9378	-42.6746+i81.9378	-0.6345+i11.2469	-0.6345-i11.2469

The controller structure of our stable inversion method is shown in Figure 6.5. It is the structure of the Approach II. The stabilizing signal u_s is superimposed on the feed-forward nominal control u_d to obtain the total control input to the plant. Since the flexible modes of the arm are not measurable, the controller uses only the rigid-angle measurement for feedback. It is noticed that the input/output map from the joint torque to the rigid angle is of minimum phase. The PD joint-angle stabilizing feedback is given by

$$\gamma(\theta) = -K_p\theta - K_d\dot{\theta}. \tag{6.68}$$

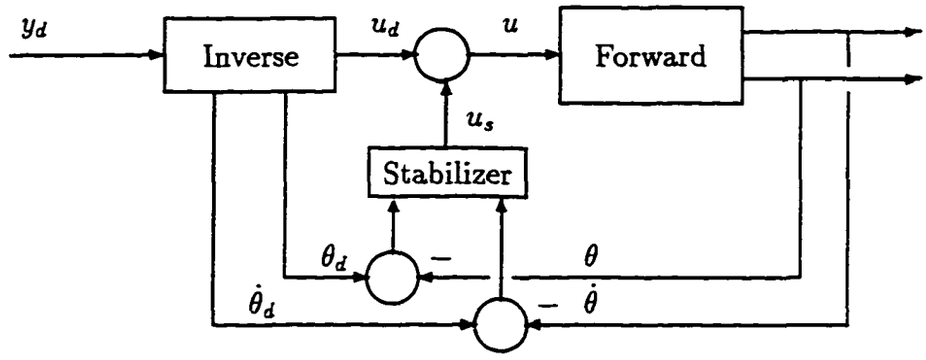

Figure 6.5 Control Scheme of Stable Inversion

The feed-forward plus feedback controller has the following overall form:

$$\begin{aligned} u &= u_d + u_s \\ &= u_d + \gamma(\theta) - \gamma(\theta_d) \\ &= u_d - K_p[\theta - \theta_d] - K_d[\dot{\theta} - \dot{\theta}_d], \end{aligned} \tag{6.69}$$

where

$$K_p = K_d = \begin{bmatrix} 0.5 & 0 \\ 0 & 0.375 \end{bmatrix}. \tag{6.70}$$

The gain matrices are selected to stabilize the two linearizations of the forward dynamics at t_0 and t_f. The eigenvalues of the linearization of the forward dynamics (6.29) at $\theta = [0°, 90°]^T$ and $q = 0$ after stabilization are given in Table 6.3.

Table 6.3 Eigenvalues of Closed-Loop Dynamics

-43.8221+i81.2408	-43.8221-i81.2408	-16.3544+i54.6808	-16.3544+i54.6808
-0.9070+i11.6319	-0.9070-i11.6319	-1.7529+i5.8291	-1.7529-i5.8291
-1.4119+i1.0185	-1.4119-i1.0185	-0.2608+i0.6814	-0.2608-i0.6814

Using control law (6.69), computer simulation of the closed-loop system is carried out in Matlab. Figure 6.6 plots the output trajectories using the tracking controller against the desired reference output trajectories. It is concluded that the tips of the robot arm follow the desired trajectories exactly without any undershoot, overshoot, or steady-state errors.

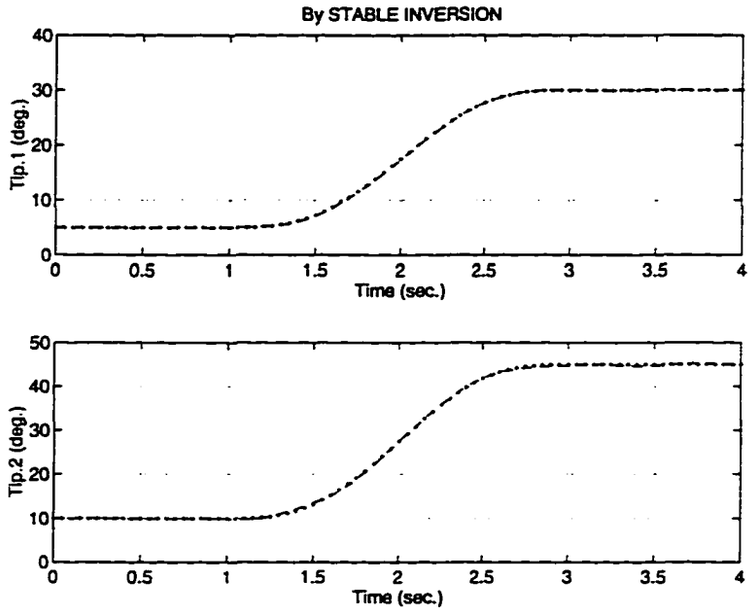

Figure 6.6 Reference Trajectory and Trajectory by Stable Inversion

As a comparison, the well-known computed torque technique [62] is considered. Similarly, only rigid modes are assumed to be measurable and used for feedback. The input torque to the system by the computed torque method can then be expressed as follows,

$$\tau^* = M_{11}(\theta_d)\ddot{\theta}_d + H_1(\theta_d, \dot{\theta}_d) - \tilde{K}_d(\dot{\theta} - \dot{\theta})_d - \tilde{K}_p(\theta - \theta_d), \tag{6.71}$$

where θ_d is computed by $\theta_d = y_d$. The feedback gains $\tilde{K}_d$ and $\tilde{K}_p$ are chosen in such a way as to optimize the output tracking.

For the same reference trajectory, the output profiles generated by the computed torque method are shown in Figure 6.7. Clearly, the computed torque technique causes significant output tracking error. The error is entirely due to the design in which the

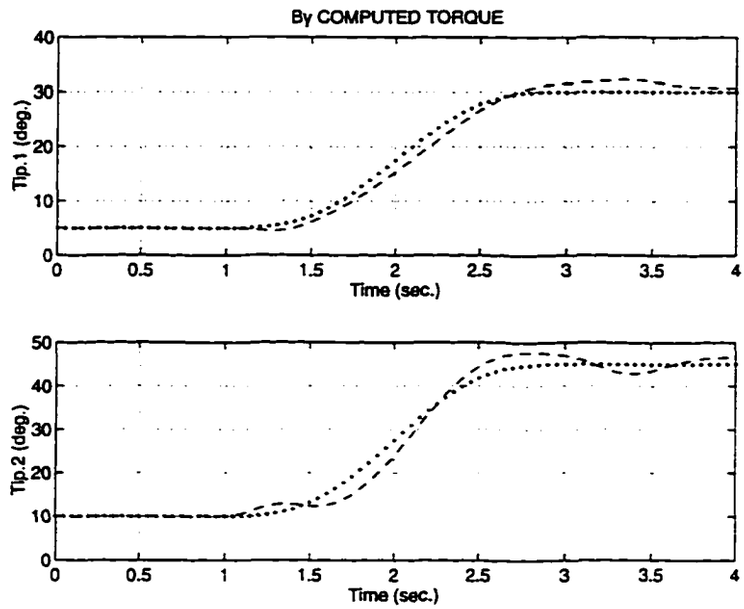

Figure 6.7 Reference Trajectory and Trajectory by Computed Torque

flexibility is not taken into consideration. Not like the robot system studied in the preceding chapter, this two-link flexible manipulator system has a non-minimum phase property that is not "weak".

6.5 Conclusions

Stable inversion based tracking control for nonlinear non-minimum phase systems is successfully applied to the tip trajectory tracking for a two-link flexible robot manipulator in this chapter. Simulation results demonstrate that the stable inversion approach is very effective for obtaining stable and remarkably accurate output tracking for multi-link flexible manipulators.

CHAPTER 7 OPTIMAL MOTION PLANNING AND CONTROL OF A FLEXIBLE SPACE ROBOT

This chapter investigates a new optimal motion control strategy for a flexible space robot. The robot is assumed to consist of a two-link flexible manipulator attached to rigid spacecraft floating in space. The control strategy is optimal in the sense that the system performance measured by the maneuvering time together with control effort and structural vibrations is optimized while the interference from the arm to spacecraft is kept satisfactorily small.

7.1 Introduction

Structural flexibility of space robot arms and limited solar energy supplied by spacecraft impose great challenges to a satisfactory space robot motion control. Firstly, any control strategy clearly has to result in a minimum energy consumption because of limited resource. Secondly, any movement of the robot manipulator would transmit an undesirable interference force from the arm to spacecraft. Finally, any control forces or disturbances applied to the arm are very likely to excite structural vibrations in the arm as well as in spacecraft. Therefore, a good motion control design for a space robot should have the following properties: *1) achieving desired motion with the shortest possible time; 2) not exciting structural vibrations; 3) using a minimal amount of energy; and 4) producing satisfactorily small interference on spacecraft.*

Though robotics has been an active research area for the past few decades, applications are concerned primarily with massive earth-bound industrial robots. Investigations concerning space robots have been mostly carried out by considering a rigid-link assumption [43]. To deal with the flexibility, a perturbation approach has been utilized to design separate motion controllers for the rigid and the flexible parts by assuming relatively small elastic vibrations [40]. Using reaction wheels or attitude control jets [61], the effect of interference from manipulator motion to spacecraft can be compensated. Another method to reduce the interference is to include spacecraft in trajectory planning and to use kinematic redundancy to optimize robot trajectories [39]. All the methods either lead to slow motion in order to keep down energy consumption and vibration excitation, or neglect the transient impact on spacecraft.

A fundamentally different approach to the tracking control of flexible structures is by using non-causal inversion. The idea was first presented by Bayo [2] to solve for inverse dynamics of one-link flexible robots. Since one-link robots are linear systems, the Fast Fourier Transform method worked successfully. By using feedback linearization and locally exponentially stable joint controllers, the method was extended to multi-link flexible robots [50]. With these results, the stable inversion concept was introduced to design exact and stable output tracking controls for a general class of nonlinear non-minimum phase systems [11, 12]. Furthermore, as studied in chapter 3, stable inverses have a nice minimum energy property. Specifically, stable inversion can achieve a given reference trajectory using a minimal amount of control energy and causing a minimal amount of internal vibrations.

In this chapter, we investigate a new motion control strategy by using the stable inversion approach for space manipulators with two flexible links and no control jets or reaction wheels. Section 7.2 briefly describes the equations of motion of the flexible space robot. It also presents the formulation of a nonlinear optimal control problem that characterized the optimal motion control. Section 7.3 is devoted to introduce an

approach to solve the optimal motion control problem by applying stable inversion. The approach involves an optimal trajectory planning and output tracking control design. Section 7.4 is intended to provide a closed-form solution of stable inverses to simplify the trajectory planning problem. In Section 7.5, a simulation study is set up and carried out to demonstrate the effectiveness of the proposed motion control strategy. Computation of the stable inverse is carried out using the numerical approach developed in Chapter 3. Finally, some remarks are made in section 7.6.

7.2 Forward Dynamics and Problem Statement

Consider a flexible space robot that consists of a rigid platform, representing spacecraft, and a robot arm with two flexible links. Both joints of the links are considered to be revolute, and input torque is applied at these joints. Both links are assumed to be slender such that the Euler-Bernoulli beam assumption is valid. A planar maneuver is assumed, and out-of-plane deflections of both links are neglected. Any possible effect from the sun and the earth is also neglected which means that there are no external forces acting on the system.

7.2.1 Forward system dynamics

Figure 7.1 depicts the space robot system together with its reference coordinate frames. The link connected to spacecraft is referred to as link one and the link attached to the tip of the first link is link two. The rotation angle θ_1 of link one is the angle between the undeformed link position and the vertical axis of the body frame of spacecraft. The angle θ_2 is the joint rotation of rigid base of the second link measuring the undeformed second link position from the tangent line at the tip of the first link. z_i measures the distance of a point at link i in the direction of the undeformed link position and w_i is

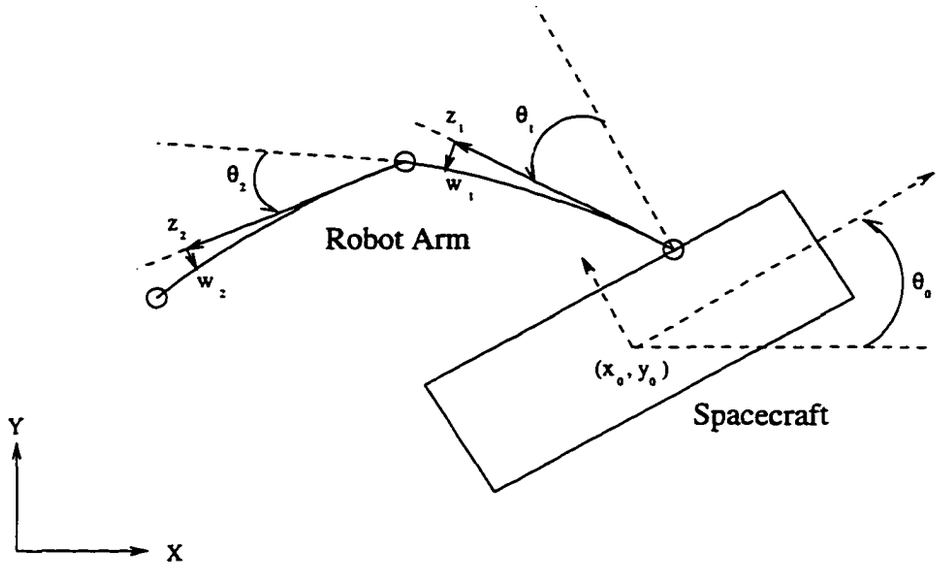

Figure 7.1 Flexible Space Robot

the deformation for the ith link at z_i for $i = 1$ and 2.

The assumed modes method is used to parameterize the continuous deformation of both flexible links. The admissible functions are chosen to be the ones for clamped-free beams [37], and two flexible modes are assigned to each link:

$$w_i(z_i,t) = \sum_{j=1}^{2} \sigma_{ij}(z_i) q_{ij}(t) \stackrel{\text{def}}{=} \sigma_i(z_i) q_i(t), \quad \forall i = 1,2, \tag{7.1}$$

where σ_i is of dimension one by two and q_i two by one for $i = 1$ and 2. $\sigma_{ij}(z_i)$, the jth admissible function of link i for $i = 1$ and 2, is given by

$$\begin{aligned} \sigma_{ij}(z_i) &= \tilde{k}_j[\cosh(\beta_{ij}l_i) + \cos(\beta_{ij}l_i)][\cosh(\beta_{ij}z_i) - \cos(\beta_{ij}z_i)] \\ &\quad -[\sinh(\beta_{ij}l_i) - \sin(\beta_{ij}l_i)][\sinh(\beta_{ij}z_i) - \sin(\beta_{ij}z_i)], \end{aligned} \tag{7.2}$$

where l_i is the length of link i for $i = 1$ and 2, $\tilde{k}_j$ a constant, and β_{ij} for $j = 1$ and 2 are the first two low-frequency solutions of the following equations

$$1 + \cosh(\beta_{ij}l_i)\cos(\beta_{ij}l_i) = 0, \quad \forall i = 1,2. \tag{7.3}$$

Denote the whole system's generalized coordinates as

$$\psi \stackrel{\text{def}}{=} [\, x_0, y_0, \theta_0, \theta_1, \theta_2, q_{11}, q_{12}, q_{21}, q_{22}\,]^T, \tag{7.4}$$

which consists of the coordinates v for spacecraft, the rigid modes θ and the flexible modes q for the arm:

$$v \stackrel{\text{def}}{=} [\, x_0, y_0, \theta_0 \,]^T, \quad \theta \stackrel{\text{def}}{=} [\, \theta_1, \theta_2 \,]^T, \quad q \stackrel{\text{def}}{=} [\, q_{11}, q_{12}, q_{21}, q_{22} \,]^T. \tag{7.5}$$

By the Lagrange's method [5], the equations of motion can be written as

$$M_{11}(\psi)\ddot{v} + M_{12}(\psi)\ddot{\theta} + M_{13}(\psi)\ddot{q} + H_1(\psi, \dot{\psi}) = 0, \tag{7.6}$$

$$M_{21}(\psi)\ddot{v} + M_{22}(\psi)\ddot{\theta} + M_{23}(\psi)\ddot{q} + H_2(\psi, \dot{\psi}) = u, \tag{7.7}$$

$$M_{31}(\psi)\ddot{v} + M_{32}(\psi)\ddot{\theta} + M_{33}(\psi)\ddot{q} + H_3(\psi, \dot{\psi}) + C_q\dot{q} + K_q q = 0, \tag{7.8}$$

which can be put in a more compact form

$$M(\psi)\ddot{\psi} + H(\psi, \dot{\psi}) + C\dot{\psi} + K\psi = B_u u, \tag{7.9}$$

where u is the vector of joint torque and B_u the torque distribution matrix given by

$$B_u = \begin{bmatrix} O_{2\times3} & I_2 & O_{2\times4} \end{bmatrix}^T. \tag{7.10}$$

K is the stiffness matrix

$$K = \begin{bmatrix} O_{5\times5} & O_{5\times4} \\ O_{4\times5} & K_q \end{bmatrix} = \begin{bmatrix} O_{5\times5} & O_{5\times2} & O_{5\times2} \\ O_{2\times5} & K_1 & O_{2\times2} \\ O_{2\times2} & O_{2\times2} & K_2 \end{bmatrix}, \tag{7.11}$$

and their elements are given by

$$[K_i]_{jk} = \int_0^{l_i} e_i \sigma_{ij}''(z_i)\sigma_{ik}''(z_i)\, dz_i, \quad \forall i = 1, 2, \tag{7.12}$$

where e_i denotes product of the Young's modulus constant and the area moment of inertia of link i for $i = 1$ and 2, and $\sigma_{ij}''(\cdot)$ the second derivative of $\sigma_{ij}(\cdot)$ with respect to spatial variable z_i. The damping matrix C is taken to be proportional to matrix K by damping ratios α_{d1} and α_{d2} of the two links respectively:

$$C = \begin{bmatrix} O_{5\times5} & O_{5\times4} \\ O_{4\times5} & C_q \end{bmatrix} = \begin{bmatrix} O_{5\times5} & O_{5\times2} & O_{5\times2} \\ O_{2\times5} & C_1 & O_{2\times2} \\ O_{2\times2} & O_{2\times2} & C_2 \end{bmatrix}, \tag{7.13}$$

where

$$C_1 = \alpha_{d1} K_1, \quad \text{and} \quad C_2 = \alpha_{d2} K_2. \tag{7.14}$$

$M(\psi)$ is the positive definite symmetric inertia matrix and its detailed definition is given in Appendix C. $H(\psi, \dot{\psi})$, the part containing centrifugal and coriolis terms, can be obtained from $M(\psi)$ as follows:

$$H(\psi, \dot{\psi}) = \dot{M}(\psi)\dot{\psi} - \frac{1}{2}\frac{\partial(\dot{\psi}^T M(\psi)\dot{\psi})}{\partial \psi}. \tag{7.15}$$

The Cartesian coordinates of the tip position of the manipulator relative to spacecraft are chosen to be the system's output vector. Each component is given by

$$y_1 = l_1 \sin(\theta_1 + \frac{\sigma_1(l_1)}{l_1} q_1) + l_2 \sin(\theta_1 + \theta_2 + \sigma_1'(l_1) q_1 + \frac{\sigma_2(l_2)}{l_2} q_2), \tag{7.16}$$

$$y_2 = l_1 \cos(\theta_1 + \frac{\sigma_1(l_1)}{l_1} q_1) + l_2 \cos(\theta_1 + \theta_2 + \sigma_1'(l_1) q_1 + \frac{\sigma_2(l_2)}{l_2} q_2). \tag{7.17}$$

In a more compact form, the output equation can be written as

$$y = h(\psi). \tag{7.18}$$

Equation (7.9) together with (7.18) constitutes the forward system dynamics of the flexible space robot system. It is noticed that the system dynamics is smooth, square (with the same number of inputs and outputs), and affine in control input u.

7.2.2 Statement of the problem

Consider a typical task usually performed by a robot manipulator attached to spacecraft. The task would be to grasp an object, say a satellite, from space and put it into spacecraft. To fulfill the task, motion control needs to be applied to move the robot arm from an initial configuration to a final configuration.

A good motion control design should, as mentioned earlier, achieve the desired configuration change with the shortest possible maneuvering time $t_f - t_0$ where t_0 and t_f

respectively denote the initial and final time of the maneuver. Due to a scarcity of fuel in space and limited solar energy, the motion should require a minimal amount of control effort which could be characterized by the $\mathcal{L}_2$-norm and the magnitude of control input u. Relatively long and flimsy robot arms used for space purpose render themselves more structural flexibility and are more likely to cause structural vibrations. The $\mathcal{L}_2$-norm and the magnitude of the flexible coordinates q could be used to characterize the structural vibrations which should be kept as small as possible for a good maneuver. The undesirable interference from the manipulator to spacecraft can adversely affect the space mission and should be kept within a sufficiently small range. The magnitude of $\dot{v}$ could be one characterization of this interference.

Based on the above discussion, an optimization problem is set up as follows. The performance index is set up such that the optimized motion control minimizes a linear combination of $t_f - t_0$, $\| u \|_{\mathcal{L}_2(-\infty,+\infty)}$ and $\| q \|_{\mathcal{L}_2(-\infty,+\infty)}$. Limitations on magnitudes of those undesirable quantities are set up as constraints (7.22), and a feasible set $\mathbb{U}$ is defined according to magnitude requirement on control input as well as the saturation levels of joint actuators installed:

$$\mathbb{U} \stackrel{\text{def}}{=} \{\, u \;\mid\; \| u_i \|_{\mathcal{L}_\infty(-\infty,+\infty)} \leq \epsilon_{u_i},\ \ \forall i = 1,2 \,\}. \tag{7.19}$$

Let $y_d(t_0)$ and $y_d(t_f)$ respectively denote the initial and the final configurations of the arm. The problem that characterizes the motion control design is thus given by

Definition 7 (Optimal Motion Control Problem)

$$\min_{u \in \mathbf{U}} \ \mathcal{J}(u) = w_t[\, t_f - t_0 \,] + w_u \| u \|_{\mathcal{L}_2(-\infty,+\infty)} + w_q \| q \|_{\mathcal{L}_2(-\infty,+\infty)} \tag{7.20}$$

subject to

$$y(t) = y_d(t_0), \quad \forall t \leq t_0, \quad \text{and} \quad y(t) = y_d(t_f), \quad \forall t \geq t_f, \tag{7.21}$$

$$\| q \| \leq \epsilon_q, \quad \text{and} \quad \| \dot{v} \| \leq \epsilon_{\dot{v}}, \tag{7.22}$$

$$\text{forward system dynamics (7.9) \& (7.18)}, \tag{7.23}$$

and t_0 is given.

Constraint (7.21) specifies the desired configuration change and the norm $\|\cdot\|$ in (7.22) is taken to be the component-wise infinity norm. w_t, w_u and w_q are weighting constants.

It is noticed that (7.20)-(7.23) is a highly nonlinear and non-convex optimal control problem. Not having any structure on $\mathbb{U}$ as well as the hard (equality) constraints (7.21) on initial and final configurations makes it impossible to solve the Hamilton-Jacobi-Bellman equation associated with the Pontryagin Minimum Principle. By taking advantage of a minimum energy property of stable inversion, we propose an approach that would lead to a suboptimal solution of the problem stated.

7.3 Optimal Motion Control in Two Stages

Firstly, each feasible control $u \in \mathbb{U}$ (with a specified initial state condition) corresponds to an output trajectory y through the input/output map of forward dynamics (7.9) & (7.18). Secondly, the set of all smooth trajectories satisfying the required configuration change renders itself a better structure than that of $\mathbb{U}$. These facts suggest a reorganization of searching over controls by a trajectory planning problem searching over output trajectories combined with a control optimization for each such trajectory.

Following this idea, it is easy to see that the optimization problem (7.20) can be reorganized into two stages. In the outer-stage, an optimization is searching over all smooth trajectories satisfying the requirement on initial and final configurations. For each such trajectory, an inner-stage optimization is performed to find an optimal control input that minimizes the performance index. Thus, optimization over both control inputs and output trajectories are performed. This two-stage problem can be stated as follows:

Definition 8 (Motion Control in Two-Stage)

$$\min_{y_d \in \mathbb{Y}} \left\{ \begin{array}{l} \min \ \mathcal{J}(u) = w_t[t_f - t_0] + w_u \| u \|_{\mathcal{L}_2(-\infty,+\infty)} + w_q \| q \|_{\mathcal{L}_2(-\infty,+\infty)} \\ u \in \mathbf{U} \\ \text{s.t. } y \equiv y_d \end{array} \right\} \tag{7.24}$$

subject to

$$\| q \| \leq \epsilon_q, \quad \text{and} \quad \| \dot{v} \| \leq \epsilon_{\dot{v}}, \tag{7.25}$$

$$\text{forward system dynamics (7.9) \& (7.18)}, \tag{7.26}$$

and t_0 is given.

The set $\mathbb{Y}$ contains all smooth trajectories satisfying the hard constraints on initial and final configurations:

$$\mathbb{Y} \stackrel{\text{def}}{=} \{ \, y_d \mid y_d(t) = y_d(t_0), \ \forall t \leq t_0, \ \ \& \ \ y_d(t) = y_d(t_f), \ \forall t \geq t_f \, \}. \tag{7.27}$$

Notice that the only constraint in the inner optimization is an output tracking requirement $y(t) \equiv y_d(t)$ and all other constraints are left to the outer optimization. Hence, the inner-stage is an unconstrained exact output tracking control problem minimizing $\mathcal{J}(u)$. The newly developed stable inversion theory provides a solution that precisely addresses this issue.

7.3.1 Inner-stage by stable inversion

Recall the interesting energy feature of the stable inverse solution established in Chapter 3, Theorem 3 and Theorem 5 on the minimum energy property of system's internal vibrations and the nominal control input u_d. Specifically, let η be any coordinate for the invariant zero dynamics manifold of the system (2.3)-(2.4) and η_d denote the solution of the two-point boundary value problem (2.29)-(2.30) which corresponds to

the stable inverse x_d and u_d. Then, it has been proved in the two theorems that (1) among infinitely many solutions for η that corresponding to $y \equiv y_d$, η_d is the only one with finite $\mathcal{L}_2(-\infty, +\infty)$-norm; (2) among infinitely many input trajectories that are able to produce $y \equiv y_d$, u_d is the only trajectory with finite $\mathcal{L}_2(-\infty, +\infty)$-norm. In another word, for a given y_d and the requirement $y \equiv y_d$, u_d and η_d from stable inversion give the minimum energy solution for the input as well as the internal vibrations.

Now consider the inner-stage optimization problem for a given y_d:

Definition 9 (Inner-Stage Optimization Problem)

$$\min_{u \in U} \; \mathcal{J}(u) = w_t[t_f - t_0] + w_u \| u \|_{\mathcal{L}_2(-\infty,+\infty)} + w_q \| q \|_{\mathcal{L}_2(-\infty,+\infty)} \tag{7.28}$$

subject to

$$y(t) \equiv y_d(t), \tag{7.29}$$

$$\text{forward system dynamics (7.9) \& (7.18)}, \tag{7.30}$$

and t_0 is given.

The forward dynamics of the space robot given by (7.9) is clearly linear in input and can be written in the form of equation (2.3). Furthermore, let us assume that all conditions for stable inversion are satisfied (the assertion is to be discussed later). q and $\dot{q}$ can be used as the coordinates for the zero dynamics of the robot which is in fact the structural vibration dynamics.

Since the performance index $\mathcal{J}(u)$ contains $\mathcal{L}_2$-norms of both control input u and internal state q, it is easy to see that the stable inverse is the only solution to the inner-stage optimization problem (7.28) based on the minimum energy property. The optimal performance index is then given by

$$\begin{aligned} \mathcal{J}(y_d) &\stackrel{\text{def}}{=} \mathcal{J}^*(u)\Big|_{y \equiv y_d} \\ &= w_t[t_f - t_0] + w_u \| u_d(y_d) \|_{\mathcal{L}_2(-\infty,+\infty)} + w_q \| q_d(y_d) \|_{\mathcal{L}_2(-\infty,+\infty)}, \end{aligned} \tag{7.31}$$

where u_d and q_d denote the stable inverses for a given y_d.

7.3.2 Optimal trajectory planning

For the two-stage problem (7.24), the inner-stage is automatically solved by stable inversion. The problem is then reduced to the outer-stage. By substituting the optimal solution from the inner-stage (7.31), the remaining outer-stage is an optimal trajectory planning problem given as follows.

Definition 10 (Optimal Trajectory Planning Problem)

$$\min_{y_d \in \mathbb{Y}} \ \mathcal{J}(y_d) = w_t[t_f - t_0] + w_u \| u_d \|_{\mathcal{L}_2(-\infty,+\infty)} + w_q \| q_d \|_{\mathcal{L}_2(-\infty,+\infty)} \tag{7.32}$$

subject to

$$\| u_d \| \leq \epsilon_u, \tag{7.33}$$

$$\| q_d \| \leq \epsilon_q, \quad \text{and} \quad \| \dot{v}_d \| \leq \epsilon_{\dot{v}}, \tag{7.34}$$

and t_0 is given.

The constraint (7.33) rewrites the definition (7.19) on feasible set $\mathbb{U}$.

There are two difficulties in solving this problem. First, the optimization is still an infinite-dimensional searching over trajectory space specified by $\mathbb{Y}$. Secondly, every constraint or index evaluation requires solutions of stable inversion which itself is an iterative procedure in general. Thus, tremendous computing effort is demanded.

To handle the first difficulty, we parameterize every trajectory $y_d \in \mathbb{Y}$ as a linear combination of a finite number of base time functions. By doing so, the optimization problem (7.32) is reduced to a finite-dimensional problem. However, only a suboptimal solution is pursued. It can be verified that choosing sinusoidal base functions as follows is a valid parameterization:

$$\begin{aligned} y_d(p_1, \ldots, p_{\bar{n}}, t) = y_d(t_0) + [\, y_d(t_f) - y_d(t_0) \,] \frac{t - t_0}{t_f - t_0} \\ - [\, y_d(t_f) - y_d(t_0) \,] (*) \left[\sum_{i=1}^{\bar{n}} \frac{p_i}{2\pi i} \sin(2\pi i \frac{t - t_0}{t_f - t_0}) \right], \end{aligned} \tag{7.35}$$

where $p_1 + \cdots + p_{\bar{n}} = [1, 1]^T$, and each p_i for $i = 1, \ldots, \bar{n}$ is a two by one constant vector, the design parameter, and the operation $(*)$ is defined as a component-wise vector multiplication.

To deal with the second difficulty, we derive a closed-form stable inverses from linearized system dynamics. Thus avoiding iterations on every constraint or index evaluation. The derivation of the closed-form stable inverses is outlined in the following section.

7.4 Closed-Form Stable Inverses

In this section, we try to derive a closed-form stable inverse to simplify the optimal trajectory planning problem (7.32). Firstly, it can be verified that the system dynamics (7.9) and (7.18) have a well-defined vector relative degree for the output defined. Secondly, the smoothness and smallness of y_d can be guaranteed by selecting an appropriate feasible trajectory set $\mathbb{Y}$ in motion planning. However, it is noticed that zero dynamics of flexible space robots with joint torque as input and tip position as output does not have a hyperbolic equilibrium point at the origin due to zero eigenvalues corresponding to the generalized coordinates of the spacecraft. To make stable inversion applicable, system dynamics is first modified such that it renders hyperbolic zero dynamics without destroying the relative degree condition. Then, a closed-form stable inverses is derived through a linearization approach.

7.4.1 Augmented forward dynamics

To deal with the non-hyperbolicity of zero dynamics, we augment both system's input and output vectors. Let $\bar{y} = v$ be the augmented output component, and $\bar{u}$ the augmented input that consists of three components: two thrusters acting on spacecraft in directions aligned with the body axes, and a torque on the mass center of spacecraft.

Then, the augmented forward system dynamics can be written as

$$M_{11}(\psi)\ddot{v} + M_{12}(\psi)\ddot{\theta} + M_{13}(\psi)\ddot{q} + H_1(\psi,\dot{\psi}) = B_1(\psi)\bar{u}, \tag{7.36}$$

$$M_{21}(\psi)\ddot{v} + M_{22}(\psi)\ddot{\theta} + M_{23}(\psi)\ddot{q} + H_2(\psi,\dot{\psi}) = u, \tag{7.37}$$

$$M_{31}(\psi)\ddot{v} + M_{32}(\psi)\ddot{\theta} + M_{33}(\psi)\ddot{q} + H_3(\psi,\dot{\psi}) + C_q\dot{q} + K_q q = 0, \tag{7.38}$$

$$\begin{cases} y = h(\psi), \\ \bar{y} = v, \end{cases} \tag{7.39}$$

where $B_1(\psi)$ is a nonsingular force distribution matrix given by

$$B_1(\psi) = \begin{bmatrix} \cos\theta_0 & -\sin\theta_0 & 0 \\ \sin\theta_0 & \cos\theta_0 & 0 \\ 0 & 0 & 1 \end{bmatrix}. \tag{7.40}$$

Since we assume that no forces from spacecraft could be used, a non-holonomic constraint by setting $\bar{u} = 0$ in equation (7.36) is added to our motion control problem (7.20). This constraint will also appear in the optimal trajectory planning problem (7.32).

With the coordinates of spacecraft specified as part of the output, this augmented dynamics shares the same zero dynamics as those for two-link flexible robots. Thus, hyperbolic zero dynamics is guaranteed (see Chapter 6).

7.4.2 Stable inverse dynamics

In the flexible space robot case, the stable inverse dynamics can be easily derived from the augmented dynamics (7.36)-(7.39). For any given y_d, We first get inverse kinematics from output equation (7.39) as follows:

$$\theta_1 = \arcsin\left(\frac{1}{2l}\sqrt{y_{1d}^2 + y_{2d}^2}\right) - \arcsin\left(\frac{y_{2d}}{\sqrt{y_{1d}^2 + y_{2d}^2}}\right) - \frac{\sigma(l)}{l}q_1, \tag{7.41}$$

$$\theta_2 = \pi - 2\arcsin\left(\frac{1}{2l}\sqrt{y_{1d}^2 + y_{2d}^2}\right) + \frac{\sigma(l)}{l}[q_1 - q_2] - \sigma' q_1. \tag{7.42}$$

It is noticed that in the above derivations we have assumed that the both links are of the same length $l_1 = l_2 = l$ and the same mode shapes are used $\sigma_1 = \sigma_2 = \sigma$. Let θ_y be the tip angle seeing from the hub of link 1 measuring from the vertical axis of spacecraft body frame. The equations (7.41)-(7.42) are valid for $0 < \theta_y < 180^o$. Outside this range the inverse may not exist or different expressions should be used due to singularity and nonlinearity.

Rewrite equations (7.41)-(7.42) in a more compact form as follows:

$$\theta = f_\theta(y_d) + M_\theta q. \tag{7.43}$$

Substituting (7.43) and $v = \bar{y}_d$ into dynamics (7.37)-(7.38) yields the stable inverse dynamics:

$$\begin{aligned}[M_{32}(\cdot)M_\theta + M_{33}(\cdot)]\ddot{q}_d + C_q\dot{q}_d + K_q q_d \\ + H_3(\cdot) + M_{32}(\cdot)\ddot{f}_\theta(y_d) + M_{31}(\cdot)\ddot{\bar{y}}_d = 0,\end{aligned} \tag{7.44}$$

$$u_d = [M_{22}(\cdot)M_\theta + M_{23}(\cdot)]\ddot{q}_d + H_2(\cdot) + M_{22}(\cdot)\ddot{f}_\theta(y_d) + M_{21}(\cdot)\ddot{\bar{y}}_d, \tag{7.45}$$

where the subscript d stands for stable inverse solutions by imposing required boundary conditions (see Section 2.2), and matrices $M_{21}(\cdot), \ldots, M_{33}(\cdot)$ are functions of $(q_d, y_d, \bar{y}_d)$ and $H_2(\cdot)$ and $H_3(\cdot)$ are those of $(q_d, y_d, \bar{y}_d)$ and their derivatives. With the same substitution, the non-holonomic constraint can be written as

$$[M_{12}(\cdot)M_\theta + M_{13}(\cdot)]\ddot{q}_d + H_1(\cdot) + M_{12}(\cdot)\ddot{f}_\theta(y_d) + M_{11}(\cdot)\ddot{\bar{y}}_d = 0. \tag{7.46}$$

A standard linearization on equations (7.44)-(7.46) yields

$$[M^0_{32}M_\theta + M^0_{33}]\ddot{q}_d + C_q\dot{q}_d + K_q q_d + M^0_{32}M_y\ddot{y}_d + M^0_{31}\ddot{\bar{y}}_d = 0, \tag{7.47}$$

$$[M^0_{12}M_\theta + M^0_{13}]\ddot{q}_d + M^0_{12}M_y\ddot{y}_d + M^0_{11}\ddot{\bar{y}}_d = 0, \tag{7.48}$$

and an expression for u_d, where the equilibrium point with $q^0_d = [0, 0, 0, 0]^T$, $\theta^0_d = [25^o, 45^o]^T$ and $\bar{y}^0_d = [0, 0, 30^o]^T$ is chosen as the linearizing point.

From (7.48) we have

$$\tilde{\bar{y}}_d = -M_{11}^{0\,-1}[\,[\,M_{12}^0 M_\theta + M_{13}^0\,]\tilde{q}_d + M_{12}^0 M_y \tilde{y}_d\,], \tag{7.49}$$

where the invertibility is guaranteed since the system inertia matrix is positive definite. Substituting (7.49) into (7.47) we obtain

$$M_1^0 \tilde{q}_d + M_2^0 \dot{q}_d + M_3^0 q_d + M_4^0 \tilde{y}_d = 0, \tag{7.50}$$

where the coefficient matrices $M_1^0, \ldots, M_4^0$ are obviously defined. The equation (7.50) is actually the zero dynamics in linearization. It can be written in a state-space form

$$\dot{\bar{q}} = A_q \bar{q} + B_q \tilde{y}_d, \tag{7.51}$$

where $\bar{q} = [q_d^T, \dot{q}_d^T]^T$, and matrices A_q and B_q are defined accordingly.

7.4.3 Closed-form stable inverses

To solve for a stable $\tilde{q}$, the dynamics (7.51) is first decoupled by a transformation

$$\bar{q} \stackrel{\text{def}}{=} \begin{bmatrix} X_s & X_u \end{bmatrix} \tilde{q} \stackrel{\text{def}}{=} \begin{bmatrix} X_{sq} & X_{uq} \\ X_{s\dot{q}} & X_{u\dot{q}} \end{bmatrix} \tilde{q}, \tag{7.52}$$

which leads to

$$\begin{bmatrix} \dot{\tilde{q}}_1 \\ \dot{\tilde{q}}_2 \end{bmatrix} = \begin{bmatrix} J_s & 0 \\ 0 & J_u \end{bmatrix} \begin{bmatrix} \tilde{q}_1 \\ \tilde{q}_2 \end{bmatrix} + \begin{bmatrix} B_s \\ B_u \end{bmatrix} \tilde{y}_d, \tag{7.53}$$

where both J_s and $-J_u$ are Hurwitz. This is guaranteed by the hyperbolicity assumption on the zero dynamics.

Time-scaling is carried out to simplify the calculation $\bar{t} = [t - t_0]/[t_f - t_0]$. From the boundary conditions requirement of stable inversion we know that the dynamics lies in unstable manifold of the zero dynamics at time t_0 and in stable manifold at time t_f. Equivalently, $\tilde{q}_1(\bar{t} = 0) = 0$ and $\tilde{q}_2(\bar{t} = 1) = 0$. Solving (7.53) with these boundary conditions, we obtain

$$\tilde{q}_1(\bar{t}) = \int_0^{\bar{t}} \exp\{J_{sf}[\bar{t} - \tau]\} B_{sf} \tilde{y}_d(\tau)\, d\tau, \quad \forall \bar{t} \geq 0, \tag{7.54}$$

$$\tilde{q}_2(\bar{t}) = \int_1^{\bar{t}} \exp\{-J_{uf}[\tau - \bar{t}]\} B_{uf} \bar{y}_d(\tau)\, d\tau, \quad \forall \bar{t} \leq 1, \tag{7.55}$$

where by time-scaling

$$J_{sf} \stackrel{\text{def}}{=} t_f J_s, \quad J_{uf} \stackrel{\text{def}}{=} t_f J_u, \quad B_{sf} \stackrel{\text{def}}{=} \frac{B_s}{t_f} \quad B_{uf} \stackrel{\text{def}}{=} \frac{B_u}{t_f}. \tag{7.56}$$

Straightforward integrations on equations (7.54) and (7.55) with y_d parameterized by (7.35) provides for all $\bar{t} \geq 0$,

$$\tilde{q}_1(\bar{t}) = \sum_{i=1}^{\bar{n}} M_\omega^{-1} \left[\frac{1}{\omega_i} \left[e^{J_{sf}\bar{t}} - \cos(\omega_i \bar{t}) I \right] B_{sf} - \frac{1}{\omega_i^2} J_{sf} B_{sf} \sin(\omega_i \bar{t}) \right] p_{\omega_i}, \tag{7.57}$$

and for all $\bar{t} \leq 1$,

$$\tilde{q}_2(\bar{t}) = \sum_{i=1}^{\bar{n}} M_\omega^{-1} \left[\frac{1}{\omega_i} \left[e^{-J_{uf}[1-\bar{t}]} - \cos(\omega_i \bar{t}) I \right] B_{uf} - \frac{1}{\omega_i^2} J_{uf} B_{uf} \sin(\omega_i \bar{t}) \right] p_{\omega_i}, \tag{7.58}$$

where

$$M_\omega \stackrel{\text{def}}{=} I + \frac{1}{\omega_i^2} J_{uf}^2, \tag{7.59}$$

$$\omega_i \stackrel{\text{def}}{=} 2\pi i, \quad \text{and} \quad p_{\omega_i} \stackrel{\text{def}}{=} \omega_i [y_d(1) - y_d(0)](*) p_i. \tag{7.60}$$

Recall that the operation $(*)$ is defined in equation (7.35) as a component-wise vector multiplication.

Now the transformation (7.52) gives us a closed-form solution of $\bar{q}$, equivalently, $(q_d, \dot{q}_d)$:

$$q_d = \begin{cases} X_{uq} e^{J_{uf}\bar{t}} \tilde{q}_2(0), & \forall \bar{t} \leq 0; \\ X_{sq} \tilde{q}_1(\bar{t}) + X_{uq} \tilde{q}_2(\bar{t}), & \forall 0 \leq \bar{t} \leq 1; \\ X_{sq} e^{J_{sf}(\bar{t}-1)} \tilde{q}_1(1), & \forall \bar{t} \geq 1, \end{cases} \tag{7.61}$$

where $\tilde{q}_1(\bar{t})$ and $\tilde{q}_2(\bar{t})$ are given by equations (7.57)-(7.58). Using this solution and an integration on equation (7.49) with time-scaling carefully involved will bring us the solution of $\dot{v}_d$. Finally, substituting of solutions of q_d and $\dot{v}_d$ into equation (7.45) in its linearized form yields u_d. Expressions of $\dot{v}_d$ and u_d are considerably messy. However, their derivations are straightforward.

7.5 Optimal Motion Planning and Control

In this section, we present a simulation study to demonstrate the effectiveness of the proposed optimal motion control strategy. The optimal trajectory planning problem (7.32) is firstly solved to yield a planned tip trajectory y_d^* satisfying the required configuration change. Then, the stable inverse is computed and an output tracking controller is designed incorporating the inverse to drive system output, the tip of the manipulator, to track y_d^*.

7.5.1 Simulation setup

The flexible space robot is assumed to have the following properties: spacecraft has $100(kg)$ of total mass and $150(kgm^2)$ of moment of inertia; the arm consists of two identical links and each link has length $5(m)$, mass per unit length $0.2(kg/m)$, damping ratio 0.025, the product of the area moment inertia and the Young's modulus $40(N/m^2)$. Each link is also assumed to have $0.1(kg)$ of tip mass and $20(kgm^2)$ of rigid hub inertia.

We assume that the initial and final configurations of the arm are

$$\theta_d(t_0) = [0^o, 5^o]^T, \quad \text{and} \quad \theta_d(t_f) = [50^o, 80^o]^T, \tag{7.62}$$

which may be visualized from Figure 7.2 corresponding to positions 1 and 5.

The coefficients $\tilde{k}_j$ for $j = 1$ and 2 in the admissible function (7.2) are taken as $\tilde{k}_1 = 1$ and $\tilde{k}_2 = 0.01$. Since a non-causal control is expected, we set $t_0 = 10$ (second). We also set small constraint bounds on $\dot{v}$, u and q to represent slow movement of spacecraft and allowable sizes of control torque and structural vibrations:

$$\epsilon_u = [5, 5]^T, \quad \epsilon_q = [0.125, 0.125, 0.125, 0.125]^T, \quad \epsilon_{\dot{v}} = [0.25, 0.5, 0.75]^T. \tag{7.63}$$

Tip trajectories are parameterized with three different frequency components by taking $\bar{n} = 3$ in (7.35). The weights in the performance index are chosen as $w_t = 0.5$, $w_u = 0.05$ and $w_q = 0.45$.

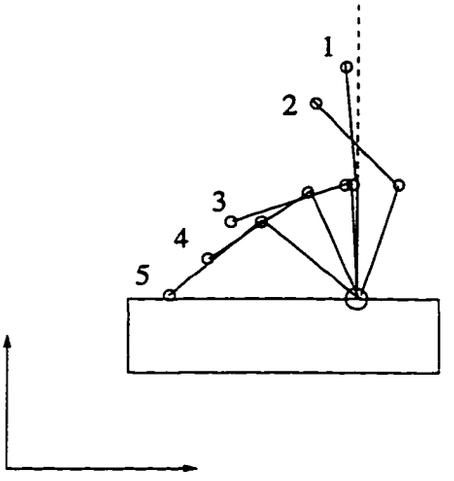

Figure 7.2 Planned Motion with only Rigid Dynamics

7.5.2 Optimal tip trajectory planning

To solve the trajectory planning problem (7.32), the following procedure is followed:

- to simplify the problem by parameterizing output trajectories (7.35) and by utilizing the closed-form solution of stable inverses (section 6.4);
- to solve for a suboptimal solution as the planned trajectory by utilizing Matlab Optimization Toolbox.

With the above simulation set up and the procedure, after running on an SGI workstation for about ten minutes a solution to the trajectory planning is found as follows:

$$t_f^* = 10.60(\text{second})$$
$$p_1^* = \begin{bmatrix} 0.6616 \\ 0.8795 \end{bmatrix}, \quad p_2^* = \begin{bmatrix} 0.2211 \\ -0.0046 \end{bmatrix}, \quad \text{and} \quad p_3^* = \begin{bmatrix} 0.1173 \\ 0.1250 \end{bmatrix}. \tag{7.64}$$

The corresponding output trajectory y_d^* can be obtained by substituting this solution into the parameterization equation (7.35). Figure 7.3 shows the trajectory obtained. The upper part is the first component of output y_1 and the lower the second component of output vector y_2.

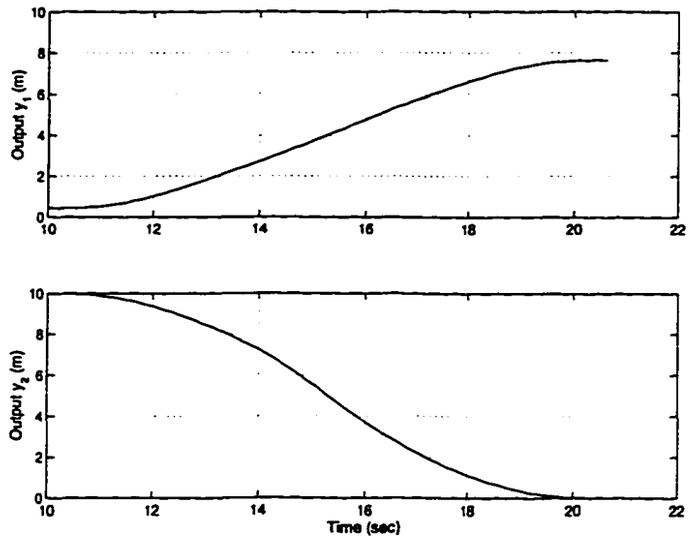

Figure 7.3 Suboptimal Tip Trajectory Planned

7.5.3 Output tracking control design

By solving the trajectory planning problem, we obtain the prescribed trajectory y_d^* satisfying the desired configuration change. The next is to compute the stable inverse for an output tracking controller. The following procedure is followed:

- to modify the system dynamics such that it meets the hyperbolic zero dynamics requirement;
- to carry out a numerical algorithm on the modified dynamics to compute the stable inverse for given y_d^*.

While in solving the trajectory planning problem, a coordinate trajectory of spacecraft v_d^* corresponding to y_d^* can also be obtained from equation (7.49). The forward dynamics equations (7.7)-(7.8) with v substituted by v_d^* together with the output equation (7.18) constitute the modified forward system dynamics:

$$M_{22}(\theta,q)\ddot{\theta} + M_{23}(\theta,q)\ddot{q} + [\, H_2(\theta,q,\dot{\theta},\dot{q}) + M_{21}(\theta,q)\ddot{v}_d^*] = u, \tag{7.65}$$

$$M_{32}(\theta,q)\ddot{\theta} + M_{33}(\theta,q)\ddot{q} + C_q\dot{q} + K_q q + [\, H_2(\theta,q,\dot{\theta},\dot{q}) + M_{31}\ddot{v}_d^*] = 0, \tag{7.66}$$

$$y = h(\theta, q). \tag{7.67}$$

With the coordinates of spacecraft specified, this modified dynamics is essentially the dynamics for two-link flexible robots (Chapter 6). Thus, it meets the requirements to apply stable inversion.

The algorithm developed in Section 3.2 is carried out on the modified dynamics (7.65)-(7.67). The dynamics is firstly stabilized by

$$\gamma(\theta) = -K_p\theta - K_d\dot{\theta}. \tag{7.68}$$

Coded in Matlab, the algorithm is executed on an SGI workstation. The procedure converges to a satisfactorily small error after only three iterations. The computing time is about three to four minutes. Only three iterations When the algorithm converges, we obtain the stable inverse pair $\left(u_d^* - \gamma(\theta_d^*), (\theta_d^*, q_d^*, \dot{\theta}_d^*, \dot{q}_d^*)\right)$ of the modified dynamics (7.65)-(7.67). This stable inverse is then used to approximate the stable inverse of the original dynamics (7.9) and (7.18). Shown in Figure 7.4 is the u_d^*.

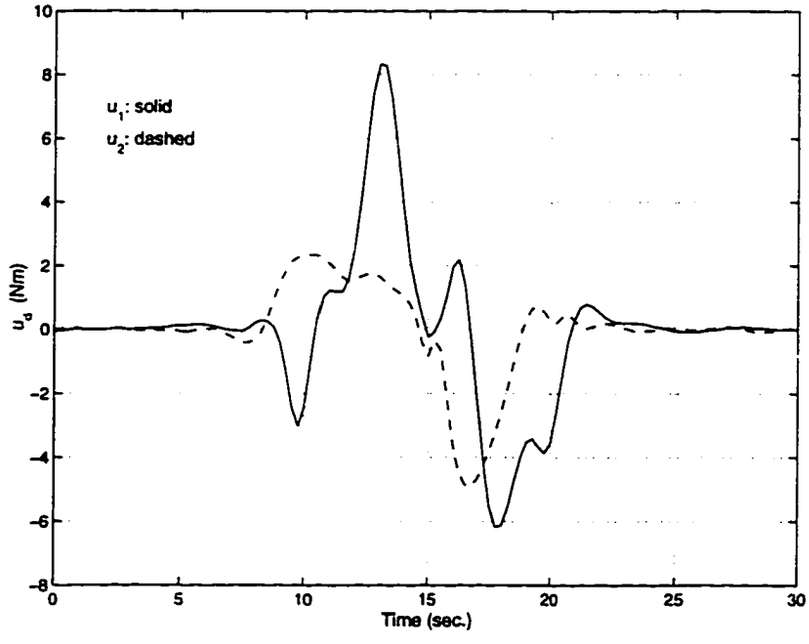

Figure 7.4 Approximated Nominal Control Input u_d^*

A closed-loop tracking controller is then designed using the stable inverse pair and it's structure is the same as that used in the preceding chapter for flexible manipulators. A feed-forward plus feedback control law is given by

$$\begin{aligned} u &= u_d^* + \gamma(\theta) - \gamma(\theta_d^*) \\ &= u_d^* - K_p[\theta - \theta_d^*] - K_d[\dot{\theta} - \dot{\theta}_d^*]. \end{aligned} \tag{7.69}$$

It is noticed that the stabilizing feedback is also a simple linear joint-angle PD feedback. See Chapter 4 and a reference by Chen [10] for tracking performance and stability analysis for various controller structures incorporating stable inverses.

The tip movement by forward simulation is shown in Figure 7.5 together with the planned tip trajectory y_d^*. It is seen that an excellent output tracking has been achieved. The error between the simulated trajectory and the planned one is mainly due to the approximation made to the forward system dynamics in order to render hyperbolic zero dynamics. The desired configuration change is thus fulfilled by the motion control which uses only joint-angle measurement and joint torque but not any control forces from spacecraft.

7.5.4 Suboptimal path vs. sinusoidal trajectory

Before concluding this application study, let us make a brief comparison study. An output trajectory y_s with sinusoidal acceleration profile is chosen as another planned trajectory. Such smooth trajectories are considered to be the best trajectories as a common practice in manipulator control area. This trajectory y_s is constructed such that it requires the same amount of time to fulfill the maneuver and it also satisfies the requirement on the configuration change. The trajectory can be obtained from the parameterization equation (7.35) with

$$\bar{n} = 1, \quad \text{and} \quad p_1 = [1, 1]^T. \tag{7.70}$$

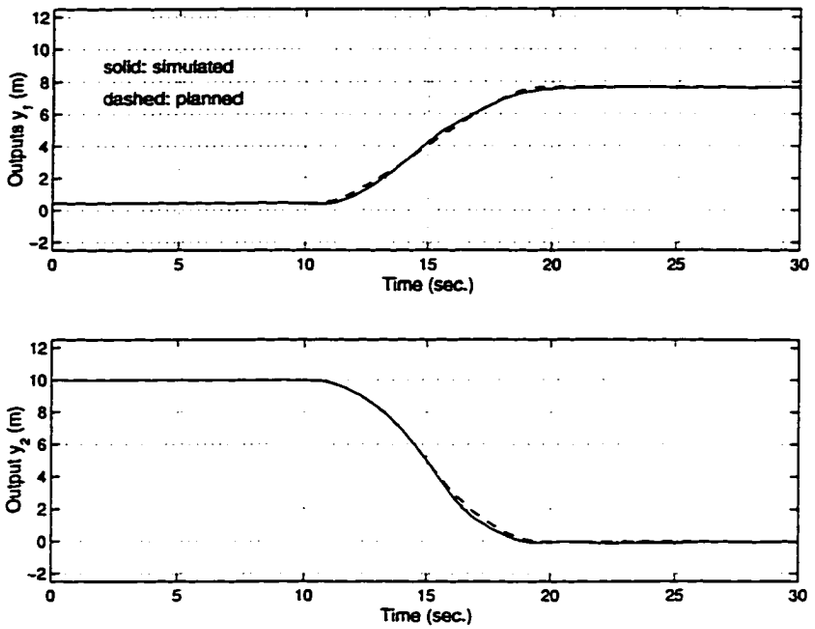

Figure 7.5 Planned Trajectory and Trajectory by Simulation

With this sinusoidal output trajectory y_s, the same procedure is carried out to compute the stable inverse. The same tracking controller structure is also assumed. Simulation results are summarized in Table 7.1. It is clearly seen that the sinusoidal trajectory requires more control energy and exhibits more structural vibrations.

Table 7.1 A Comparison on Performance

	Suboptimal y_d^*	Sinusoidal y_s
Time $t_f - t_0$	10.60	10.60
Control $\| u \|_{\mathcal{L}_2(-\infty,+\infty)}$	14.40	16.27
Vibration $\| q \|_{\mathcal{L}_2(-\infty,+\infty)}$	0.57	0.65
Index $\mathcal{J}(u)$	6.28	6.41

7.6 Conclusions

In this chapter, a new strategy has been developed for motion control of a flexible space robot. The motion control is formulated as a nonlinear optimal control problem and rearranged into two stages. The inner-stage is as an unconstrained exact output tracking problem for which stable inversion provides the unique optimal solution. With this, the outer-stage becomes an optimal trajectory planning involving system output alone. A suboptimal solution is obtained using parameterization with a finite number of base functions. Finally, the stable inversion based output tracking controller is designed to realize the planned motion.

It is noticed that an error exists between the achieved and the planned output trajectories. This is due to an approximation used in computing the stable inverse for the planned trajectory. Specifically, we have used the reduced dynamics model (7.65)-(7.67)) by replacing the generalized coordinate for spacecraft v with v_d^*, the same coordinate computed in trajectory planning process using linearized dynamics (7.49). The approximation is necessary in order to satisfy a condition in stable inversion. However, if we are allowed to use reaction wheels or attitude control jets, conditions in stable inversion will be automatically satisfied. In that case, we expect that the error would be eliminated.

It is also worth pointing out that the "optimality" of the proposed approach is affected by a few simplifications made in the study. Firstly, a linearized model has been used to obtain closed-form stable inverse solutions. Secondly, feasible trajectories have been parameterized with a ramp function and three sinusoidal functions of different frequencies. On the other hand, the true solution to the optimal control problem by the Pontryagin Minimum Principle is in general extremely difficult if not impossible. The reason is that there is no solutions available to the associated HJB equations for problems of highly nonlinear and non-convex nature.

CHAPTER 8 CONCLUSIONS

This thesis addressed the stable inversion problem and its applications to output tracking control for various robotic systems. Main contributions were presented from Chapter 3 to Chapter 7.

A minimum energy property was established in Chapter 3 for stable inverses. It claimed that out of infinitely many possible inverse solutions, the one provided by the stable inversion process is the only one that has finite energy measured by $\mathcal{L}_2(-\infty, +\infty)$-norm. Based on this property, a numerical procedure was developed to provide an approach to construct stable inverses. The algorithm is based on constructing and solving an optimal control problem minimizing control input energy. The algorithm was applied in Chapter 7 for motion control of a flexible space robot.

Output tracking control design was addressed in Chapter 4. The design incorporates stable inverses into a dead-beat tracking controller. Tracking performance was analyzed via standard Lyapunov arguments. Furthermore, uncertainties were also considered and assumed to satisfy the "matching conditions". A modified controller structure was presented for those systems with such uncertainties. The robust tracking performance was also discussed.

From Chapter 5 to Chapter 7 three applications of the tracking control design developed in Chapter 4 to various robotic systems were studied. Whereas tracking control of a single-link flexible-joint robot system was designed in Chapter 5, Chapter 6 dealt with tip trajectory tracking of a two-link flexible manipulator. A space robot system without usage of any reaction wheels or attitude control jets was considered in Chapter 7. For

such a system, an optimal motion control problem with trajectory planning was solved using stable inversion and optimization technique.

The work presented in this thesis is just the beginning towards the objective of designing output tracking control systems using stable inversion for various robotic systems. There are many issues related to the area addressed in this thesis that require a deeper study. These issues may include:

- Extending stable inversion to those systems without a well-defined relative degree or their zero dynamics does not have a hyperbolic equilibrium point at the origin:
- Further exploring the energy property of stable inverses within a finite time horizon and the relationship between stable inversion and energy optimal control problems:
- Extending the stable inversion approach to allow more general reference output trajectories such as those having no compact support or those generated by exosystems on $[0, \infty)$;
- Defining and constructing robust stable inverse solutions for systems with various uncertainties or those subjected to disturbances;
- Real time implementing of tracking controllers using stable inversion is an interesting issue to explore due to the non-causality of the inverse control signals;
- Constructing a more efficient numerical procedure to solve for stable inverses which includes solving the two-point boundary value problems with instability existing in both positive and negative time directions;
- Extending the robotic models currently considered to include deformation due to other effects such as shear strain and rotary inertia and to allow three dimensional motion.

APPENDIX A AN ITERATIVE ALGORITHM

The key to obtaining the stable inverse pair x_d and u_d is to solve for a bounded and convergent η_d from equations (2.29)-(2.30), the two-point boundary value problem. An iterative approach by Chen [9] to such a solution was developed which is presented in detail in this appendix for references.

In each iteration, the differential equation (2.29) is linearized along the solution obtained from the previous iteration to yield equation (A.1). The stable eigenspace $\mathbb{E}^s$ and the unstable eigenspace $\mathbb{E}^u$ of the zero dynamics corresponding to (A.1) are used for the boundary conditions instead of $\mathbf{W}^s$ and $\mathbf{W}^u$. We thus obtain a linear time-varying two-point boundary value problem at this iteration:

$$\dot{\eta} = A(t)\eta + B(t), \tag{A.1}$$

subject to

$$\eta(t_0) \in \mathbb{E}^u, \quad \text{and} \quad \eta(t_f) \in \mathbb{E}^s. \tag{A.2}$$

The boundary condition (A.2) can be characterized by two equality conditions. To do this, let matrix $X_s(t_0)$ ($Y_s(t_0)$) contain the real right (left) eigenvectors and the generalized eigenvectors of $A(t_0)$ associated with eigenvalues having negative real parts, and $X_u(t_0)$ ($Y_u(t_0)$) contain those associated with eigenvalues having positive real parts. Then, we have

$$\begin{bmatrix} Y_s(t_0) \\ Y_u(t_0) \end{bmatrix} A(t_0) \begin{bmatrix} X_s(t_0) & X_u(t_0) \end{bmatrix} = \begin{bmatrix} J_s(t_0) & O \\ O & J_u(t_0) \end{bmatrix}, \tag{A.3}$$

where $J_s(t_0)$ and $J_u(t_0)$ are the corresponding real Jordan canonical forms of the stable and unstable subspaces respectively. In particular, from (A.3) we have

$$Y_s(t_0)A(t_0)X_u(t_0) = O. \tag{A.4}$$

On the other hand, the condition $\eta(t_0) \in \mathbb{E}^u$ can be characterized by $\eta(t_0)$ expressed as a linear combination of unstable right eigenvectors and generalized eigenvectors. That is,

$$\eta(t_0) = X_u(t_0)z_u, \tag{A.5}$$

for some vector z_u. Combining (A.5) with (A.4) yields an equivalent equality condition for $\eta(t_0) \in \mathbb{E}^u$:

$$C_s\eta(t_0) = 0, \tag{A.6}$$

where

$$C_s \stackrel{\text{def}}{=} Y_s(t_0)A(t_0). \tag{A.7}$$

A similar derivation at $t = t_f$ can be made to replace '$\eta(t_f) \in \mathbb{E}^s$ by

$$C_u\eta(t_f) = 0, \tag{A.8}$$

where

$$C_u \stackrel{\text{def}}{=} Y_u(t_f)A(t_f). \tag{A.9}$$

The linear problem (A.1), (A.6)-(A.9) is then solved and the solution is taken to be the new approximation of the current iteration. The iteration continues until the solutions in the adjacent two iterations are satisfactorily close to each other. Solving the boundary value problem in (A.1), (A.6)-(A.9) is done following a technique from linear-quadratic optimal control and is carried out in the following steps.

First, apply a change of state variable:

$$\zeta \stackrel{\text{def}}{=} \begin{bmatrix} \zeta_1 \\ \zeta_2 \end{bmatrix} \stackrel{\text{def}}{=} \begin{bmatrix} C_s \\ C_u \end{bmatrix} \eta. \tag{A.10}$$

Since $C_s\eta = 0$ in (A.6) characterizes the unstable eigenspace of the zero dynamics, therefore $\zeta_1 = C_s\eta$ is, roughly speaking, the stable part of η. Similarly, $\zeta_2 = C_u\eta$ is the unstable part. The inverse transformation is given by

$$\eta = \begin{bmatrix} C_s \\ C_u \end{bmatrix}^{-1} \zeta \stackrel{\text{def}}{=} \begin{bmatrix} T_s & T_u \end{bmatrix} \begin{bmatrix} \zeta_1 \\ \zeta_2 \end{bmatrix}. \tag{A.11}$$

Differentiating ζ_1 and ζ_2 using equations (A.10)-(A.11) and (A.1), we get

$$\dot{\zeta}_1 = A_{11}(t)\zeta_1 + A_{12}(t)\zeta_2 + B_1(t), \tag{A.12}$$

$$\dot{\zeta}_2 = A_{21}(t)\zeta_1 + A_{22}(t)\zeta_2 + B_2(t), \tag{A.13}$$

and the boundary conditions in (A.6)-(A.9) become $\zeta_1(t_0) = 0$ and $\zeta_2(t_f) = 0$. It is worth pointing out that $\zeta_1(t_0) = 0$ and equation (A.12) form an initial value problem while $\zeta_2(t_f) = 0$ and equation (A.13) form a final value problem. However, these two problems are coupled.

The second step is to decouple the ζ_1 and ζ_2 dynamics. Since ζ_1 and ζ_2 satisfy a pair of linear differential equations, their solutions are also linearly related. That is,

$$\zeta_2(t) = S(t)\zeta_1(t) + \sigma(t), \tag{A.14}$$

for some functions $S(t)$ and $\sigma(t)$ with suitable final value conditions

$$S(t_f) = 0 \quad \text{and} \quad \sigma(t_f) = 0. \tag{A.15}$$

Differentiating both sides of equation (A.14) yields

$$\dot{\zeta}_2(t) = \dot{S}(t)\zeta_1(t) + S(t)\dot{\zeta}_1(t) + \dot{\sigma}(t).$$

Substituting the values of $\dot{\zeta}_1$ and $\dot{\zeta}_2$ from (A.12) and (A.13) and comparing the coefficients of $\zeta_1(t)$ lead to

$$\dot{S}(t) = A_{21}(t) + A_{22}(t)S(t) - S(t)A_{11}(t) - S(t)A_{12}(t)S(t), \tag{A.16}$$

$$\dot{\sigma}(t) = [A_{22}(t) - S(t)A_{12}(t)]\sigma(t) + [B_2(t) - S(t)B_1(t)], \tag{A.17}$$

with final conditions specified in equation (A.15).

The third step is backward and forward integrations. Since equation (A.16) contains only known functions except $S(t)$, it can be integrated backward in time to get $S(t)$. Once this is done, equation (A.17) can also be integrated backward in time to solve for $\sigma(t)$. With $S(t)$ and $\sigma(t)$ as known functions, equation (A.12) can be rewritten as

$$\dot{\zeta}_1(t) = [A_{11}(t) + A_{12}(t)S(t)]\zeta_1(t) + B_1(t) + A_{12}(t)\sigma(t), \tag{A.18}$$

and it can be integrated forward in time with $\zeta_1(t_0) = 0$ to obtain $\zeta_1(t)$. With these, the algebraic equation (A.14) can be used to obtain $\zeta_2(t)$.

The final step is to use the inverse transformation in equation (A.11) to obtain $\eta(t)$ that will be the solution of the current iteration.

It is worth pointing out that even though all stable inversion results are local and this appendix presents a local linearization approach to construct stable inverses, the stable inverse solutions can be, but do not have to be, always locally constructed.

APPENDIX B USEFUL LEMMAS AND THEOREMS

Useful lemmas and theorems are quoted in this appendix. They are from both theory of ordinary differential equations and nonlinear systems theory. See the corresponding references for proofs.

Theorems from Theory of Differential Equations

The following two theorems concerns local properties of solutions to a dynamical system near the origin. One deals with solutions inside stable or unstable manifolds of the origin. Another one is about solutions on neither stable nor unstable manifold. The system is assumed to have a hyperbolic equilibrium point at the origin.

Theorem 10 (See Wiggins [63] for a proof.) *Let* $\mathbf{W}^s$ *and* $\mathbf{W}^u$ *be the local stable and unstable manifolds of a hyperbolic equilibrium point of a dynamical system. Then the solutions of the dynamic system with initial conditions in* $\mathbf{W}^s$ *(respectively* $\mathbf{W}^u$*) approach the equilibrium point at an exponential rate asymptotically as* $t \to +\infty$ *(respectively* $t \to -\infty$*).*

Let the origin be the hyperbolic equilibrium point of a dynamic system. Denote by $B(h)$ a spherical neighborhood with center at the origin and radius of h.

Theorem 11 (See Miller and Michel [41] for a proof.) *Let* $\mathbf{W}^s$ *and* $\mathbf{W}^u$ *be the local stable and unstable manifolds of a hyperbolic equilibrium point of a dynamic system. Then there exists a* $\delta_1 > 0$ *(respectively* $\delta_2 > 0$*) such that if* $(\tau, \eta(\tau)) \in \mathbb{R} \times B(\delta_1)$

(respectively $\mathbb{R} \times B(\delta_2)$) for some solution η of the system but $\eta(\tau) \notin \mathbf{W}^s$ (respectively $\mathbf{W}^u$), then $\eta(t)$ must leave the ball $B(\delta_1)$ (respectively $B(\delta_2)$) at some finite time $t_1 > \tau$ (respectively $t_2 < \tau$).

Theorems from Nonlinear Systems Theory

Theorem 12 (See Khalil [33] for a proof.) *Let $x = 0$ be an equilibrium point for the nonlinear system*

$$\dot{x} = f(t, x), \tag{B.1}$$

where $f : [0, \infty) \times \mathbb{D} \to \mathbb{R}^n$ is continuously differentiable, $\mathbb{D} = \{x \in \mathbb{R}^n \mid \|x\|_2 < r\}$, and the Jacobian matrix $[\partial f / \partial x]$ is bounded and Lipschitz on $\mathbb{D}$, uniformly in t. Let

$$A(t) = \frac{\partial f}{\partial x}(t, x)\bigg|_{x=0}. \tag{B.2}$$

Then, the origin is an exponentially stable equilibrium point for the nonlinear system, if and only if it is an exponentially stable equilibrium point for the linear system

$$\dot{x} = A(t)x. \tag{B.3}$$

The following result is the converse Lyapunov theorem for the case when the origin is an exponentially stable equilibrium point.

Theorem 13 (See Khalil [33] for a proof.) *Let $x = 0$ be an equilibrium point for the nonlinear system*

$$\dot{x} = f(t, x), \tag{B.4}$$

where $f : [0, \infty) \times \mathbb{D} \to \mathbb{R}^n$ is continuously differentiable, $\mathbb{D} = \{x \in \mathbb{R}^n \mid \|x\|_2 < r\}$, and the Jacobian matrix $[\partial f / \partial x]$ is bounded on $\mathbb{D}$, uniformly in t. Let k, γ, and r_0 be positive constants with $r_0 < \gamma / k$. Let $\mathbb{D}_0 = \{x \in \mathbb{R}^n \mid \|x\|_2 < r_0\}$. Assume that the trajectories of the system satisfy

$$\| x(t) \|_2 \leq k \| x(t_0) \|_2 e^{-\gamma[t - t_0]}, \quad \forall x(t_0) \in \mathbb{D}_0, \quad \forall t \geq t_0 \geq 0. \tag{B.5}$$

Then, there is a function $V : [0,\infty)\times\mathbb{D}_0 \to \mathbb{R}$ *that satisfies the inequalities:*

$$c_1\| x(t)\|_2^2 \le V(t,x) \le c_2\| x(t)\|_2^2, \tag{B.6}$$

$$\frac{\partial V}{\partial t} + \frac{\partial V}{\partial x} f(t,x) \le -c_3\| x(t)\|_2^2, \tag{B.7}$$

$$\left\| \frac{\partial V}{\partial x}(t) \right\|_2 \le c_4\| x(t)\|_2 \tag{B.8}$$

for some positive constants c_1, c_2, c_3 *and* c_4.

Consider the system

$$\dot{x} = f(t,x) + g(t,x), \tag{B.9}$$

as a perturbation of the nominal system

$$\dot{x} = f(t,x). \tag{B.10}$$

The following Lyapunov-like theorem is very useful in dealing with such perturbed systems with non-vanishing perturbation $g(t,0) \neq 0$.

Theorem 14 (See Khalil [33] for a proof.) *Let* $\mathbb{D} = \{x \in \mathbb{R} \mid \|x\| < r\}$ *and the map* $f : [0,\infty)\times\mathbb{D} \to \mathbb{R}^n$ *be piecewise continuous in* t *and locally Lipschitz in* x. *Let* $V : [0,\infty)\times\mathbb{D} \to \mathbb{R}$ *be a continuously differentiable function such that*

$$\alpha_1(\| x(t)\|_2) \le V(t,x) \le \alpha_2(\| x(t)\|_2), \tag{B.11}$$

$$\frac{\partial V}{\partial t} + \frac{\partial V}{\partial x} f(t,x) \le -\alpha_3(\| x(t)\|_2), \qquad \forall \|x(t)\|_2 \ge \mu > 0, \tag{B.12}$$

$\forall t \ge 0$, $\forall x \in \mathbb{D}$, *where* $\alpha_1(\cdot)$, $\alpha_2(\cdot)$, *and* $\alpha_3(\cdot)$ *are class* $\mathcal{K}$ *functions defined on* $[0,r)$ *and* $\mu < \alpha_2^{-1}(\alpha_1(r))$. *Then, there exists a class* $\mathcal{KL}$ *function* $\beta(\cdot,\cdot)$ *and a finite* t_1 *such that*

$$\| x(t)\|_2 \le \beta(\| x(t_0)\|_2, t - t_0), \qquad \forall t_0 \le t < t_1, \tag{B.13}$$

$$\| x(t)\|_2 \le \alpha_1^{-1}(\alpha_2(\mu)), \qquad \forall t \ge t_1, \tag{B.14}$$

$\forall \| x(t_0) \|_2 < \alpha_2^{-1}(\alpha_1(r))$. *Moreover, if all the assumptions hold with* $r = \infty$, *that is* $\mathbb{D} = \mathbb{R}^n$, *and* $\alpha_1(\cdot)$ *belongs to class mathcal*K_∞, *then inequalities (B.13)-(B.14) hold for any initial state* $x(t_0)$. *Furthermore, if* $\alpha_i(r) = k_i r^c$ *for some positive constants* k_i *and* c, *then* $\beta(r, s) = kr \exp(-\gamma s)$ *with* $k = [k_2/k_1]^{1/c}$ *and* $\gamma = [k_3/k_2 c]$.

The following theorem deals with the perturbed system (B.9) when the origin of the nominal system (B.10) is exponentially stable.

Theorem 15 (See Khalil [33] for a proof.) *Let* $x = 0$ *be an exponentially stable equilibrium point of the nominal system (B.10). Let* $V(t, x)$ *be a Lyapunov function of the nominal system that satisfies (B.6)-(B.8) in* $[0, \infty) \times \mathbb{D}$, *where* $\mathbb{D} = \{x \in \mathbb{R}^n \mid \|x\|_2 < r\}$. *Suppose the perturbation term* $g(t, x)$ *satisfies*

$$\| g(t, x) \|_2 \leq \delta \leq \frac{c_3}{c_4} \sqrt{\frac{c_1}{c_2}} \theta r, \tag{B.15}$$

for all $t > 0$, $x \in \mathbb{D}$, *and some positive* $\theta < 1$. *Then, for all* $\| x(t_0) \|_2 < \sqrt{c - 1/c_2} r$, *the solution of the perturbed system* $x(t)$ *satisfies*

$$\| x(t) \|_2 \leq k \exp\{-\gamma [t - t_0]\} \| x(t_0) \|_2, \qquad \forall t_0 \leq t < t_1, \tag{B.16}$$

and

$$\| x(t) \|_2 \leq b, \qquad \forall t \geq t_1, \tag{B.17}$$

for some finite t_1, *where*

$$k = \sqrt{\frac{c_2}{c_1}}, \quad \gamma = \frac{[1 - \theta] c_3}{2 c_2}, \quad b = \frac{c_4}{c_3} \sqrt{\frac{c_2}{c_1}} \frac{\delta}{\theta}. \tag{B.18}$$

The following lemma is known as the Barbalat's lemma.

Lemma 5 (See Khalil [33] for a proof.) *Let* $\phi : \mathbb{R} \to \mathbb{R}$ *be a uniformly continuous function on* $[0, \infty)$. *Suppose that*

$$\lim_{t \to \infty} \int_0^t \phi(\tau) \, d\tau \tag{B.19}$$

exists and is finite. Then,

$$\phi(t) \to 0 \qquad \text{as} \qquad t \to \infty. \tag{B.20}$$

APPENDIX C INERTIA MATRIX FOR SPACE ROBOTS

In this appendix, detailed and complete description of system inertia matrix $M(\psi)$ for the flexible space robot studied in Chapter 7 is given.

Notations and Definitions

A list of system's parameters is as follows:

i_{b_i}: inertia of rigid hub of the ith link, $i=1,2$,

m_{e_i}: tip mass of the ith link, $i=1,2$,

l_i: length of the ith link, $i=1,2$,

e_i: product of area moment of inertia and Young's Modulus, $i=1,2$,

ρ_i: mass per unit length of the ith link, $i=1,2$,

m_{x_0}: total mass of spacecraft,

i_{x_0}: moment of inertia of spacecraft about its mass center.

For the convenience of notations, we define the following variables for all $i = 1$ and 2:

$$m_{x_i} = \int_0^{l_i} \rho_i^{=} \, dz_i, \quad i_{x_i} = \int_0^{l_i} \rho_i^{=} z_i^2 \, dz_i, \quad i_{y_i} = \int_0^{l_i} \rho_i^{=} z_i \, dz_i, \tag{C.1}$$

and matrices N_i of dimensions two by one, N_{i+2} of two by one, M_i of two by two where their elements are given by

$$[N_i]_j = \int_0^{l_i} \rho_i^{=} z_i \sigma_{ij} \, dz_i, \quad [N_{i+2}]_j = \int_0^{l_i} \rho_i^{=} \sigma_{ij} \, dz_i, \quad \forall j = 1,2 \tag{C.2}$$

$$[M_i]_{jk} = \int_0^{l_i} \rho_i^{=} \sigma_{ij} \sigma_{ik} \, dz_i, \quad \forall j = 1,2, \; k = 1,2, \tag{C.3}$$

where

$$\rho_i^* = \rho_i + m_{e_i}\delta(z_i - l_i). \tag{C.4}$$

We also define

$$\bar{\theta}_2 \stackrel{\text{def}}{=} \theta_2 + \sigma'_{11}(l_1)q_{11} + \sigma'_{12}(l_1)q_{12}, \tag{C.5}$$

$$f_1(\cdot) = h\cos(\cdot) - d\sin(\cdot), \quad f_2(\cdot) = h\cos(\cdot) + d\sin(\cdot), \quad f_3(\cdot) = -h\sin(\cdot) + d\cos(\cdot), \tag{C.6}$$

where h is the distance between the mass center of spacecraft and the rigid hub of link one in the horizontal direction of spacecraft body frame, and d is that in the vertical direction of the body frame.

System Inertia Matrix

The inertia matrix $M(\psi)$ is given by $M(\psi) = U\bar{M}(\psi)U^T$ where

$$U = \begin{bmatrix} I_3 & O & O \\ O & I_2 & O \\ O & B_3 & I_4 \end{bmatrix}, \quad B_3 = \begin{bmatrix} 0 & 0 & 0 & 0 \\ \sigma'_{11}(l_1) & \sigma'_{12}(l_1) & 0 & 0 \end{bmatrix}, \tag{C.7}$$

and $\bar{M}(\psi)$ is positive definite symmetric and its elements are given by:

$$\bar{m}_{11} = m_{x_0} + m_{x_1} + m_{x_2}, \qquad \bar{m}_{12} = 0,$$

$$\bar{m}_{13} = -[\,m_{x_1} + m_{x_2}\,]f_2(\theta_0) - [\,i_{y_1} + m_{x_2}l_1\,]\cos(\theta_0 + \theta_1) - i_{y_2}\cos(\theta_0 + \theta_1 + \bar{\theta}_2),$$

$$\bar{m}_{14} = -[\,i_{y_1} + m_{x_2}l_1\,]\cos(\theta_0 + \theta_1) - i_{y_2}\cos(\theta_0 + \theta_1 + \bar{\theta}_2),$$

$$\bar{m}_{15} = -i_{y_2}\cos(\theta_0 + \theta_1 + \bar{\theta}_2),$$

$$[\bar{m}_{16} \quad \bar{m}_{17}] = -[\,N_3^T + m_{x_2}\sigma_1(l_1)\,]\cos(\theta_0 + \theta_1),$$

$$[\bar{m}_{18} \quad \bar{m}_{19}] = -N_4^T\cos(\theta_0 + \theta_1 + \bar{\theta}_2);$$

$$\bar{m}_{22} = m_{x_0} + m_{x_1} + m_{x_2},$$

$$\bar{m}_{23} = [\,m_{x_1} + m_{x_2}\,]f_3(\theta_0) - [\,i_{y_1} + m_{x_2}l_1\,]\sin(\theta_0 + \theta_1) - i_{y_2}\sin(\theta_0 + \theta_1 + \bar{\theta}_2),$$

$$\bar{m}_{24} = -[\, i_{y_1} + m_{x_2} l_1 \,] \sin(\theta_0 + \theta_1) - i_{y_2} \sin(\theta_0 + \theta_1 + \bar{\theta}_2),$$

$$\bar{m}_{25} = -i_{y_2} \sin(\theta_0 + \theta_1 + \bar{\theta}_2),$$

$$[\bar{m}_{26} \quad \bar{m}_{27}] = -[\, N_3^T + m_{x_2} \sigma_1(l_1) \,] \sin(\theta_0 + \theta_1),$$

$$[\bar{m}_{28} \quad \bar{m}_{29}] = -N_4^T \sin(\theta_0 + \theta_1 + \bar{\theta}_2);$$

$$\bar{m}_{33} = i_{x_0} + i_{x_1} + i_{x_2} + i_{b_1} + i_{b_2} + m_{x_1}[\, h^2 + d^2 \,] + m_{x_2}[\, h^2 + d^2 + l_1^2 \,] +$$

$$+2[\, i_{y_1} + m_{x_2} l_1 \,] f_1(\theta_1) + 2 i_{y_2} f_1(\theta_1 + \bar{\theta}_2) + 2 i_{y_2} l_1 \cos\bar{\theta}_2,$$

$$\bar{m}_{34} = i_{x_1} + i_{x_2} + i_{b_1} + i_{b_2} + m_{x_2} l_1^2 + [\, i_{y_1} + m_{x_2} l_1 \,] f_1(\theta_1) +$$

$$+ i_{y_2} f_1(\theta_1 + \bar{\theta}_2) + 2 i_{y_2} l_1 \cos\bar{\theta}_2,$$

$$\bar{m}_{35} = i_{x_2} + i_{b_2} + i_{y_2} f_1(\theta_1 + \bar{\theta}_2) + i_{y_2} l_1 \cos\bar{\theta}_2,$$

$$[\bar{m}_{36} \quad \bar{m}_{37}] = N_1^T + m_{x_2} l_1 \sigma_1(l_1) + [\, N_3^T + m_{x_2} \sigma_1(l_1) \,] f_1(\theta_1) + i_{y_2} \sigma_1(l_1) \cos\bar{\theta}_2,$$

$$[\bar{m}_{38} \quad \bar{m}_{39}] = N_2^T + N_4^T l_1 \cos\bar{\theta}_2 + N_4^T f_1(\theta_1 + \bar{\theta}_2);$$

$$\bar{m}_{44} = i_{x_1} + i_{x_2} + i_{b_1} + i_{b_2} + m_{x_2} l_1^2 + 2 i_{y_2} l_1 \cos\bar{\theta}_2, \qquad \bar{m}_{45} = i_{x_2} + i_{b_2} + i_{y_2} l_1 \cos\bar{\theta}_2,$$

$$[\bar{m}_{46} \quad \bar{m}_{47}] = N_1^T + m_{x_2} l_1 \sigma_1(l_1) + i_{y_2} \sigma_1(l_1) \cos\bar{\theta}_2,$$

$$[\bar{m}_{48} \quad \bar{m}_{49}] = N_2^T + N_4^T l_1 \cos\bar{\theta}_2;$$

$$\bar{m}_{55} = i_{x_2} + i_{b_2}, \qquad [\bar{m}_{56} \quad \bar{m}_{57}] = i_{y_2} \sigma_1(l_1) \cos\bar{\theta}_2, \qquad [\bar{m}_{58} \quad \bar{m}_{59}] = N_2^T.$$

$$\begin{bmatrix} \bar{m}_{66} & \bar{m}_{67} \\ \bar{m}_{76} & \bar{m}_{77} \end{bmatrix} = M_1 + m_{x_2} \sigma_1^T(l_1) \sigma_1(l_1), \qquad \begin{bmatrix} \bar{m}_{68} & \bar{m}_{69} \\ \bar{m}_{78} & \bar{m}_{79} \end{bmatrix} = \sigma_1^T(l_1) N_4^T \cos\bar{\theta}_2;$$

$$\begin{bmatrix} \bar{m}_{88} & \bar{m}_{89} \\ \bar{m}_{98} & \bar{m}_{99} \end{bmatrix} = M_2.$$

BIBLIOGRAPHY

[1] M. Azam and S. N. Singh. Invertibility and trajectory control for nonlinear maneuvers of aircraft. *J. of Guidance, Control, and Dynamics*, 17(1):192–200, 1994.

[2] E. Bayo. A finite-element approach to control the end-point motion of a single-link flexible robot. *J. of Robotic Systems*, 4(1):63–75, 1987.

[3] E. Bayo, Papadopoulos P., and J. Stubbe. Inverse dynamics and kinematics of multilink elastic robots: An iterative frequency domain approach. *Int. J. of Robotics Research*, 8(6):49–62, 1989.

[4] E. Bayo and B. Paden. On trajectory generation for flexible robots. *J. of Robotic Systems*, 4(2):229–235, 1987.

[5] W. J. Book, O. Maizza-Neto, and D. E. Whitney. Feedback control of two beam, two joint systems with distributed flexibility. *J. of Dynamic Systems, Measurement, and Control*, 94(4):424–431, 1975.

[6] R. W. Brockett and M. D. Mesarovic. The reproducibility of multivariable systems. *J. of Mathematical Analysis and Applications*, 11(3):548–563, 1965.

[7] A. E. Bryson and Y. C. Ho. *Applied Optimal Control.* Hemisphere, New York, 1975.

[8] R. H. Cannon and E. Schmitz. Initial experimental on the end point control of a flexible one-link robot. *Int. J. of Robotics Research*, 3(3):62–75, 1984.

[9] D. Chen. An iterative solution to stable inversion of nonlinear nonminimum phase systems. *Proceedings of the 1993 American Control Conference*, pages 2960–2964, 1993.

[10] D. Chen. Output tracking control of nonlinear non-minimum phase systems. *Proceedings of the 33rd IEEE Conference on Decision and Control*, pages 2340–2345, 1994.

[11] D. Chen and B. Paden. Stable inversion of nonlinear nonminimum phase systems. *Proceedings of the Japan/USA Symposium on Flexible Automation*, pages 791–797, 1992.

[12] D. Chen and B. Paden. Stable inversion of nonlinear nonminimum phase systems. *Int. J. of Control*, 64(1):81–97, 1996.

[13] E. J. Davison. The robust control of a servomechanism problem for linear time-invariant multivariable systems. *IEEE Trans. on Automatic Control*, 21(1):25–34, 1976.

[14] A. De Luca and B. Siciliano. Inversion-based nonlinear control of robot arms with flexible links. *J. of Guidance, Control, and Dynamics*, 16(6):1169–1176, 1993.

[15] A. De Luca and B. Siciliano. Regulation of flexible arms under gravity. *IEEE Trans. on Robotics and Automation*, 9(4):463–467, 1993.

[16] E. Delaleau and M. Fliess. An algebraic interpretation of the structure algorithm with an application to feedback decoupling. *Proceedings of the IFAC Symposium on Nonlinear Control Systems Design*, pages 179–184, 1992.

[17] S. El Asmi and M. Fliess. Invertibility of discrete-time systems. *Proceedings of the IFAC Symposium on Nonlinear Control Systems Design*, pages 335–339, 1992.

[18] M. Fliess. A new approach to the structure at infinity of nonlinear systems. *Systems & Control Letters*, 7(5):419–421, 1986.

[19] M. Fliess. A note on the invertibility of nonlinear input-output differential systems. *Systems & Control Letters*, 8(2):147–151, 1986.

[20] B. A. Francis. The linear multivariable regulator problem. *SIAM J. on Control & Optimization*, 15(3):486–505, 1977.

[21] B. A. Francis and W. M. Wonham. The internal model principle for linear multivariable regulators. *Applied Mathematics & Optimization*, 2(2):170–194, 1975.

[22] R. A. Freeman. *Robust Control of Nonlinear Systems.* PhD thesis, University of California, Santa Barbara, 1995.

[23] R. A. Freeman and P. V. Kokotovic. *Robust Nonlinear Control Design: State-Space and Lyapunov Techniques.* Birkhauser, Boston, 1996.

[24] J. W. Grizzle. On a rank invariant of analytic discrete-time nonlinear systems. *Proceedings of the IFAC Symposium on Nonlinear Control Systems Design*, pages 331–334, 1992.

[25] R. M. Hirschorn. Invertibility of control systems on lie groups. *SIAM J. on Control and Optimization*, 15(6):1034–1049, 1977.

[26] R. M. Hirschorn. Invertibility of multivariable nonlinear control systems. *IEEE Trans. on Automatic Control*, 24(6):855–865, 1979.

[27] R. M. Hirschorn. Invertibility of nonlinear control systems. *SIAM J. on Control and Optimization*, 17(2):289–297, 1979.

[28] L. R. Hunt, R. Su, and G. Meyer. Global transformation of nonlinear systems. *IEEE Trans. on Automatic Control*, 28(1):24–31, 1983.

[29] A. Isidori. *Nonlinear Control Systems: An Introduction.* Springer-Verlag, New York, 1989.

[30] A. Isidori and C. I. Byrnes. Output regulation of nonlinear systems. *IEEE Trans. on Automatic Control*, 35(2):131–140, 1990.

[31] A. Isidori, A. J. Krener, C. Gori-Giorgi, and S. Monaco. Nonlinear decoupling via feedback: A differential geometric approach. *IEEE Trans. on Automatic Control.* 26(2):331–345, 1981.

[32] A. Isidori and C. H. Moog. *On the Nonlinear Equivalent of the Notion of Transmission Zeros.* Springer-Verlag, New York, 1991.

[33] H. K. Khalil. *Nonlinear Systems.* Macmillan, New York, 1992.

[34] Ülle Kotta. *Inversion Method in the Discrete-Time Nonlinear Control Systems Synthesis Problems.* Springer-Verlag, New York, 1995.

[35] A. J. Krener and A. Isidori. Nonlinear zero distribution. *Proceedings of the 19th IEEE Conference on Decision and Control*, pages 665–668, 1980.

[36] D. S. Kwon and Book. W. J. An inverse dynamic method yielding flexible manipulator state trajectories. *Proceedings of the 1990 American Control Conference*, pages 186–192, 1990.

[37] S. K. Madharan and S. N. Singh. Inverse trajectory control and zero dynamics sensitivity of an elastic manipulator. *Proceedings of the 1991 American Control Conference*, pages 1879–1884, 1991.

[38] L. Meirovitch. *Analytical Methods in Vibrations.* Macmillan, New York, 1967.

[39] L. Meirovitch and Y. Chen. Trajectory and control optimization for flexible space robots. *Proceedings of the AIAA Guidance, Navigation, and Control Conference*, pages 1625–1638, 1992.

[40] L. Meirovitch and S. Lim. Maneuvering and control of flexible space robots. *J. of Guidance, Control, and Dynamics*, 17(3):520–527, 1994.

[41] R. K. Miller and A. N. Michel. *Ordinary Differential Equations.* Academic Press. New York, 1982.

[42] B. Morton. A dynamic inversion control approach for high-mach trajectory tracking. *Proceedings of the 1992 American Control Conference*, pages 1332–1336. 1992.

[43] D. Nenchev, Y. Umetani, and K. Yoshida. Analysis of a redundant free-flying spacecraft/manipulator system. *IEEE Trans. on Robotics and Automation*, 8(1):1–6, 1992.

[44] H. Nijmeijer. Invertibility of affine nonlinear control systems: A geometric approach. *Systems & Control Letters*, 2(3):163–168, 1982.

[45] H. Nijmeijer. Right invertibility for a class of nonlinear control systems: A geometric approach. *Systems & Control Letters*, 7(2):125–132, 1986.

[46] H. Nijmeijer and J. M. Schumacher. Zeros at infinity for affine nonlinear control systems. *IEEE Trans. on Automatic Control*, 30(6):566–573, 1985.

[47] H. Nijmeijer and A. van der Schafr. *Nonlinear Dynamical Control Systems.* Springer-Verlag, New York, 1990.

[48] J. M. Ortega. *Matrix Theory.* Plenum Press, New York, 1987.

[49] R. Ortega and M. W. Spong. Adaptive motion control of rigid robots: A tutorial. *Proceedings of the 27th IEEE Conference on Decision and Control*, pages 1575–1584, 1988.

[50] B. Paden, D. Chen, R. Ledesma, and E. Bayo. Exponentially stable tracking control for multi-link flexible manipulators. *ASME J. of Dynamic Systems, Measurement. and Control*, 115(1):53–59, 1993.

[51] M. K. Sain and J. L. Massey. Invertibility of linear time-invariant dynamical systems. *IEEE Trans. on Automatic Control*, 14(2):141–149, 1969.

[52] B. Siciliano and W. J. Book. A singular perturbation approoach to control lightweight flexible manipulators. *Int. J. of Robotics Research*, 7(4):79–90. 1988.

[53] L. M. Silverman. Inversion of multivariable linear systems. *IEEE Trans. on Automatic Control*, 14(3):270–276, 1969.

[54] S. N. Singh. A modified algorithm for invertibility in nonlinear systems. *IEEE Trans. on Automatic Control*, 26(2):595–599, 1981.

[55] S. N. Singh. Generalized functional reproducibility conditions for nonlinear systems. *IEEE Trans. on Automatic Control*, 27(4):958–960, 1982.

[56] S. N. Singh. Functional reproducibility in nonlinear systems using dynamic compensation. *IEEE Trans. on Automatic Control*, 29(5):446–450, 1984.

[57] S. N. Singh. Asymptotically decoupled discontinuous control of systems and large aircraft maneuver. *IEEE Trans. on Aerospace and Electronic Systems*, 25(5):677–688, 1989.

[58] S. N. Singh and W. J. Rugh. Decoupling in a class of nonlinear systems by state variable feedback. *ASME J. of Dynamic Systems, Measurement, and Control*, 94(3):323–324. 1972.

[59] S. S. Skaar. Closed form optimal control solution for conntinuous linear elastic system. *J. of Astronautical Science*, 32(4):447–461, 1984.

[60] W. H. Sunada and S. Dubowsky. On the dynamic analysis and behavior of industrial robotic manipulators with elastic members. *J. of Mechanisms, Transmissions, and Automation in Design*, 105(1):42–51, 1983.

[61] Z. Vafa and S. Doubowsky. On the dynamics of manipulators in space using the virtual manipulator approach. *Proceedings of the 26th IEEE Int. Conference on Robotics and Automation*, pages 579–585, 1987.

[62] M. Vukobratovic and D. Stokic. *Applied Control of Manipulation Robots.* Springer-Verlag, New York, 1989.

[63] S. Wiggins. *Introduction to Applied Nonlinear Dynamical Systems and Chaos.* Springer-Verlag, New York, 1990.

[64] K. A. Wise. Nonlinear aircraft flight control using dynamic inversion. *Proceedings of the 1992 American Control Conference*, pages 1322–1326, 1992.